Cancer Dynamics under a Chemotherapeutic Stress Gradient Using a Microfluidic *in vitro* Tumor Environment

Ke-Chih Lin

A Dissertation
Presented to the Faculty
of Princeton University
in Candidacy for the Degree
of Doctor of Philosophy

Recommended for Acceptance
by the Department of
Electrical Engineering
Adviser: Professor James C Sturm

June 2019

Abstract

In this dissertation, we use the microfluidic cancer-on-chip system we have developed to explore cancer population dynamics and how cancer acquires drug resistance. The microfluidic cell culture device, the "evolution accelerator" (EA), generates an *in vitro* landscape of stress heterogeneity across a tumor population. The system allows for high-magnification real-time observations of different cancer cell lines and downstream analysis of cell phenotype as a function of position on the stress landscape. With the EA technology, we investigate the adaptation and evolution dynamics in prostate cancer cell metapopulations under a stress landscape of a chemotherapeutic drug (docetaxel). High-resolution time-lapse scanning provides abundant information about the change in cell morphology, population dynamics, cell motility and cell migration over time on a cellular level.

We further implement this technology to study quantitatively the emergence of polyploid, mesenchymal and stem-like cancer cells in the context of complex heterogeneous yet controllable *in vitro* environments with a spatially-varying drug concentration. Within our microfluidic stress landscape, we observe: (1) a previously-unobserved surprisingly large number of polyploid giant cancer cells (PGCCs) which emerged in a highly stressful region in response to chemotherapy; (2) the transition of the epithelial to the mesenchymal state; (3) the stem-like characteristics of PGCCs. We argue that the elevated emergence of PGCCs in a high drug environment is due to migration of diploid epithelial cells from regions of low drug concentration, where they proliferate, to regions of high drug concentration, where they rapidly convert to PGCCs. The coexistence of the emerging drug-resistance PGCCs and the altruistic proliferative diploid cells may serve as a survival strategy for the cancer population. This suggests the clinical value of identifying vulnerabilities of PGCCs that might be considered critical targets.

Finally, we present a microfluidic device, the static diffuser, which, unlike earlier work using continuous flows, generates a long-term chemical gradient within tumor microenvironment based on a static diffusion mechanism. Due to the simplicity of the experimental setup, the system allows not only well-controlled continuous microscopic studies of the interaction among various cell types, but also parallel experimentation for up to 18X time-resolved downstream cellular assays. As a proof of concept, we report the co-culture of human bone marrow stromal cell line (HS-5) and bone-metastatic prostate cancer cell line (PC3) using the static diffuser.

Taken together, the experimental platform and cancer studies presented in this dissertation show the power of sophisticated *in vitro* environments to enable the discovery of new pathways and mechanisms underlying evolution of drug resistance in cancer.

Acknowledgements

Thank you to all who helped make this thesis possible. First and foremost, I would like to express my greatest appreciation to my advisor, Prof. James Sturm, for his exceptional amount of support towards my thesis work. Prof. Sturm dedicates himself to the development of his students, including the abilities to conduct independent research and the exploration of various career opportunities. He has always been on my side when I need to make important life decisions. I have been very fortunate to have Prof. Sturm as my academic advisor and mentor.

I would like to thank Prof. Robert Austin for all his mentoring and guidance throughout the years. Prof. Austin, a.k.a. Uncle Bob, is my role model with respect to his amazing research enthusiasm and work ethic. Uncle Bob provides me with the opportunities to do research in several multidisciplinary collaborations, which has truly broadened my horizons.

I would like to thank all fellow students in Sturm Lab and Austin Lab, both past and present. The members of the group create a supportive working environment, where people are willing to share pieces of knowledge and ideas. My special thanks to Dr. Amy Wu, Dr. Yu Chen, and Dr. Joseph D'Silva for introducing me to the equipment, experiment protocols, and facilities in the lab when I joined the group. I would also like to thank Average Phan, Matthew Black, and Weibin Liang for countless discussion that are hugely inspiring and tons of fun. Many thanks to Yusha Sun and Kumar Mritunjay for being tremendously helpful in the cancer research projects.

I am truly grateful to our collaborators at Johns Hopkins Medical Institute, Prof. Kenneth Pienta and Dr. Gonzalo Torga. They have been really supportive and provided much of the cancer biology and implications insight. Many thanks to Prof. Robert Axelrod at University of Michigan and Dr. Robert Gatenby at Moffitt Cancer Centerfor for their exceptional amount of insight in our research projects. I would

also like to thank Prof. Gabor Balazsi and Mariola Szenk for initiating the cancer metastasis collaboration. Many thanks to Prof. Kaushik Sengupta, Prof. Daniel Cohen, and Prof. Sujit Datta for their advice and comments throughout the years of my Ph.D. studies.

The past 5 years have been a wonderful journey for me. I could not have gone this far without the support and understanding from my family. I will never forget what my parents taught me, and I will strive to pass their teaching on. And finally, to Yi-Chen, for sharing all the challenging yet joyful moments with me at Princeton. My beloved wife sacrificed her own career just to be here with me, and I'll always be grateful for that.

To my parents Jia Lin, Yung-Fang Shih and my wife, Yi-Chen.

Contents

List of Tables

List of Figures

Chapter 1

Introduction

1.1 Motive

Cancer has been a major concern in the US and around the world. According to World Health Organization (https://www.who.int/news-room/fact-sheets/detail/cancer), cancer is the second leading cause of death globally, and is responsible for an estimated 9.6 million deaths in 2018. In 2018, in the US alone, 1.7 million new cases of cancer were diagnosed and 0.6 million people died of cancer according to National Cancer Institute (https://www.cancer.gov/about-cancer/understanding/statistics).

In the past 30 years, the 5-year relative survival rate for all cancers has only increased 18%, from 50% in 1975 to 68% in 2007, according to NIH Fact Sheets (https://report.nih.gov/nihfactsheets/viewfactsheet.aspx?csid=75). The majority of that increase in survival is due to improvements in prevention (diet and habits), early detection (screening programs, better imaging systems and biochemical markers) and the improved ability to ablate tumors (radiotherapy, surgical procedures), but not other forms of treatment. Metastatic cancer, on the whole, remains incurable: cancer metastasis has caused over 90% of cancer related deaths, and

the prognosis of metastatic cancers have not been improved over several decades. [1] Regardless of the myriad of attempts and money invested in drug development and screening, as well as the enormous improvements archived in the capacity to design targeted agents, our ability to predict the outcome of a given therapy through either animal or *in vitro* models has barely changed. The gap between the lab bench and patient bedside remains wide.

The classic idea that cancer recapitulates Darwinian evolution, in which a series of mutagenic episodes end up becoming a tumor that eventually kills the patient may be conceptually correct, but has also been demonstrated to be too simplistic. [2, 3] It is unlikely that the generation of a lethal cancer is simply the result of a statistical repetition of independent events. [4] There is clear evidence of cross-talk between cancer cells, host-cells and cancer cells, and cancer-influenced host cells (e.g., cancer-associated fibroblasts, myofibroblasts, and macrophages) with other host cells. Thus, cancer is better described in an ecological framework that explains Darwinian evolution in the context of an evolving and dynamic environment that applies pressures as well as presents opportunities for genetic and epigenetic changes. [5, 6]

Interactions between the different cells in the cancer microenvironment have been proven fundamental for the cancer to survive by escaping immunosurveillance, promoting matrix degradation and angiogenesis, and promoting cancer cells to undergo Epithelial-to-Mesenchymal Transitions (EMT) to become more invasive and aggressive. Better *ex vivo* models are required to recreate the dynamic ecosystems where cancer cells reside. To break the therapeutic logjam in our current treatments for metastatic cancer, tumors must be studied within microenvironments which contain cancer clones, components of stroma and the immune system, and components of extracellular matrices within a dynamic resource environment (changing oxygen tension and nutrients) that allows quantitative studies of their interactions in terms of cooperation or competition.

In Section 1.2, we will discuss the advantages and drawbacks of the existing preclinical tumor models as reviewed by D. Caballero *et al.*[7] We then summarize the essential features of an *in vitro* tumor model in Section 1.3, and introduce our approach to the problem in Section 1.4.

1.2 Existing preclinical tumor models in biomedical research

1.2.1 Conventional 2D *in vitro* models

Conventional two-dimensional (2D) models are defined as the cell culture techniques performed on flat tissue culture-treated surfaces, provided with uniform growth medium and reagents of interest. Standard culturewares include cell culture dishes, flasks, or multi-well plates. These standard 2D model are the most widely adopted *in vitro* models for standard cellular assays such as cell motility, proliferation, genetic and epigenetic studies, cell signaling, and drug screening.

The history of 2D cell cultures can be dated back to over a century ago. It has always been the default platform for molecular biological studies for several reasons. First, the culturewares are typically made out of polystyrene (PS), which has high optical clarity, relative ease of manufacture, and low production cost. Secondly, the maintenance of a cell culture is straightforward, and the downstream cellular protocols can be easily automated. Therefore, 2D *in vitro* models, such as 96 well-plates, offer remarkable experiment capacity and reproducibility, making it the top choice for general biological research and high-throughput drug screening in pharmaceutical industry. [8]

The aforementioned advantages, however, can also be the Achilles' heel of 2D *in vitro* models. 2D culture provides fixed and uniform external conditions for cell

growth. The homogeneous culture environment produces statistics for understanding cell dynamics in a mean-field approach, which fails to take into account the architectural complexity and heterogeneous ecological factors in a tumor. Moreover, cells in a 2D environment display different phenotypes and altered gene expression compared to cells *in vivo*. Therefore, albeit being valuable for general purposes, standard 2D culturewares do not serve as a suitable platform to mimic tumor dynamics.

1.2.2 3D *in vitro* models

To capture the fundamental features of a tumor which 2D *in vitro* models fail to offer, several attempts have been made to develop 3D *in vitro* models. These models offer an environment for reconstructing inter-cellular and cell-ECM interaction so that cell morphology and physiological function are preserved compared to their *in vivo* counterparts. There is currently no 3D model that describes every aspect of *in vivo* biological system, but these models are still very informative under different scenarios.

Hydrogel and collagen matrix

As the most abundant protein in mammals making 25% to 35% of the whole-body protein content, collagen is the major extracellular structural protein in various connective tissues including bone, tendon, cartilage, blood vessels, intestines, etc. Therefore, to study cell physiology while preserving cell phenotypic response as they were *in vivo*, culturing cells in collagen or hydrogel matrix is a rather straightforward approach.

It is simple and cost efficient to prepare collagen matrix for *in vitro* cell culture as the protocol has been well-established in most cases. The main components for collagen matrix formation are concentrated collagen solution and concentrated phosphate buffer (PBS). The mechanical properties of the gelled collagen matrix can be

fine-tuned and customized based on the concentration of collagen solution, the concentration of PBS, the pH of mixed reagent, and the incubation temperature.

Common cell seeding methods in collagen matrix include 3D sandwich culture and 3D entrapment. [9] 3D sandwich culture is a layer-by-layer culture method. Cells are re-suspended and seeded onto a sheet of gelled collagen matrix. After cell attachment, the culture is then covered with another sheet of collagen matrix for another round of cell seeding. The process is then repeated consecutively to achieve the desired thickness of sample. This approach avoids exposing cells to a stressful environment, the collagen solution which contain concentrated PBS and is typically prepared below 4 °C. However, the distribution of cells is not uniform across the vertical dimension. For some scientific purposes such as studying the electrophysiological characteristics of neurons in a 3D environment, the fact that the cells remain in-plane after weeks of culture limits the physiological and morphological relevance.

For the 3D entrapment method, the cells are mixed with collagen reagents and then incubated during the gel formation process. The advantage of entrapment method is that the sample preparation is less labor-intensive and the cells are distributed uniformly across the collagen matrix. However, it would be more challenging to adjust cell culture protocol for sensitive cells which are more likely to die out in the sample preparation and gelling process.

Microcarriers in bioreactors

Microcarriers are artificial supportive materials that allow for the culture of adherent cells. They are usually made of glass, polystyrene, acrylamide, collagen, or alginate with 100 - 200 μm in diameter. The materials and surface treatments of the microcarriers can be specifically modified to optimize or influence the cellular dynamics.

Microcarriers have been applied in various studies which highlight their superior ability to mimic the permeability of nutrients, metabolites, or growth factors in a

biological system. Scientists have shown that seeding together cancer cells and fibroblasts on gelatin microsphere allows for the recapitulation of desmoplastic reaction of pancreatic cancer. [10] The results are of great interest because of the presented microcarrier cancer model replicates the complexity of the tumor microenvironment and could potentially be utilized as a drug screening platform. It has also been shown that cell-seeded microcarriers can be guided and organized into desired geometry, enabling efficient generation of diverse structures in a configurable way. [11]

Spheroids

Spheroid cultures are a subset of 3D culturing methods where cells are cultured to form aggregates either spontaneously or guided by external geometrical constrains.[12] The size of a spheroid can depend heavily on the type of cells and the fabrication techniques, but typically tens of microns to hundreds of microns in diameter. Spheroids are usually maintained in standard culturewares such as 96-well plates, and are amenable to high-throughput screening (HTS). As one of the most popular scaffold-free 3D culture techniques, spheroids have been shown to have advantages over other 3D culture approaches in simulating tumor microenvironment and cellular functions, especially in the context of cell-cell interaction among different cell types.

A spheroid culture, unlike collagen matrix or some of the microcarriers, does not relay on cell adhesion to foreign materials. Tumoral cells can be co-cultured within spheroids with various cell types including fibroblasts, immune cells, and endothelial cells to foster a self-organized heterogeneous tumor microenvironment. Cells within the spheroid can produce extracellular matrix and growth factors while interacting with other cell types as well as self-secreted matrix in a natural and undisturbed manner. [12] Moreover, spheroids can be used as building blocks for more complicated tissue engineering to improve the physiological relevance of *in vitro* studies. These advantages promote the study of several fundamental metastatic events such as

angiogenesis[13], epithelial-to-mesenchymal transition (EMT)[14], tumor-associated fibroblast differentiation[15], and tumor progression.

1.2.3 Model organisms

Model organisms are *in vivo* animal models that are studied to understand specific biological phenomena, which may be transferable and provide further insight into the biological function of other organisms. Depending on the questions to be answered, model organisms with different level of complexity can be chosen, ranging from simple organisms (e.g. C.elegans, zebrafish) to mammalians (e.g. mice, rabbits, pigs). Genomic data is used to make close comparisons between species and determine suitable model animals with high phylogenetic relatedness. For instance, homo sapiens share roughly 99% of our genome with chimpanzees and over 90% with mice. Therefore, taking into account the cost effectiveness, genetically engineered mice have become the primary source of pre-clinical animal model.

In cancer research, an animal model can be coarsely classified as spontaneous models or induced models. Spontaneous models are either normal animals with phenotypic features resemble those of humans or abnormal members of a species that arise via spontaneous mutations. Induced models are animals subjected to well-controlled manipulation including surgery, genetic modification, and chemical treatment, leading to an alteration to their normal physiologic state. Both models are extensively utilized as a pre-clinical drug development platform, while induced models are the most common in cancer research and metastatic diseases.

Animal models, among all existing preclinical tumor models, offer the highest physiological relevance and still maintain reasonable genetic similarity to humans. However, animal testing has long been acknowledged to have significant limitations in predicting human outcomes.

In 2004, the FDA chief announced that only 8% of drugs that pass preclinical phase, including animal testing, make it to the marketplace.[16] More recent studies suggest that the approval rate has not been improved, despite the efforts throughout the years to enhance the predictability of animal models. Although there are many other potential factors that reduce the approval rate of drugs, the statistics clearly demonstrated that no animal is sufficiently similar to humans to waive clinical human testing.

Moreover, animal testing is time-consuming process. It would take several months or even years to finish a series of animal testing, from establishing hypotheses, generating induced animal model, to the actual experimentation and analysis. Therefore, it is possible to revolutionize the pharmaceutical industry and speedup the drug development pipeline if there exists a preclinical screening platform that is more time efficient and more capable of predicting the results of human testing.

1.2.4 Microfluidic cancer-on-chip model

Microfluidics has been prophesized to bridge the gap between over-simplified 2D *in vitro* model and animal models which are too complex to support controllable quantitative studies. [8, 17, 7] A wide range of microfluidic cancer-on-chip models have been designed based on the advances in micro/nanofabrication technologies, bio-compatible materials, and tissue engineering. These models enable various multimodal cancer research projects with divergent system complexity and physiological relevance.

Microfluidics has been widely implemented since the late 1970s. Microfluidics is defined as a subset of technologies which manipulate and control small volume of fluidic dynamics to achieve specific tasks including but not limited to gradient generation, particle processing, mass transport, and precise chemical reaction. Because of the ability to precisely manipulate small volume of liquids in the scale of nL, pL

of even fL, microfluidic technologies have been proven to be especially influential on biotechnology.

The advances in organ-on-a-chip technologies in the past few decades demonstrated the potential of utilizing microfluidic systems as pre-clinical models or research platforms for cancer research. [18] Complicated intercellular behaviors can be monitored in a well-controlled physical and biochemical environment. [19, 20] For instance, cancer metastasis is a complicated sequence of events which involves: (1) primary tumor progression,[21, 22, 23] (2) angiogenesis,[24, 25, 26] (3) epithelial-to-mesenchymal transition, (4) invasion, (5) intravasation into the circulatory system,[27, 28, 29] (6) surviving the harsh circulation environment, (7) extravasation out of the circulatory system,[30, 31, 32] and (8) dormancy and subsequent secondary tumor growth. Customized organ-on-chip devices construct biomimetic systems to more accurately reproduce part of the cancer metastasis process, which has not been realized in most of the aforementioned 2D and 3D models.

To sum up, microfluidic cancer-on-chip models can bridge the gap between the oversimplified conventional 2D cultures and the complicated animal models, which have limited ability to produce reliable and reproducible quantitative results. Microfluidic models can be designed to cover different level of biological complexity, from single cell resolution to 3D-culture compatible configurations, making it an adaptive platform to study a wide range of fundamental questions in cancer biology.

1.3 Essential features of an *in vitro* tumor model

To summarize the previous discussion on existing preclinical models, conventional cell culture was developed almost a century ago and remains the most frequently used preclinical model in biomedical research, despite its proven limited ability to predict clinical results in cancer. Despite 3D cell cultures having been developed

over 50 years ago, they could also have notable limitations, and their application for cancer drug screening remains anecdotal. Animal models remain the most effective preclinical platform to predict clinical response to putative drugs but at great cost and extended time frames of months. Among all the preclinical models descussed in Section 1.2, microfluidic cancer-on-chip models appear to be the most promising candidate to satisfy the unmet need in cancer research.

Uncovering key interactions between host cells and cancer cells and developing improved therapeutic strategies under the conditions found *in vivo* requires not only a cell culturing system with complex fitness gradients, in which the behavior of each individual cell and the interactions of multiple cell types can be tracked and monitored in real time, but also a means to localize cell populations transiently so that local interactions can take precedence over "mean field" interactions averaged over all cell types. In other words, to recreate the complex dynamics in a *in vivo* tumor, one must investigate the population and evolutionary dynamics of cancer from an ecological perspective by enabling (1) the capability to observe adaptive cellular response, both individually and collectively, to a well-controlled heterogeneous microenvironment, (2) the observation of intercellular interactions among various types of cells in a tumor-like community. Throughout this dissertation, we demonstrate the development and implementation of our microfluidic cancer-on-chip platform that satisfy these requirements.

1.4 Our approach: building an artificial microenvironment with heterogeneous stress landscape to study cancer dynamics from an ecological perspective

For many years microfluidic organ-on-chips have been prophesied to be able to overcome all of the limitations mentioned in the previous section. However, no cancer-on-chip model has offered a platform that is able to reproduce key components and interactions to mimic a tumor microenvironment in a comprehensive manner, yet simple enough to provide reliable and reproducible data.

Therefore, in this dissertation, we present our microfluidic cancer-on-chip technologies that not only allow for long-term culture among various cell types and real-time data acquisition at single-cell level, but also provide a controllable platform to support quantitative study of cancer dynamics within a well-defined varying environmental conditions over time. Our microfluidic system resembles *in vivo* stress heterogeneity and metabolic stress gradient that is not modeled in current *in vitro* assays.

Adapted from the previous work in our group, as shown in Fig. 1.1, the pattern of cell culture region in our microfluidic device consists 109 interconnected hexagonal and 24 half-hexagonal chambers in the center, resembling a honeycomb structure. Two independent media channels surround the hexagonal cell culture region, providing fresh media with fixed concentration of reagents as the boundary condition. Media channels and cell culture region are connected with small slits (about 15 μm wide), which prevent direct media flow and the resulting shear stress across cell culture area, but still allow chemicals to diffuse through small slits and exchange nutrients, metabolic waste, etc.

Cells are cultured on a gas permeable membrane, encapsulated by the microstructure through the positive back pressure on the membrane against the chip. The hexagonal array pattern was chosen for two reasons: (1) maximization of precious chip area because a hexagon is the highest sided regular polygon that can cover space; (2) a connected hexagon maximizes the number of interconnection channels between adjacent parts of the cancer cell metapopulation while still providing localized confinement.

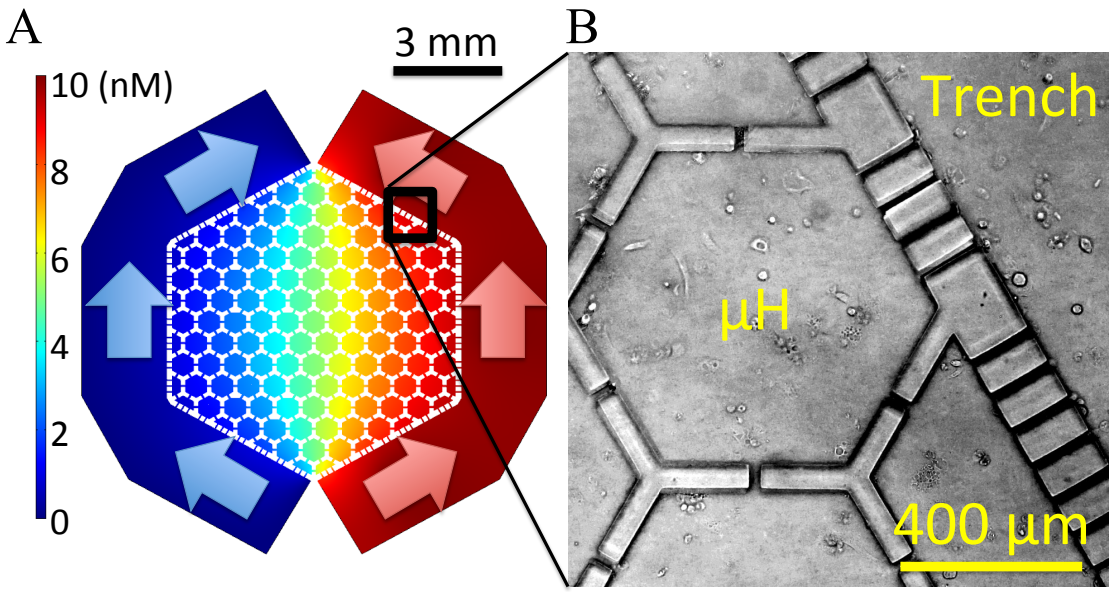

Figure 1.1: **The distribution of the chemical concentration in EA.** (A)The COMSOL Multiphysics® modeling of reagent concentration pattern. The diffusion coefficient is $10^{-9}m^2/s$ and the boundary condition at the peripheral media trenches is set as 0 (blue) and 10 nM (red). Media flow rate is 20 μL/hr. The reagent diffuses into the microhabitat array from the right three edges and out from the left. (B) A bright field image of the chip. The side of each hexagonal microhabitat (μH) is 400 μm and the depth of the trenches and habitats is 100 μm. Small slits (15 μm wide) restrict the direct media flow from the trenches into the microhabitat array. Large slits (25 μm wide) allow cell migration between adjacent habitats.

As a device with demonstrated ability to accelerate evolutionary dynamics, we name our microfluidic device the "Evolution Accelerator" (EA). The EA has two separate medium inlets, two outlets, and one central port for cell seeding or extraction of excessive medium. As shown in Fig. 1.1, the EA technology provides an

platform to investigate the emergence phenomena and cell population dynamics in a chemotherapy induced stress landscape due to the following features:

- Cells are partially confined within hexagonal wells called microhabitats, but they can move from microhabitat to microhabitat through the 25-μm wide slits on the walls.
- Fresh media with desired concentration of drug is continuously provided by syringe pump, which, combined with a similar drug-free buffer flow on the other side, secures a predetermined maximal and minimum dosage and establishes stable drug gradient via cross diffusion.
- The system allows real-time monitoring at single-cell level in bright field and fluorescent channels.
- The system allows for spatially resolved downstream immunofluorescence (IF) assays and direct sampling removal of cells for further characterization (to be demonstrated in Section 3.5 and Section 4.3).
- Our experiments are carried out over multiple weeks, with constant data collection. This observation of the emergence of phenotypes that would not be observed in short time experiments.
- The EA technology of semi-isolated populations in a gradient environment accelerates evolutionary dynamics to take place over weeks in the lab rather than months in conventional *in vitro* assays.

Therefore, the system enables numerous potential applications such as pre-clinical drug screening, *ex vivo* modeling and prediction for patient-specific treatment, etc.

1.5 Thesis organization

In this thesis, we present the microfluidic devices we have developed and how we implemented the technology to explore cancer population dynamics, phenotype variations and how cancer cells acquire drug resistance. The design concept, device fabrication process and experimental platform are introduced in Chapter 2.

In Chapter 3, we present a proof-of-principle study with the co-culture of human prostate cancer cell lines, PC3-EPI and PC3-EMT. We demonstrate the rapid adaptive behaviors of cancer cells in chemotherapy gradients with respect to the variation of cell proliferation profile and averaged motility in local population as a function of space and time. We also observe the emergence of population heterogeneity within the region where cell mortality transition occurs. This observation in turn motivate the work presented in Chapter 4.

Chapter 4 describes the characteristics of an emerging phenotype of cancer, polyploid giant cancer cells (PGCCs), that we have observed when the cells are exposed to chemotherapy gradients. We observe the rapid emergence of a surprisingly large number of polyploid giant cancer cells (PGCCs) in regions of very high drug concentration, which does not occur in conventional cell culture of uniform concentration. We present a sets of modified logistic growth equations in order to identify the underlying mechanism of the increased polyploidization events in drug gradient.

In Chapter 5, we introduce the concept of intercellular interactions within tumor microenvironments, and seek to demonstrate the potential of using static diffuser as a experiment platform to predict the population dynamics between bone marrow stromal cells (HS-5) and metastatic prostate cancer cells in bone marrow (PC3) in our engineered microenvironment.

Lastly, we summarize these studies and discuss future perspectives in Chapter 6. And finally, the protocols and data analysis procedures are presented in the appendices.

Chapter 2

Methodology and Hardware

In this chapter, I will introduce the previous work done in our lab, the design concept of our improved microfluidic cancer-on-chip system, device fabrication process, and the experimental platform. The results and figures presented in this chapter were published in Convergent Science Physical Oncology [33]. The content about the static diffuser presented in Section 2.4.2 is still in progress for a journal publication.

I was in charge of constructing the experimental EA apparatus, maintaining the cultures at Princeton, doing the experiments on the EA chips as well as data acquisitions, data processing and image analysis. The development of the technology has been supported by our collaborators at Johns Hopkins Medical Institute, Prof. Kenneth Pienta and Dr. Gonzalo Torga. A Research Experiences for Undergraduates (REU) program attendee, Wesley J Murray, was involved in the development of the gas supply system.

2.1 Previous work

Following the train of thought from the previous introductory chapter, we may infer that in order to reconstruct cellular dynamics in complex biological systems, the *in vitro* cancer models must capture two key features: (1) the ability to observe

adaptive cellular response to a well-controlled heterogeneous microenvironment, (2) the realization of interactions among various types of cells in a tumor-like community.

A practical way to achieve these features is to develop a microfluidic cell culture device that resembles *in vivo* stress heterogeneity by creating chemical gradients across the microecology. The cell culture microecology consists of hundreds of interconnected cell culture microhabitats that allows local intercellular interactions among various types of cells.

The interconnected microhabitats can be considered as a metapopulation. Metapopulation consists of a set of spatially separated populations of the same species which are permitted to interact at some limited level. According to Sewall Wright's evolutionary theory, when the population is broken down into multiple subpopulations, the individuals with better fitness advantages may emerge in response to local stress conditions, leading to rapid domination in the corresponding microhabitat. This fixated population can then sequentially explore neighboring microhabitats and achieve rapid evolution under heterogeneous stress landscape.

Several attempts have been made in our group as well as other researchers to utilize the concept of metapopulation to accelerate evolutionary dynamics of organisms. Zhang *et al.* demonstrated with a microfluidic device designed to mimic naturally occurring bacterial niches that resistance of E. coli to the antibiotic ciprofloxacin can be developed within 10 hours. Wu *et al.* showed that the degree of doxorubicin resistance of multiple myeloma increased 16-fold after 48 hrs of doxorubicin gradient exposure. Han *et al.* presented a microfluidic device that induced drug resistance in stage IV U87 glioblastoma cells to doxorubicin in 7 days.

However, these existing microfluidic systems leave much to be desired in several aspects. First of all, the packaging and assembly method of the existing devices restrict the ability to adjust gaseous stressors (e.g. normoxia or hypoxia conditions). Secondly, because the devices are not gas permeable, they offer limited ability to

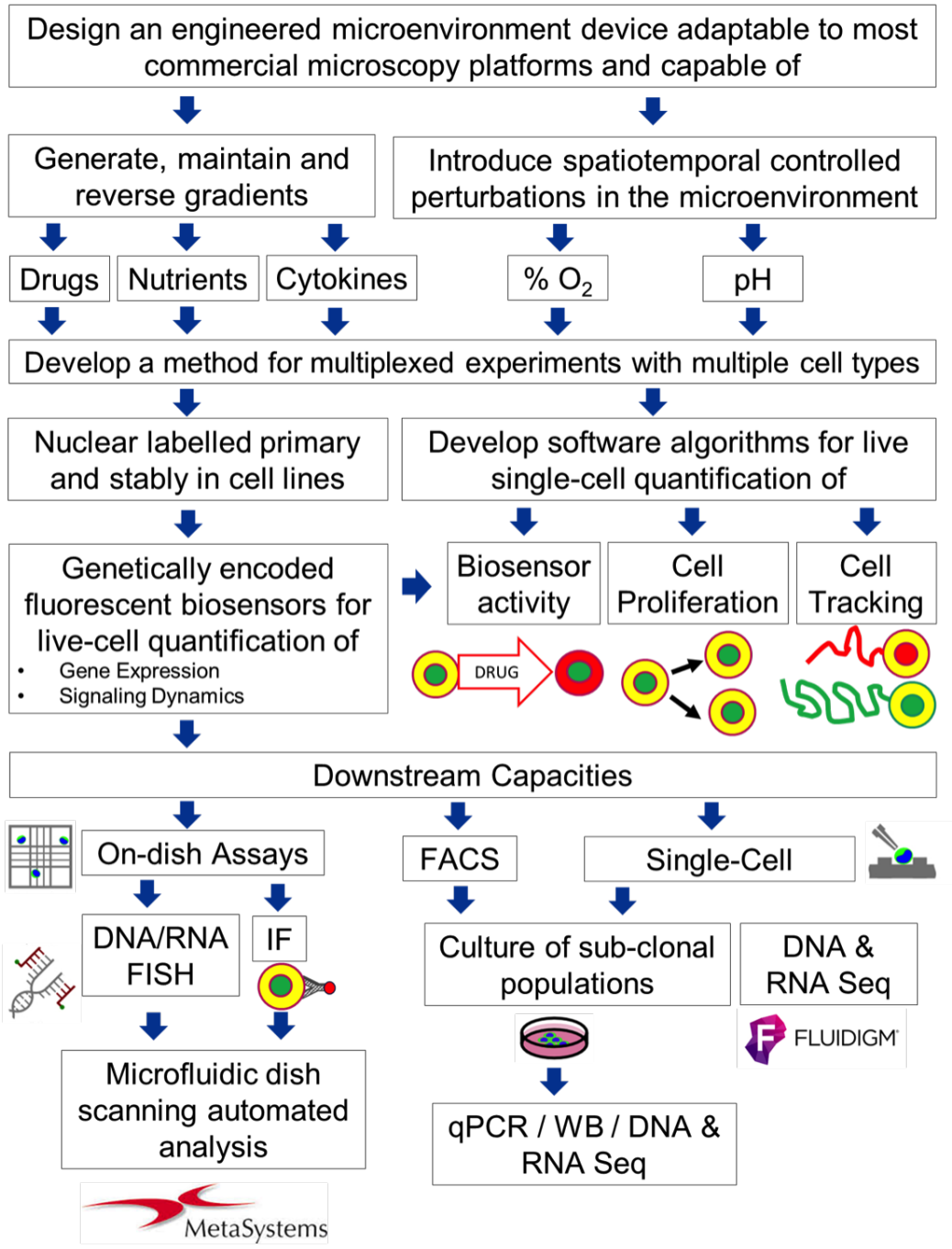

Figure 2.1: **The block diagram of the full experimental platform.**

maintain efficient oxygen and CO_2 exchange to optimize cell growth. As shown later in the next section, without efficient gas exchange, the device would fail to maintain constant pH across the entire population. Thirdly, to fully exploit the potential of cancer-on-chip technologies, it is essential to have the ability to acquire real-time multi-channel images with high temporal and spatial resolution. Lastly, the system should provide downstream experiment capacities (e.g. FACS, sub-clonal populations expansion, IF, DNA/RNA FISH, etc.) complementary to the time-lapse images taken in the course of the experiments. Last but not least, it should also be taking into consideration the difficulty of experiment implementation as well as the amenability to high-throughput experimentation. That is, the platform should be easily implemented by non-expert users, and should also provide the capacity of multiple experiments for the users to explore wider parameter space and experiment replicates.

Therefore, we have developed a novel packaging and assembly method for our microfluidic device to resolve the aforementioned issues. We have also built up the peripheral hardware for our portable on-stage cell culture microfluidic system. The overview of the capabilities of our improved microfluidic system is presented in the block diagram in Fig. 2.1.

2.2 The design of micro-structures: dealing with the effect of insufficient gas exchange on cell culture

As shown in Fig. 2.2, the original device prototype Fig. 2.2 (A) is only composed of cell culture hexagonal array and the peripheral media trenches, without the presence of the serpentine channels as seen in our current design (Fig. 2.2 (B)). The media was delivered into the chip directly through inlets, extracted out from the outlets.

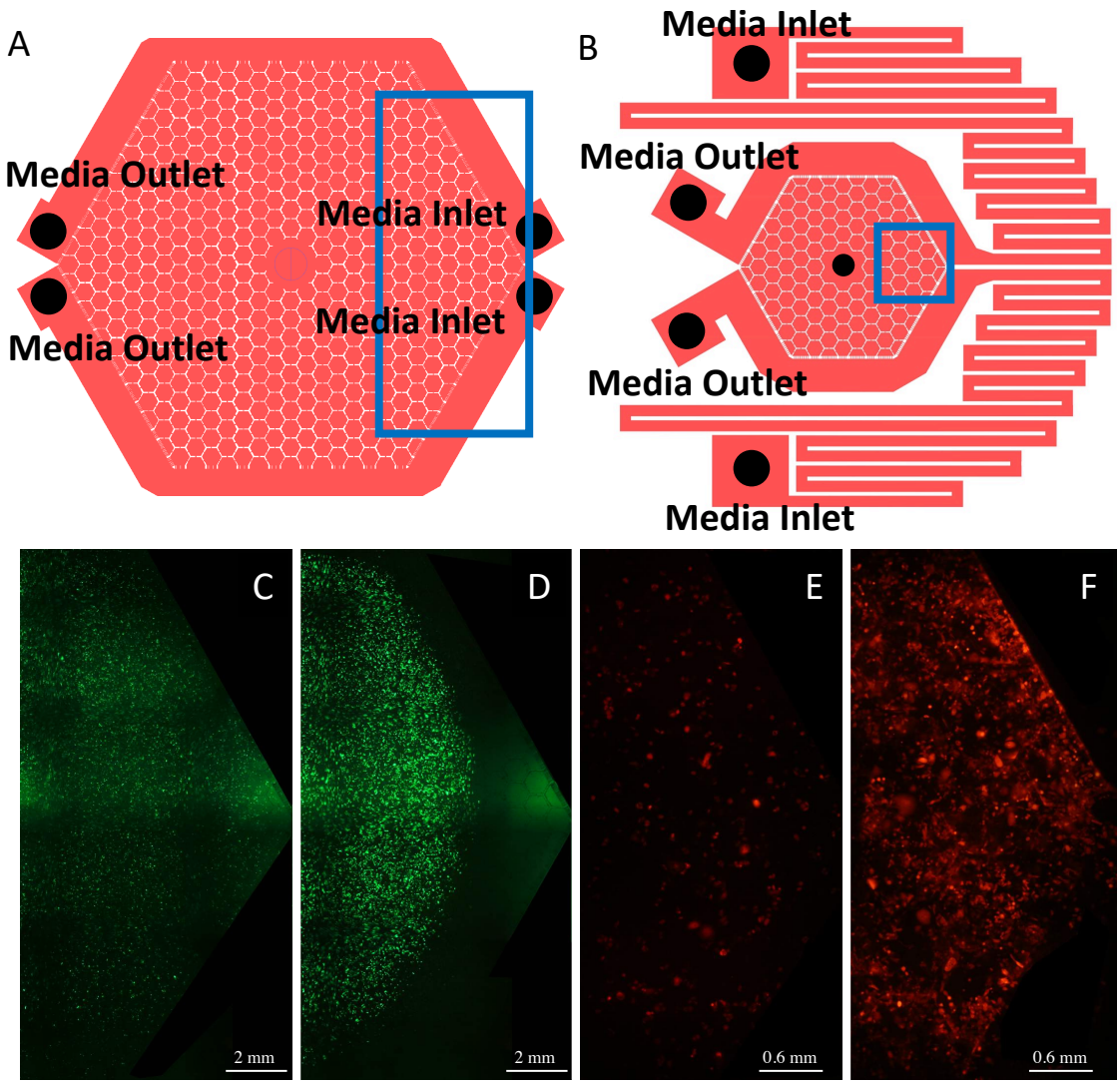

Figure 2.2: **The effect of insufficient gas exchange on cell culture.** (A) The pattern of the original prototype. Growth media is injected directly into the media trenches and extracted out from the outlets. (B) Modified design with serpentine incubation channels. (C)(D) Control experiment done with human prostate cancer cell line PC3 in the prototype chip A. As shown in C, cells were seeded uniformly to begin with. Cells around the media inlets died out after 5 days as shown in D. (E)(F) The PC3 Control experiment performed in the modified chip B. With the uniform initial seeding density shown in E, cells grew fully confluent with constant proliferation rate independent of their position.

Both the original prototype and our current design are made of PDMS with identical chip assembly method: cells are cultured on a gas-permeable Lumox membrane, encapsulated by the PDMS microstructures. Further details are described in Section 2.3.

A control experiment was performed with this prototype. Human prostate cancer cell line PC3 was cultured on the chip. Fresh normal media was provided on both sides of the media trenches to avoid any foreseeable chemical gradients. However, as shown in Fig. 2.2 (C) (D) corresponding to the square region marked in (A), after 5 days of culture, cells died out around the apex of the device near the media inlets. We argue that the dependence of cell fitness on relative distance to media inlets implies insufficient gas exchange. In order to ensure uniform oxygen level and pH value across the chip, we must secure sufficient incubation time for the media to be pre-conditioned under desired gas composition before entering the chip.

Therefore, we modified the media channels to allow thorough media conditioning, as shown in Fig. 2.2 (B). Note that between the medium inlets and the cell culture arrays, a pair of serpentine channels that allow the medium equilibrate with the atmosphere passed below the gas-permeable membrane. The serpentine channels result in significant improvement in uniformity of cell proliferation rate as a function of position, as shown in Fig. 2.2 (E) (F), corresponding to the square box marked in (B).

2.3 A compact on-stage cell culture platform: gas supply system, thermal control unit, and the PDMS microfluidic device

The full tumor-on-chip technology was designed to be a portable cell culture platform that can be installed on any inverted Epi-fluorescent microscope. The full platform is composed of three components: the gas supply that can control oxygen and CO2 levels, a customized well plate with thermal-controlled enclosure, and the PDMS microfluidic device with growth medium pump.

2.3.1 The gas supply system

As shown in Fig. 2.3 (B) and Fig. 2.5, our gas supply system consists of the CO_2 and O_2 concentration control units, a gas pump, a gas mixing chamber, a humidifier (bubbler), and three separate sets of gas valves and pressure gauges. The CO_2 and O_2 controller adjust the mixing rate of the gas from CO_2 tank, N_2 tank and the gas pump that works as an unregulated O_2 source. The gas is mixed in the mixing chamber, humidified by a bubbler and a relative humidity monitor that increase the relative humidity (RH) up to 85%, and then led to three independent gas valves with pressure gauges in order to control and monitor the gas flow rate that supports the cells cultured in the customized 3-well sample plate.

2.3.2 The customized well plate with thermal control unit

The stainless steel well sample plate is designed to hold up to 6 Lumox dishes capped by the PDMS device while being able to provide suitable environmental factors for cell culture. With the thermal control unit and the custom made gas supply system

A

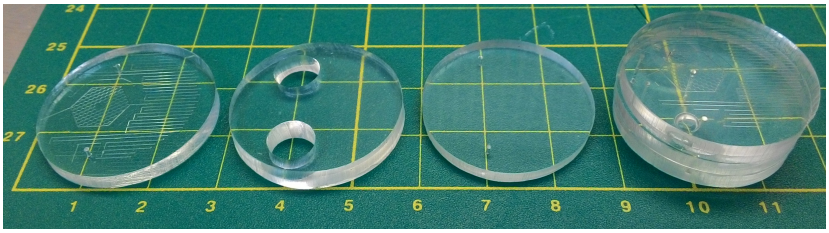

B

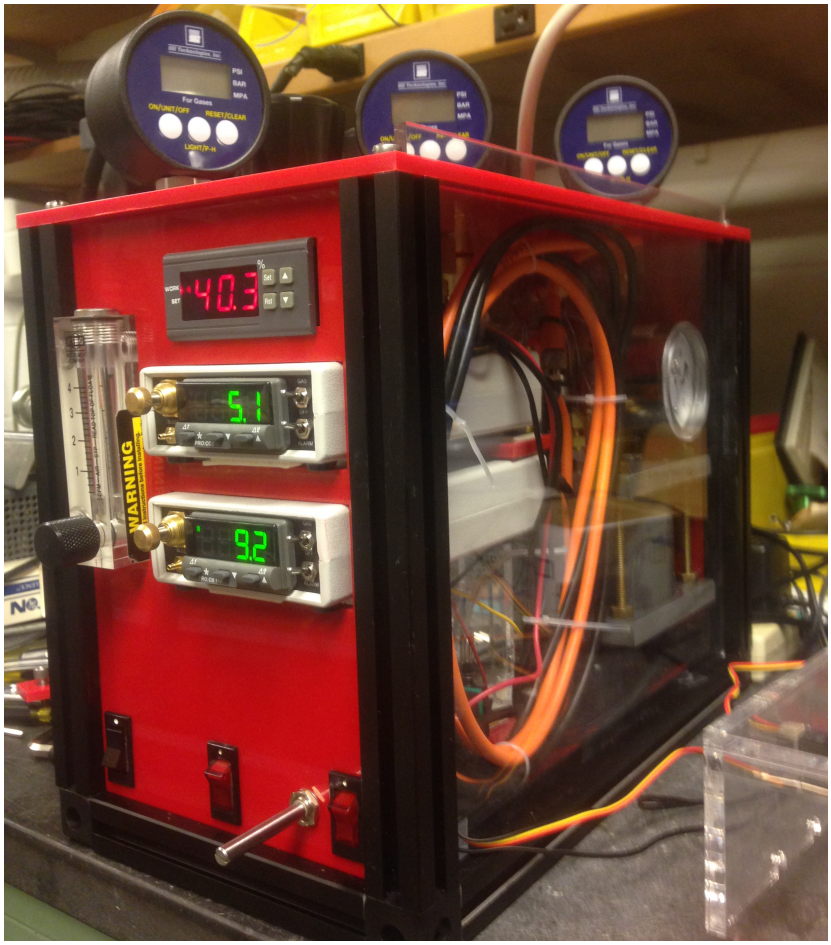

Figure 2.3: **The components of the PDMS chip and the gas supply system.** (A) The PDMS device. From left to right: the patterned layer, the reservoir layer, the capping layer, and the assembled device. The three stacks of PDMS layers were bonded by oxygen plasma treatment. The reservoirs trap bubbles in the tubing. (B) The gas supply system.

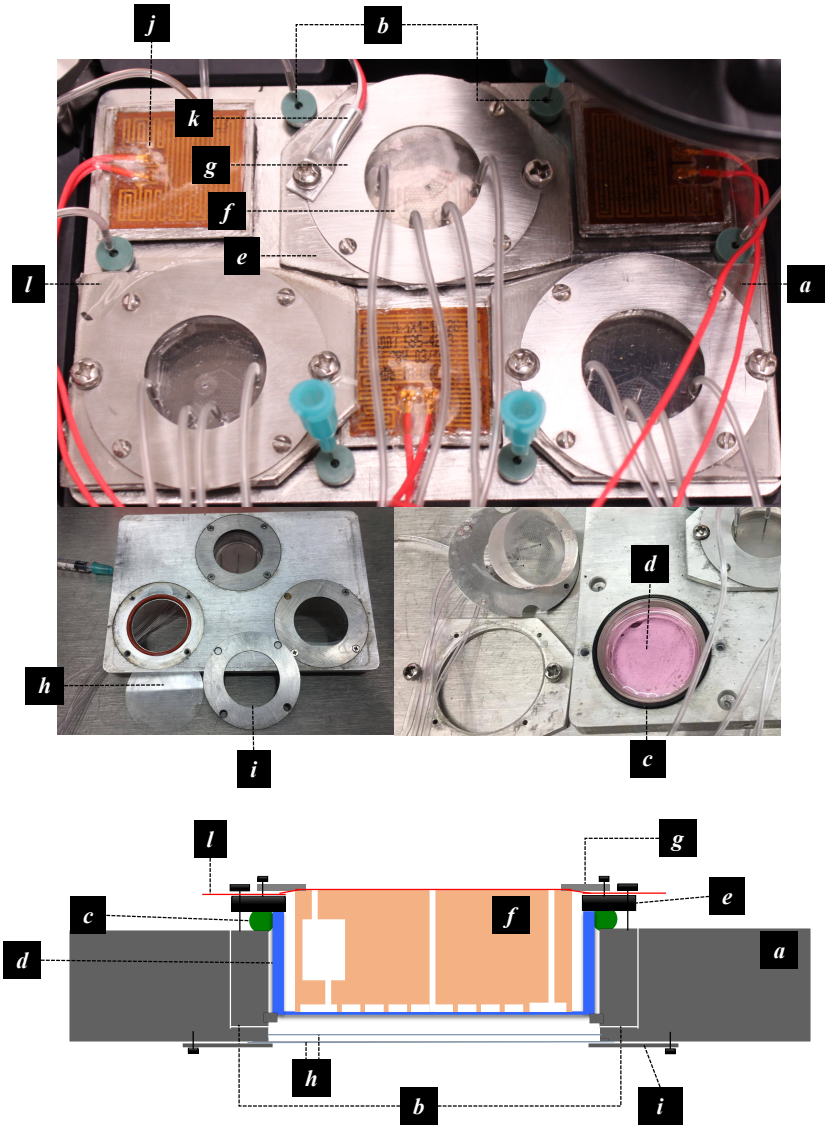

Figure 2.4: **The components of the customized 3 well sample plate.** ***a***, the main body of 3 well plate; ***b***, a pair of gas channels that allow conditioned atmosphere to be pumped in and vented out through the septa at the entrance of the gas channels; ***c***, an O-ring designed to seal the space between the well plate and the Lumox^{TM} dish; ***d***, the 35 mm diameter Lumox^{TM} dish; ***e***, the dish holder; ***f***, the PDMS device; ***g***, the PDMS chip holders; ***h***, the double layer 35 mm glass windows designed to maintain thermal isolation and prevent water condensation; ***i***, glass window holder; ***j***, heating pads; ***k***, temperature sensor; ***l***, the Microseal^{TM} B Adhesive Sealer (Biorad, Hercules, California 94547 USA) that keeps the chip from drying out.

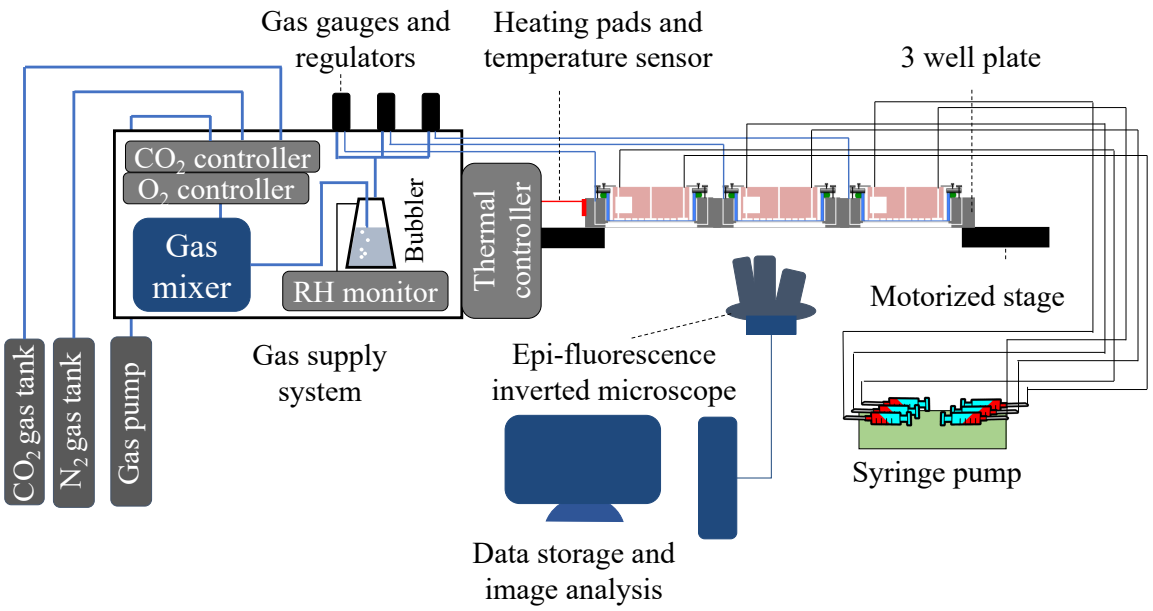

Figure 2.5: **The schematic figure of the experimental setup.** The setup of the experiment, including the gas supply system, gas channels connection, the medium supply connection and the imaging system.

which are compatible to the well plate, our cell culture platform can support cell culture on a motorized stage without the need for a full incubator enclosure.

The components of the 3-well sample plate is illustrated in Fig. 2.4. Each of the three wells is identical and independent. Each well comes with a pair of gas channels (b in Fig. 2.4), a Lumox dish holder (e), a PDMS chip holder (g), a glass window holder (i), and a pair of 35 mm glass windows (MatTek Corporation, Ashland, MA) (h). The LumoxTM dish holder clamps the Lumox dish (d) surrounded by an O-ring (c), squeezing the O-ring to create an airtight space between the Lumox dish and the well. The PDMS chip holder pushes the PDMS device (f) downward. The gas supply system is connected to the gas channels, pressurizing the space between the Lumox dish and the well, and pushing the Lumox membrane against the PDMS device to secure the sealing of the device. The temperature sensing unit (k) and heating pads (j) are connected to the 3-well plate and actively control the temperature around 37

°C. A sheet of Microseal B Adhesive Sealer (l) was taped on top of the PDMS device, clamped by the PDMS chip holder to prevent the chip from drying out. The double layer glass windows are designed to keep the space between the Lumox membrane and the well thermal isolated so that theres no water condensation due to temperature difference at the interface. The entire 3-well sample plate is set on the motorized stage of an inverted microscope for long-term image acquisition.

2.3.3 PDMS microfluidic device fabrication

The PDMS microfluidic device is fabricated by standard photolithography of a silicon wafer followed by soft lithography. The reverse patterned silicon wafer is silanized for PDMS release. PDMS Sylgard 184 (Dow Corning, Midland, MI) is poured up to create a 2 mm film in height onto a previously silanized Si wafer mold, degassed in a vacuum chamber for 30 minutes, and then heat cross-linked overnight at 70 °C. The cured PDMS film is peeled from the mold followed by punching through-holes. Oxygen plasma (Plasmatic Systems Inc., North Brunswick, NJ) is used for bonding PDMS to PDMS layers. The plasma treatment is performed on the PDMS surfaces for 60 seconds at 1 torr and 150-Watt power. The detailed configuration will be further introduced in the next section.

2.4 Experiment configurations: syringe-pump-driven gradient versus static diffuser

2.4.1 Syringe-pump-driven configuration

As shown in Fig. 2.6 (A), in the syringe-pump-driven configuration, the device is composed of 3 layers of PDMS: the bottom micro-structured layer, the middle reservoir layer, and the top cap layer. The tri-layered PDMS-based device cultures and

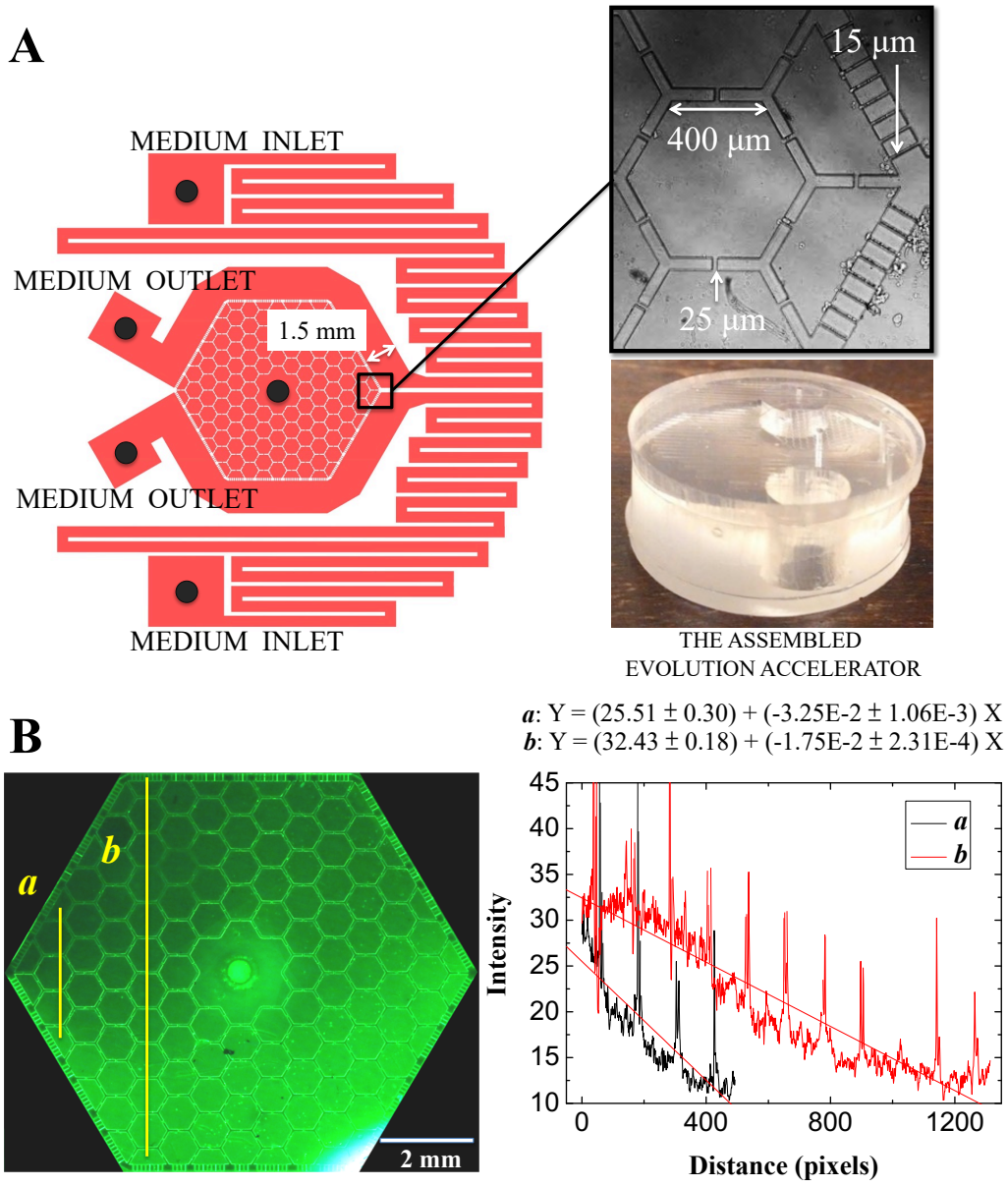

Figure 2.6: **The syringe-pump-driven configuration.** (A) The microfluidic device has two separate medium inlets, two outlets, and one central port for cell seeding or extraction of excessive medium. Note that between the medium inlets and the cell culture arrays, a pair of serpentine channels that allow the medium equilibrate with the atmosphere passed below the gas-permeable membrane. (B) The generation of gradient. The syringes pump the medium with $\sim$ 0.1 mM of fluorescein and no fluorescein respectively into the chip through the 2 medium inlets on the right, extracted out from the chip at the 2 medium outlets on the left. The concentration of fluorescein is proportional to the intensity of fluorescence signal, and is profiled near the medium inlets/outlets **a** and near the center **b**.

encapsulates cells at the bottom micro-structured level within 109 interconnected hexagonal and 24 half-hexagonal chambers in the center. The floor of the lowest level of the PDMS device upon which the cells move is a 35mm diameter hydrophilic 20 micron thick Lumox gas permeable film (Sarstedt, D 51588 Nmbrecht, Germany). Two coupled pairs of syringes with different concentration of chemicals, e.g. drugs, nutrients or cytokines, pump differing chemicals into the external flow channels. The chemicals advect and diffuse into the hexagonal chambers through the 15 micron wide and 180 microns long slits between the periphery channels and the hexagonal array. The slit width dimensions were chosen to provide hydrodynamic resistance and hence reduce advective fluid flow into the interior of the hexagonal array, since too much flow can cause cell detachment.

Each PDMS device requires four 10 mL BD Luer-Lok^{TM} tip syringes loaded onto the syringe pump and individually connected to a 50 cm Tygon microbore tube by a Luer lock 23G dispensing needle into one hollow steel pin (NE-1300-01 / 0.025 OD 0.017 ID x 0.500 long / New England Small Tube, Litchfield, NH) inserted into the PDMS chip. Sterile medium was pre-warmed at 37 °C and then degassed for 20 minutes in a vacuum chamber. A pair of syringes were loaded with desired growth media according to the cell types, while the other pair of syringes contain the same growth medium formula with chemical of interest. Two 10mL syringes per chip were fully loaded in sterile conditions with the adequate media and placed in the infusion deck of the pump while other two were placed empty in the withdraw deck. The normoxia ambient gas composition (20% O_2, 5% CO_2 and 75% N_2) with $>$ 80% humidity was provided by the homemade gas supply unit. The conditioned atmosphere was then led into 3 individual gas channels in the sample wells and vented through gas outlet channels. The flow rate of normoxia gas can be regulated by the gas valves and the gauge pressure maintained at 0.2 psi (1.4×10^4 Pa) to push the

membrane against the PDMS hexagonal array. The medium flow rate around the array was set at 20 μL/hr.

The generation of a complex gradient is demonstrated in Fig. 2.6(B), where one input syringe contain $\sim$ 0.1 mM of fluorescein while the other input syringe is free of the dye fluorescein. The gradient near the medium inlets/outlets (as shown in the line profile *a* in Fig. 2.6 (B)) can be twice as large as the gradient near the center (as shown in the line profile *b*).

There are several significant advantages of the syringe-pump-driven configuration. First, the boundary conditions are strictly fixed by the biochemical contents in the source media. Secondly, the setup allows for time-dependent gradient generation with ease. Considering that cancer is an open complex dynamic system governed by variations in blood-flow-generated heterogeneity, although it is out of the scope of this thesis, the ability to create time-varying stress gradient may be a crucial features in future perspectives.

2.4.2 Static diffuser configuration

In spite of the previous described advantage, the syringe-pump-driven configuration still has considerable limitations in research for several reasons. (i) The experimental setup is a complicated and labor-intensive process. It takes months of training to be proficient in conducting an experiment. (ii) The need of active pressure source such as a syringe-pump limits the experiment throughput.

Therefore, we designed the microfluidic device which also constructs cancer cell metapopulations and a stress landscape, yet does not requires syringe pump as an active media source. Instead, this new device, the "static diffuser," generates a stable chemical gradient through diffusion between an on-chip pre-filled reservoir and the outer media buffer. The outer media buffer is contained in a cell cultureware such as a Lumox dish, which requires media buffer replenishment every other day.

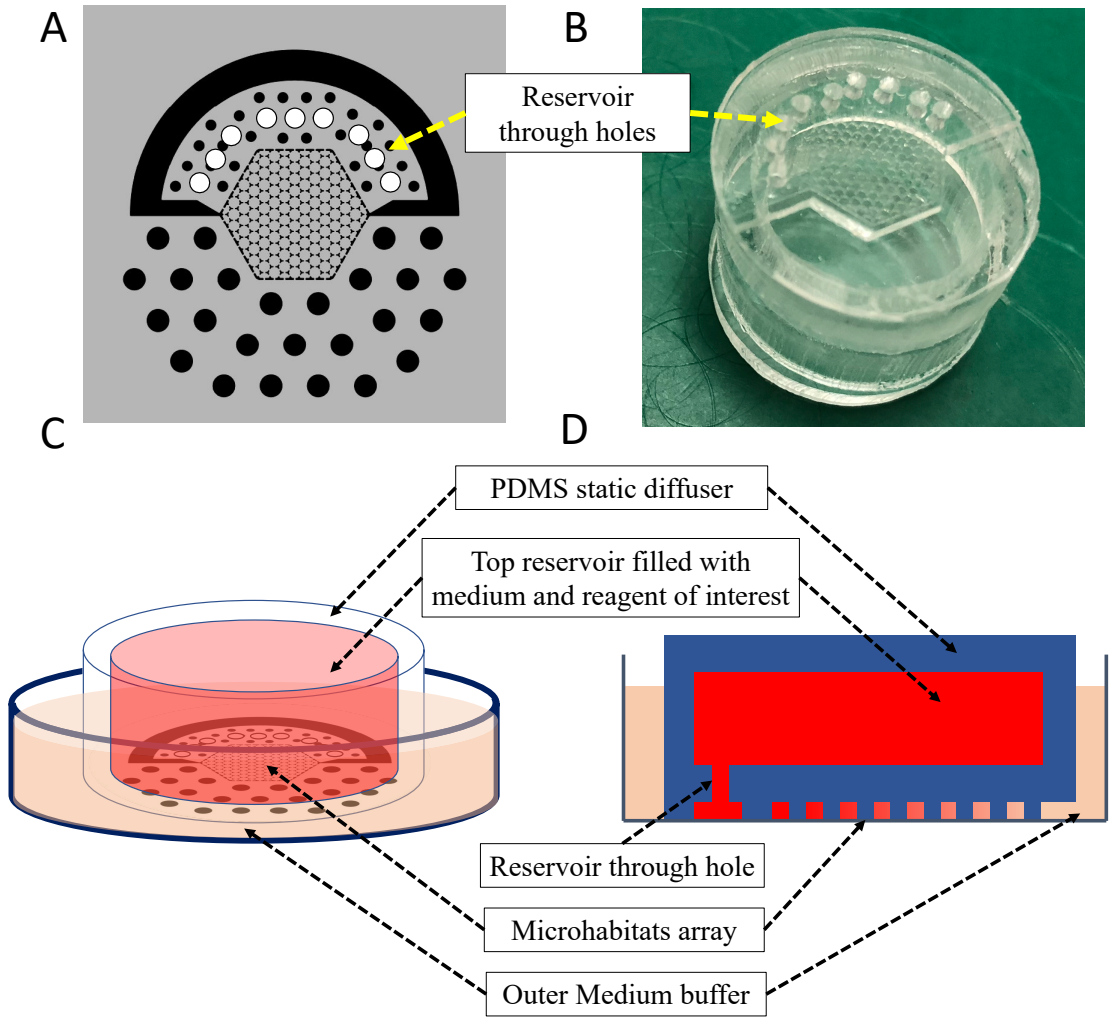

Figure 2.7: **The design of static diffuser.** (A) The design of hexagonal microhabitat array. The black structures illustrate the walls that enclose the cells and the posts that support the device. The white circles are through-holes connected to the top media reservoir. The side of each hexagonal microhabitat is 400 μm and the diameter of the entire chip is 21 mm. (B) The picture of the assembled PDMS static diffuser. (C)(D) The illustration of how gradients are generated in (C) 3D and (D) cross-section view. The media in the top reservoir (red) and in the outer buffer (orange) contain different concentrations of reagents of interest. Reagents diffuse across the hexagonal microhabitat array and generate 2D gradients within the cell culture region. Because there is no additional opening in the top reservoir, regardless of the height of outer buffer media level, there is no fluid advection in the device.

Without the bulky peripheral equipment for an active media source, the experimental setup is greatly simplified and allows high-throughput experimentation. Tens, if not hundreds, of experiments could be done simultaneously, which enables numerous potential applications such as parallel experimentation for time-resolved downstream cellular assays, high-throughput drug screening, *ex vivo* modeling and prediction for patient-specific treatment, etc.

As shown in Fig.2.7, the device consists of two compartments, the 2 mL on-chip medium reservoir and a PDMS chip with 107 interconnected hexagonal and 24 half-hexagonal chambers. The reservoir is pre-filled with medium. To initiate the experiment, one simply holds the chip upside-down and cap it on top of the cell culture membrane and filled with normal growth medium. The reagent of interest diffuses into the hexagonal cell culture region via the through-holes on the reservoir, and eventually diffuses out from the hexagonal array through the slits on the periphery of the PDMS chip and becomes diluted. Media in the outer region can be replenished by pipetting. The chip holding mechanics is the same as syringe-pump-driven configuration: pressurized Lumox membrane being sealed against the chip, holding by customized 6-well plate.

The COMSOL Multiphysics® simulation demonstrates the distribution of reagent concentration and magnitude of diffusion flux in the static diffuser at the steady state (Fig. 2.8). The diffusion coefficient is 10^{-9} m^2/s and the boundary condition is set as 10 nM. We consider two scenarios. (1) The 10 nM reagent diffuses out from the top reservoir, into the hexagonal array, and then diluted at the open boundary at the bottom. (2) The 10 nM reagent is added in the outer region, diffuses into the hexagonal array, and then diluted in the 2 mL on-chip top reservoir. The results of these 2 cases, as presented in Fig. 2.8 (A)(B) and (C)(D), are symmetrical. The line profile of diffusion flux magnitude around the chip boundary is plotted in 2.8 (E). The total loss of reagent, which is equal to the integral of total diffusion flux over time

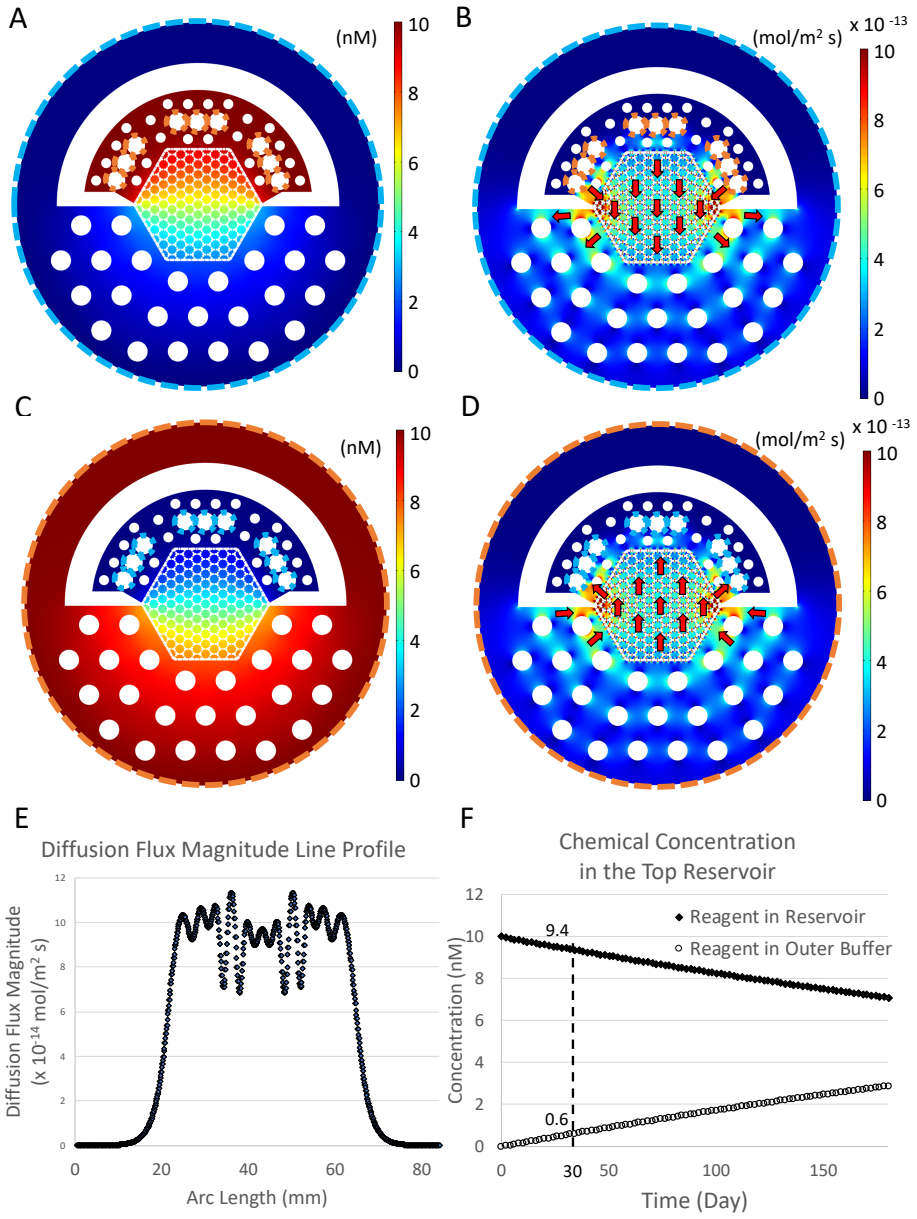

Figure 2.8: **COMSOL Multiphysics® simulation of the static diffuser.** (A)(B) The simulation of reagent concentration distribution and magnitude of diffusion flux in the case when the reagent diffuses out from the top reservoir. The reagent diffuses from the three square through-holes on the top, into the hexagonal array, and then diluted at the open boundary at the bottom. (C)(D) The simulation of reagent concentration distribution and magnitude of diffusion flux in the case when the reagent diffuses into the cell culture array from the outer region. (E) The line profile of magnitude of diffusion flux around the chip boundary. (F) The concentration of reagent in the top reservoir as a function of time. Within the period of 30 days, the concentration of reagent in the top reservoir changes only 6% by simulation, which is tolerable in many experiments.

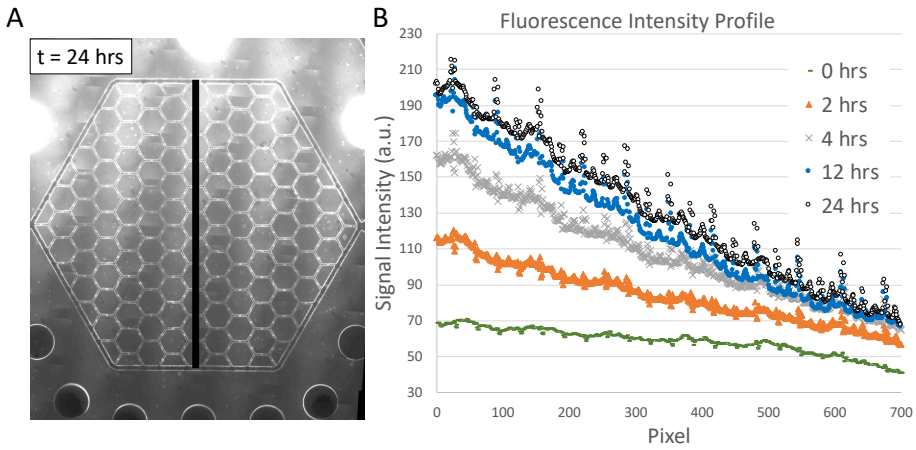

Figure 2.9: **The fluorescein gradient test for static diffuser.** The static diffuser was filled up with 0.1 mM of fluorescein. The fluorescein diffuses from the reservoir above the chip through 3 large holes at the top of the image into the outer channel (the region outside the top half of the arrray), and then through slits in the thin wall bewteen the central array and the outer media buffer region. After about 24 hours, the gradient pattern was stabilized. (A) The fluorescent images of the static diffuser taken at 24 hours after installation. (B) The line profile of fluorescent signal intensity as marked in image A.

and surface area, is negligible compared with the total amount of reagent inside the reservoir. The dissipation of reagent per second equals 4.4 x 10^{-19} mol/s while the total amount of reagent in the reservoir equals 2 x 10^{-11} mol. As demonstrated in 2.8 (F), the amount of dissipated reagent is negligible within the period of an experiment. The concentration of reagent in the top reservoir changes only 6% in 30 days, which is tolerable in many practical experiment purposes.

Compared with flow-driven gradient generators, the static diffusion mechanism requires a longer time to establish desired concentration pattern. In order to measure the timescale of gradient generation, we performed a fluorescein gradient test for static diffuser. The static diffuser was filled up with 0.1 mM of fluorescein. To block the background fluorescent signal from the fluorescein in the top reservoir, we used black PDMS chip made by mixing black dye into the PDMS elastomer during the curing process. The fluorescent intensity profile across the device is plotted in Fig. 2.9. The

gradient of fluorescent intensity, which is proportional to the gradient of fluorescein, increased monotonically and reached equilibrium at around 24 hours after device installation.

In conclusion, we may assume the concentration of reagent stays constant on the boundary. The lack of an active source (pump) guarantees a bubble-free fluid and static fluid dynamics, which ensures stable chemical gradient across the chip. Most importantly, this pump-free configuration allows multiple experiments to be conducted at the same time and therefore allows for the exploration of much wider parameter space.

In Chapter 3 and Chapter 4, the syringe-pump-driven EA is implemented to study how human prostate cancer cells react to chemotherapy gradient, while the static diffuser is tested in Chapter 5 to observe the dynamics of human bone marrow stromal cells and bone-metastatic prostate cancer cells across chemotherapy gradients.

Chapter 3

A proof-of-principle study: Epithelial and Mesenchymal Prostate Cancer Cell Population Dynamics on a Complex Drug Landscape in the Microfluidic Cell Culture Device

In this chapter, as a proof-of-principle, we present the aforementioned engineered microenvironment and cell culturing platform which allows for the quantitative study of the interactions of multiple cell types at a cell by cell resolution in response to neighboring cells and their local microenvironment over a period of several weeks. The resulting massive database presents a detailed image of cancer cell dynamics in the presence of a chemotherapy gradient.

We performed continuous observations of different cancer cell lines and carried out downstream analysis of cell phenotype as a function of position on the stress landscape. We used this technology to probe adaption and evolution dynamics in prostate cancer cell metapopulations under a stress landscape of a chemotherapeutic drug (docetaxel). The utility of this approach is highlighted by analysis of heterogenous prostate cancer cell motility changes as a function of position in the stress landscape. Because the technology presented here is easily adapted to a standard epifluorescence microscope, it has the potential for broad application in preclinical drug development and assays of likely drug efficacy.

The results and figures presented in this chapter were published in Convergent Science Physical Oncology [33]. Our collaborators at Johns Hopkins Medical Institute, Prof. Kenneth Pienta and Dr. Gonzalo Torga, provided much the cancer implications insight. The preliminary result of mass spectrometry presented in Section 3.5 were done in a collaboration with Prof. Joshua Rabinowitz and Riley Skeen-Gaar at Princeton.

3.1 Motive

The epithelial to mesenchymal transition (EMT) of cancer cells is thought to play a significant role in invasion and metastasis and is associated with resistance to chemotherapy [34]. Visualizing and tracking the emergence of EMT in a tumor cell population is a major goal in cancer cell biology. Utilizing the technology platform we have discussed above we sought simulate a tumor tissue with both epithelial (PC3-EPI) and mesenchymal (PC3-EMT) phenotypes experiencing a chemotherapy stress gradient. We observed and analyzed the behaviors of cells individually and collectively, recording how they respond to chemotherapy and develop drug resistance in real time.

The human prostate cancer line PC3, originally established from a patient with bone metastasis, was obtained from the American Type Culture Collection (ATCC, Manassas, VA). PC3-EPI and PC3-EMT cells were generated in Prof. Kenneth Pienta's lab as previously described by Roca *et al.* [35]. PC3-EPI is a E-cadherin/CDH1 positive / vimentin negative PC3 clone and PC3-EMT is its M2 macrophage-induced mesenchymal derivative that has a E-cadherin negative / vimentin positive phenotype.. All cells were routinely maintained in RPMI 1640 (Gibco, Grand Island, NY) supplemented with 10% fetal bovine serum (Sigma-Aldrich, St. Louise, MI) and 1X Anti-anti (Gibco, Grand Island, NY) at 37 ^{o}C in a humidified atmosphere containing 5% CO2.

3.2 Control experiment of cell growth and motility measurement without the presence of external stress

3.2.1 Validation of optimum cell growth on chip

The major goal of our experiment platform is to reproduce key components and interactions in a complex tumor microenvironment in a comprehensive manner, yet simple enough to provide quantitative, reliable and reproducible data. This goal can only be achieved if we have full control of the physical and biochemical environmental factors. We must either exclude the undesired factors or figure out a way to incorporate the uncontrollable factors into the quantitative model to interpret the population behaviors correctly.

The first test is to ensure optimum cell growth on the device. The cell proliferation rate on the device needs to be identical or comparable to their growth profile in conventional cultureware.

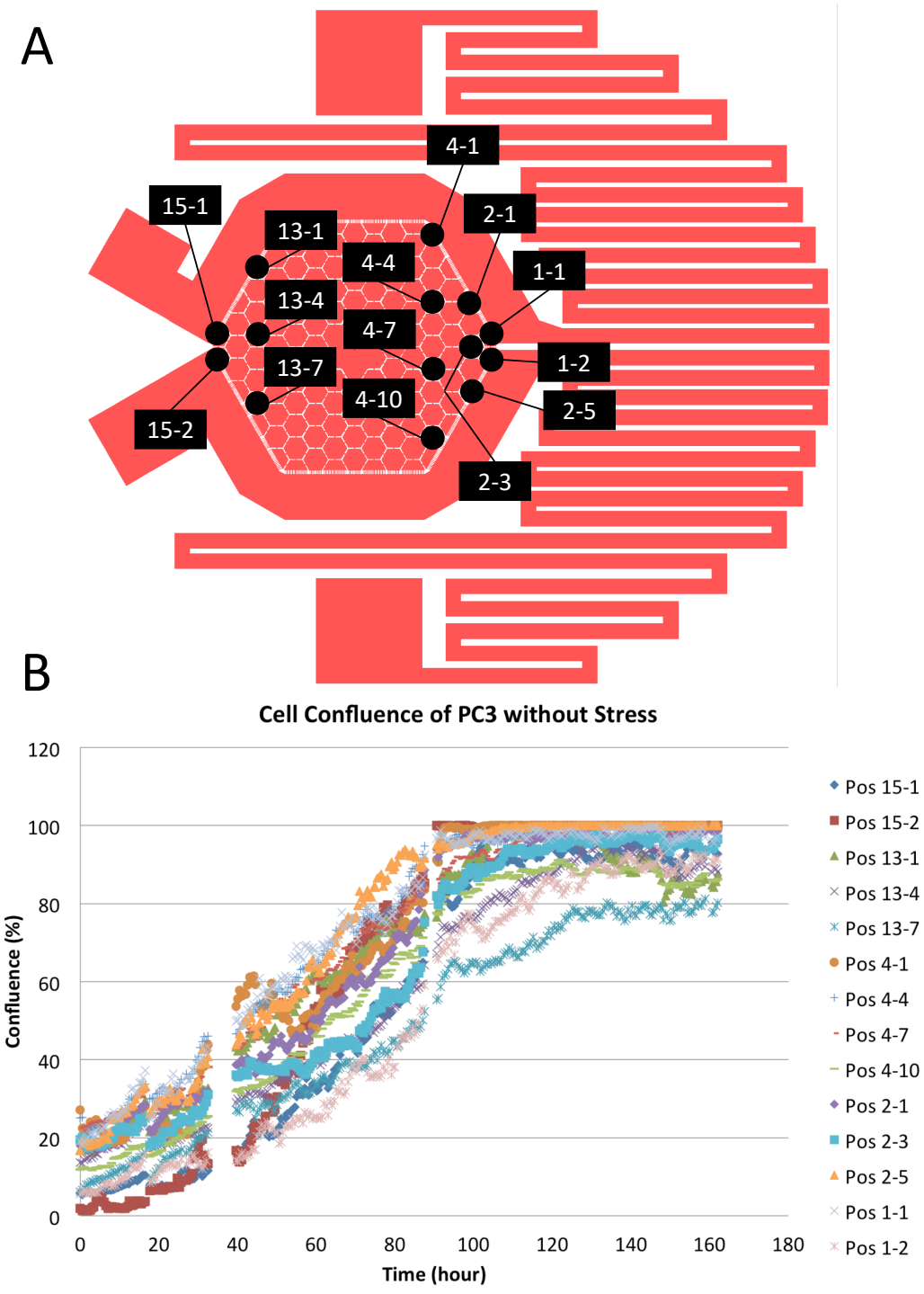

Figure 3.1: **Growth curves of PC3 in the EA without stress.** PC3 were cultured in EA without the presence of external stress. (A) The pattern of EA with position labels. (B) The growth curves of PC3 at the chosen positions in terms of cell confluence.

PC3 cells were cultured in EA without the presence of external stress. These cells were fluorescent-labeled in the cytoplasm so one could observe and quantify the population of cells using inverted fluorescent microscopy. Cells confluence, defined as the area that is covered by cells, was measured at each microhabitat at different time frames given a selected intensity threshold on the fluorescent images using Fiji.[36] The growth curves of cells at each chosen position are plotted in Fig. 3.1. The chosen positions scattered across the chip, from region near the apex of media inflow to the apex close to media outlets.

The growth curves in Fig. 3.1 (B) are well-aligned, suggesting the identicality of cell proliferation profile as a function of position across the chip. The initial slope of curves reveals the proliferation rate. The doubling time for cells in the device is around 24 hours as shown in Fig. 3.1 (B) from time 0 to 24 hrs, which is the same as the doubling time in conventional cultureware. Therefore, we may conclude that without the presence of external source of stress, the physical and biochemical factors are uniformly distributed, leading to the homogeneous and optimized cell growth from time 50 to 100 hrs.

We further considered the ability to quantify cell dynamics between sub-populations in a microenvironment. GFP-expressing PC3-EMT and the mCherry-expressing PC3-EPI cell lines were co-cultured in the EA as shown in Fig. 3.2.

Cell confluence, defined as the percentage of area covered by the cells, is measured as the indication of the size of population. Starting from 40% confluence, the co-culture grew fully confluent within 3 days. Interestingly, we may observe the progression of each phenotype in the microenvironment. While the growth curve of total confluence is in the form of logistic growth model, the population of PC3-EMT continued to expand and PC3-EPI was suppressed in the asymptotic phase.

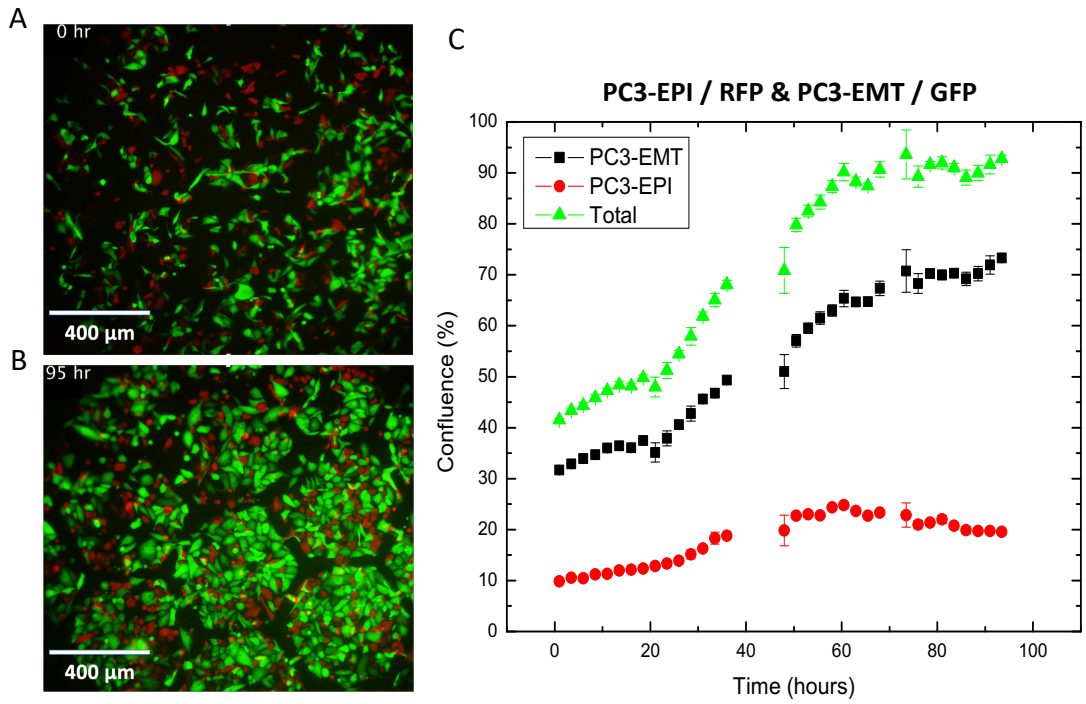

Figure 3.2: **The co-culture of PC3-EPI and PC3-EMT in the EA without stress.** PC3-EPI (red) and PC3-EMT (green) were co-cultured in the EA without the presence of external stress. (A) The overlay of two fluorescent channels at t=0. (B) The fluorescent image taken at t=95 hrs. (C) The growth curves in terms of cell confluence.

3.2.2 Demonstration of cell motility assay in a mixed population

Cell motility is an important phenotypic behavior of cell. The motility distribution of a population can provide information about the physical interaction of cells, the mechanical properties of local microenvironment, and can sometimes be analyzed as the indication of epigenetic variation of cells. Given that our improved cell culture platform allows nearly continuous imaging, the advantage of having fine temporal resolution maximizes the potential of single cell tracking in a heterogeneous population.

We use the plugin TrackMate[37] in Fiji (http://fiji.sc) with customized macro to implement and automate the tracking process. TrackMate allows user to implement

and customize tracking algorithm using a scripting language from the Fiji Script Editor. The tracking process is divided in a series of steps, the segmentation, filtering, and particle-linking processes. Tracking results can be immediately visualized on TrackMate GUI. Each step of tracking process is described as follows.

As shown in Fig. 3.3 A, each individual cell is detected using Laplacian of Gaussian (LoG) segmentation. Given an input image $f(x, y)$, this image is convolved by a Gaussian kernel $g(x, y, t)$ at a certain scale t, which gives the scale space representation $L(x, y, ; t)$. Applying the Laplacian operator to $L(x, y, ; t)$ gives $F(x, y, ; t)$ with strong negative responses for bright blobs of radius $\sqrt{2t}$.

$$g(x, y, t) = \frac{1}{2\pi t} e^{-\frac{x^2+y^2}{2t}} \tag{3.1}$$

$$L(x, y; t) = g(x, y, t) * f(x, y) \tag{3.2}$$

$$\nabla^2 L(x, y; t) = F(x, y; t) \tag{3.3}$$

Given a set of estimated blob diameter and threshold value, the locations of each cells are recorded at each time frame. Sequentially, a particle-linking algorithm, Linear Assignment Problem (LAP), is chosen to track the motion of cells across each time step.

As shown in Fig. 3.3 B, we performed a "wound healing assay" as a demonstration to study cell collective migration and cell-cell interaction. PC3-EPI and PC3-EMT cells were densely seeded in the center of the device and were allowed to freely migrate toward empty region. The normalized histogram of speed of both phenotypes is plotted in Fig. 3.3 C. The velocity of PC3-EMT is significantly higher than PC3-EPI by a factor of 1.8x, which is consistent with the fact that mesenchymal phenotype serves as a component of cutaneous wound healing with exceptional ability to migrate as opposed to the comparably stationary epithelial phenotype.

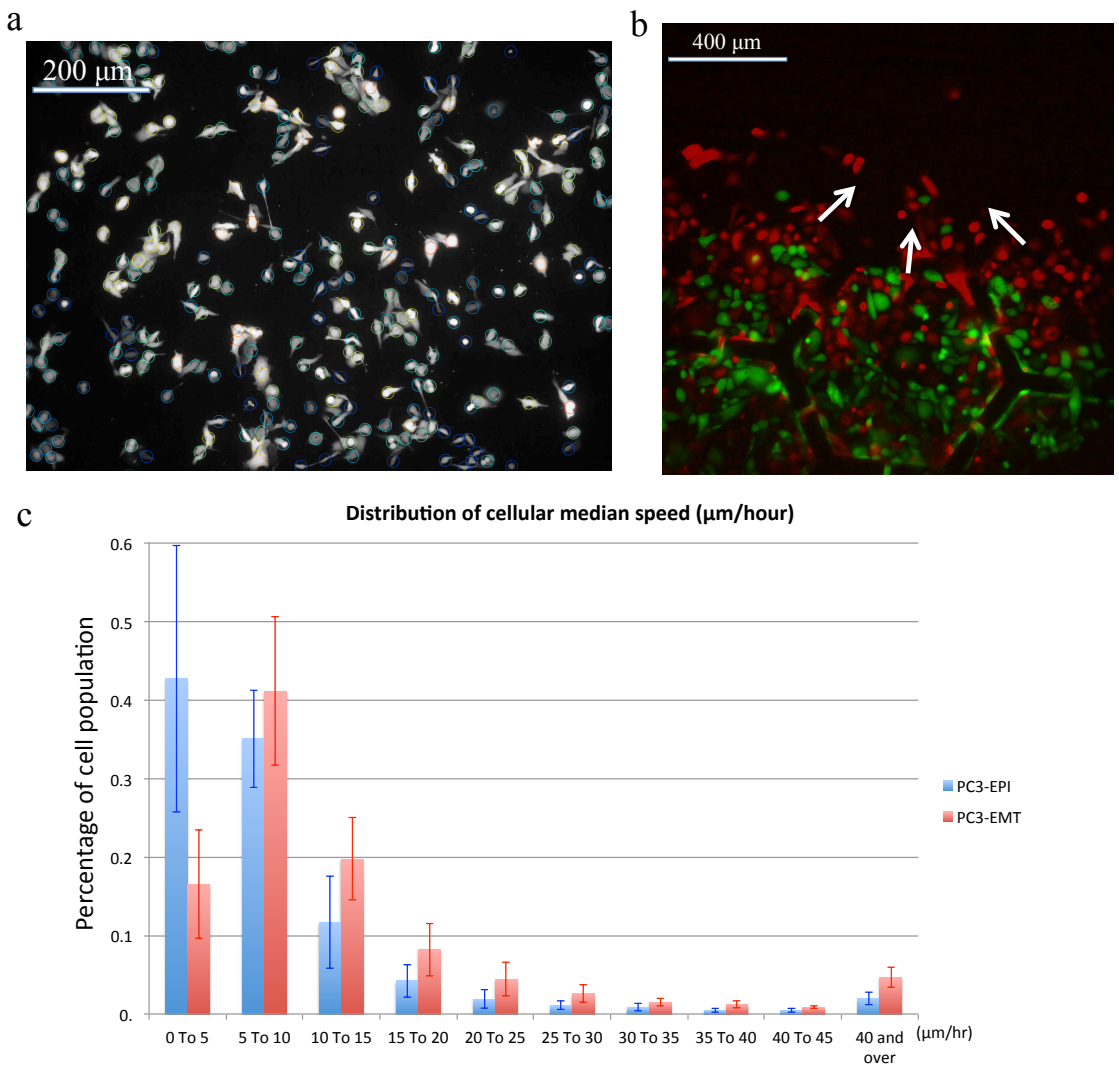

Figure 3.3: **Cell motility assay in a mixed population.** The demonstration of single cell tracking performance in a mixed population. (A) Cell detection by Laplacian of Gaussian (LoG) segmentation. The detected cells are linked from frame to frame based on the linear assignment problem. (B) The "wound healing assay" of PC3-EPI and PC3-EMT co-culture experiment. (C) The normalized histogram of cell motility. PC3-EMT is faster than PC3-EPI by a factor of 1.8x.

Further, in order to observe the progression of cell motility in a stress-free environment, we performed a long-term co-culture of PC3-EPI and PC3-EMT with uniform initial seeding density, and tracked the distribution of cell velocity varying with time. As shown in the Fig. 3.4 (A)(B), after 6 days of culture, as cells reached higher confluence, the distributions of cell speed for both phenotypes leaned toward the left tails.

We may compare the ratio of number of PC3-EPI to PC3-EMT in each class interval. As shown in Fig. 3.4 (C), regardless of the days of culture or density of cells, PC3-EMT dominated the high speed region while PC3-EPI occupied the low speed zone. Although the overall velocity decreased significantly for both phenotypes, PC3-EMT remained motile and were affected less by the crowdedness of the microenvironment as shown in Fig. 3.4 (D). The average speed of PC3-EPI dropped around 40 % while that of PC3-EMT only dropped 14%.

In conclusion, there are several factors that can affect the distribution of cell velocity and the average speed, such as the crowdedness of the population. Continuous cell tracking and monitoring over all subpopulation is essential to understand the progression of phenotypic behavior. For example, if we would like to quantify the level of mesenchymal status of an unlabeled subpopulation, it would be more informative to acquire not only the distribution of the physical quantity (e.g. velocity) of the interested subpopulation as a function of time, but also that of all the rest of the coexisting subpopulation of cells.

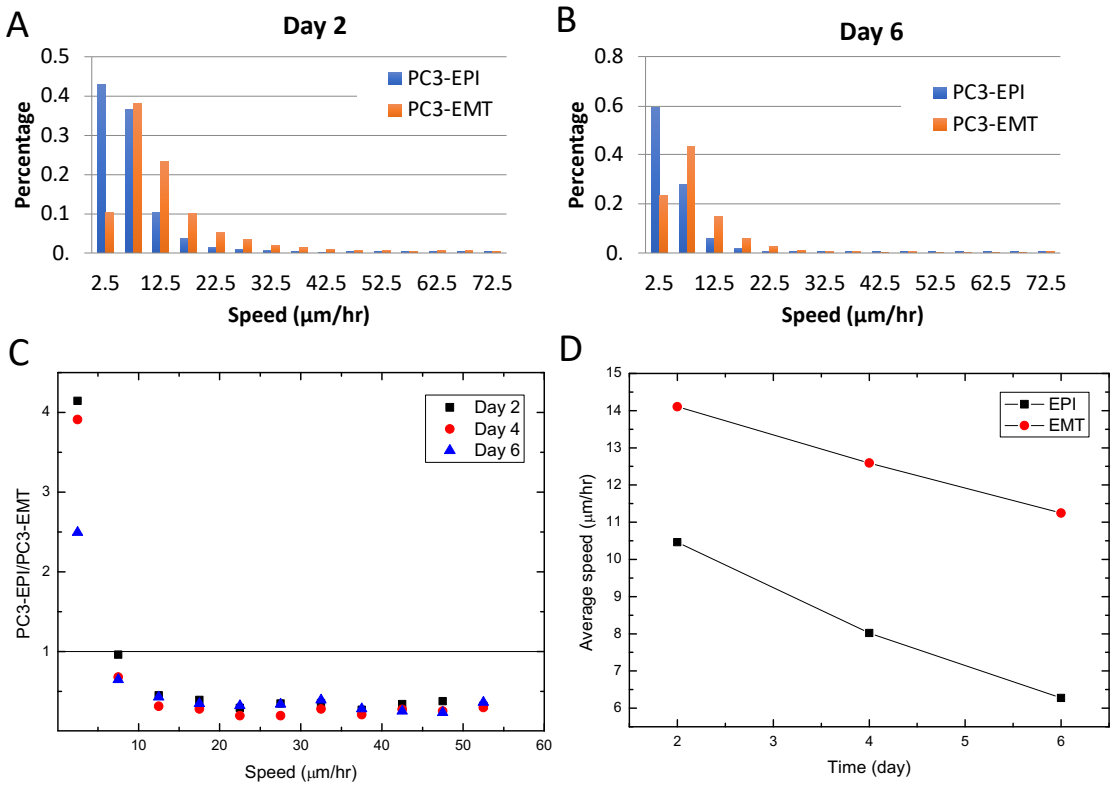

Figure 3.4: **The motility assay of a long-term co-culture of PC3-EPI and PC3-EMT.** A long-term co-culture of PC3-EPI and PC3-EMT with uniform initial seeding density. The distribution of cell velocity varies with time. (A) The normalized distribution of cell speed on day 2. (B) The normalized distribution of cell speed on day 6. (C) The ratio of number of PC3-EPI to PC3-EMT in each class interval. (D) The average speed of PC3-EPI and PC3-EMT as a function of time.

3.3 Population dynamics of epithelial and mesenchymal prostate cancer cell in chemotherapeutic gradient

The preliminary experiment presented here shows the potential of this technology. GFP-expressing PC3-EMT and the mCherry-expressing PC3-EPI cell lines were co-cultured in the presence of a 10 nM docetaxel gradient along 3 edges of the array as shown in Fig. 3.5 A. 10 nM of docetaxel is a extremely high dosage for prastate

cancer cell line PC3, as the half maximal inhibitory concentration (IC50) of docetaxel for PC3 is only 0.60 nM[38] following 72-hour drug exposure.

In the first 100 hours, both cell lines died out at the bottom, while the cells in lower-drug region continued to proliferate. A sharp boundary of cells was formed between the living cells and a region cleared of living cells. However, after 150 hours, the population started to expand and reached the high drug concentration zone where the cells had initially died out. At the end of the experiment, the cells almost occupied the entire chip, inclding the highest drug levels, with a striking patchiness of different cell origins, that is, large red and green clumps (see Fig. 3.5 A, 405 hours). This may represent a building of niche construction in the complex ecology.

The dynamics of the emergence of drug resistance is demonstrated in Fig. 3.5 where the population of cells at the PC3-EMT-rich plaque and the PC3-EPI-rich plaque was quantified in terms of cell confluency. At both PC3-EMT-rich region (Fig. 3.5 B and C) and PC3-EPI-rich region (Fig. 3.5 D and E), PC3-EMT cells died out in the first 100 hours, while the PC3-EPI cells died out within 50 hours. The microhabitats around the periphery were cleared out due to chemotherapy induced cell death, and then refilled by chemotherapy resistant cells in sequence from the lower dosage region into higher dosage region due to collective migration and cell population expansion starting from roughly 200 hours.

The re-emergence of cancer cells at high docetaxel concentration is a evidence of the acquisition of chemotherapy resistance within 10 days. This result mimics the rapid emergence of doxorubicin resistance of multiple myeloma [39] and U87 glioblastoma cells [40] in other related microfluidic devices. Image stacks with high spatial and temporal resolution can be acquired in both fluorescence and bright field channels. The population dynamics of different cell lines can be investigated at a global point of view, while most importantly the behavior of each individual cell was being tracked and monitored throughout the span of the experiment. Events

including cell division, cell fusion, cell migration, and changes in cell morphology and cell motility are studied at cellular level in real time, and the quantitative analysis of those parameters can be made with respect to different spatial or phenotypic division, providing greater perspective to approach the dynamics in a complex ecology with a heterogenous fitness landscape.

3.4 The distribution of cell motility as a function of time and space

Previous work [41] demonstrated PC3-EMT cells inherently migrate faster than PC3-EPI cells with respect to accumulated distance in control conditions. With this experiment we probed our ability not only to quantify that different motility phenotype simultaneously for both sub-populations, but also to determine how the given motility distribution changes for each sub-group over time in the presence of a docetaxel gradient.

One of the key elements to be observed is the migration and proliferation of both epithelial and mesenchymal cells after the rapid fixation in the metapopulation under stress. Time-lapse microscopy was performed daily for 41 fields per chip every 30 minutes. Accumulated distance was analyzed using Fiji software (`http://fiji.sc`) with plugins including Manual Tracking, Chemotaxis and Migration Tool Version, and TrackMate. The result of cell motility and migration in a population consisting of two different sub-clones of PC3 cells is presented in Fig. 3.6 . With the tracking algorithm, we obtain the velocity of each cell in each time frame. Usually the variance-to-mean ratio of the speed of a single cell is smaller than 1, so we picked the median speed of a single cell as a representative quantity, and took an average of those median speed of cells in each microhabitat.

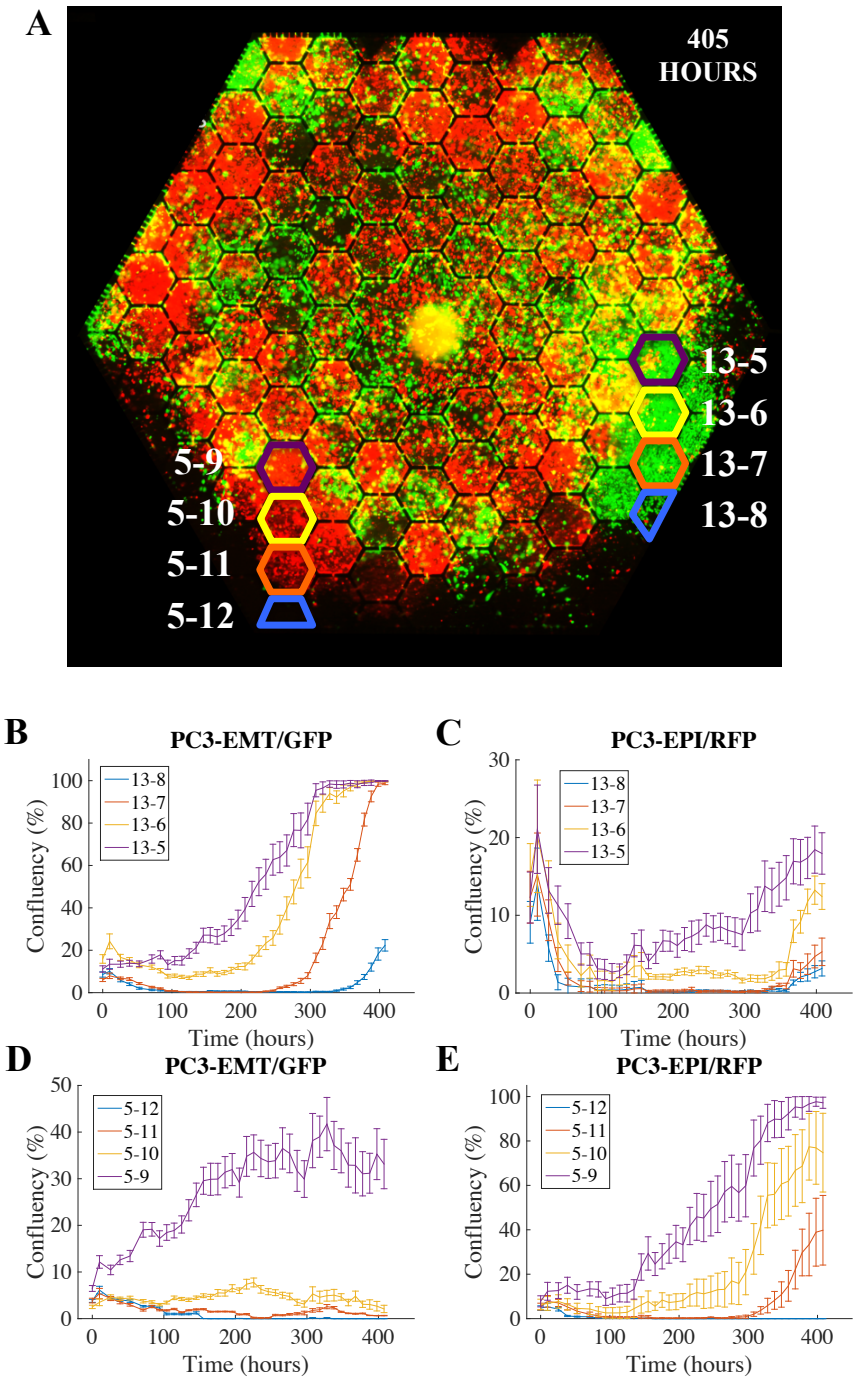

Figure 3.5: **Density of PC3-EMT (green cells) and PC3-EPI (red cells) as a function of time at high docetaxel region.** (A) The rule of labeling. Micro-habitat $i-j$ corresponds to the j^{th} hexagon in column i. (B)-(E)The confluency of PC3-EMT and PC3-EPI at the high docetaxel region. The curves show the dynamics of the cells dying out in beginning and the re-emergence of the cells in terms of the variation of population.

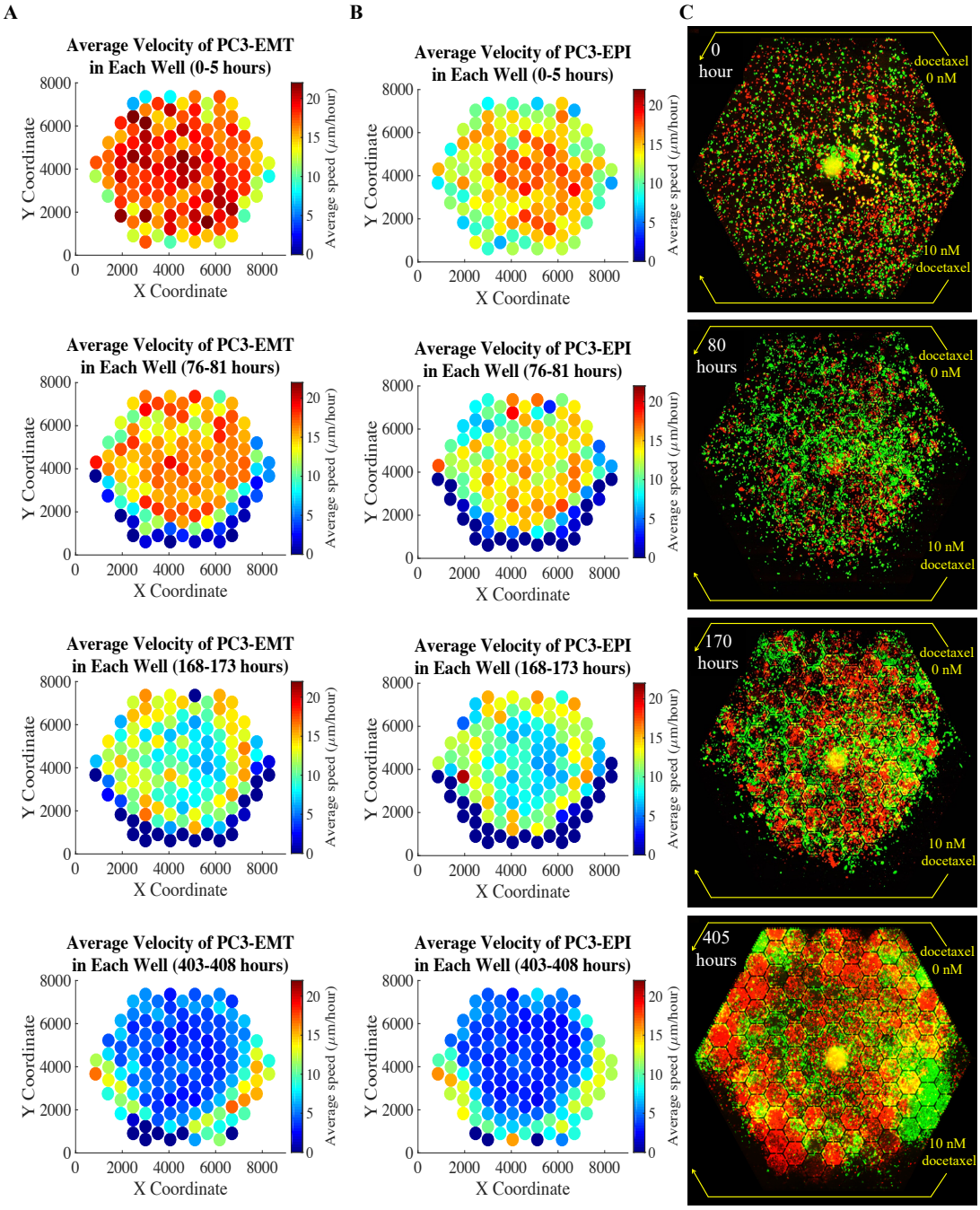

Figure 3.6: **The distribution of velocities and populations of PC3-EPI (red cells) and PC3-EMT (green cells) in the complex ecology with docetaxel gradient.** The experiment was done under the existence of docetaxel gradient across the chip, from 10 nM at the bottom three edges to 0 nM at the top three edges. The distribution of the averaged speed of (A) PC3-EMT and (B) PC3-EPI in each micro-habitat is illustrated as the 2D color-scaled graph. (C) The red and green fluorescent images were taken respectively with 10X objective, stitched and displayed together to show a global view of the distribution of the two cell lines at different time points.

The spatial distribution of the averaged speed of PC3-EMT and PC3-EPI at different time point is illustrated in Fig. 3.6 A and B with corresponding fluorescent images listed in column C. The cell tracking analysis provides further insight into the composition of a subpopulation and their phenotypic expression as a function of time and space. The cellular response to the environmental stress gradient can be monitored in real time in terms of cell morphology and motility. PC3-EMT, a mesenchymal subclone of PC3 cells, tends to be more motile than the epithelial phenotype PC3-EPI roughly by a factor of 2, in accordance with the cell motility previously reported by Shiraishi *et al* [41]. Both the motility of PC3-EMT and PC3-EPI were uniformly distributed in the beginning. As cells at high-drug region died out, the speed decreased at the edges. When the cells proliferated and aggregated to a higher degree of confluency, the cells started to slow down. After the emergence of docetaxel resistance, both PC3-EPI and PC3-EMT cells moved towards the high-drug region, generating a sharp wavefront of cell migration into the high drug regions.

The process observed on our microfluidic system, from cell growth, chemotherapy induced cell death, cell migration, to cancer relapse, is a *in vitro* demonstration of the development of drug resistance and relapse of a metastatic cancer in a patient during chemotherapy treatment. The initial chemotherapy induced cell death corresponds to the early phase of chemotherapy treatment, when the cancer population remains sensitive to the drug. Sequentially, drug resistance emerges in the cancer population, which may be acquired as a cellular response to drug exposure, or be inherent in a subpopulation of heterogeneous cancer cells. Eventually, resistant cancer cells expand and migrate to adjacent microenvironments, followed by cancer relapse and metastasis. Our microfluidic system allows for the direct observation of the aforementioned process, which offers a suitable *in vitro* platform to study the underlying mechanism of drug resistance and cancer metastasis.

Interestingly, during the experiments, we have observe a morphological transformation of PC3-EPI in the resistant population, which may be an indication of epithelial-to-mesenchymal transition (EMT) among resistant PC3-EPI cells. We have also observed the emergence of multinucleated cells within the resistant population. These observations inspire the work presented in the next chapter.

3.5 Downstream experiment capacity: mass spectrometry

Although it is a feature we have not fully explored, the thin Lumox window allows sampling of the cells or metabolic fluid locally on the device with a micro-translation stage and NanoFil syringe pump(World Precision Instruments, Sarasota, FL 34240). As demonstrated in Fig. 3.7 (A), the syringe carries 36 G blunt needle, penetrating through the 20 μm-thick Lumox membrane, extracting as small as 50 to 100 nL medium from the chip. The preliminary result is presented in Fig. 3.7 (B), where the relative concentration of metabolites can be measured for further investigation. We may also harvest, subculture and sequence the cells from specific locations and compare the genetic contents and evolution dynamics of cells under different level of environmental stress.

This capability of removing cells from specific locations in a heterogenous culture is a major advance compared to earlier devices, where the sealing surface to a chip had to be removed before one could access the culture. [39] Further, even in that case, the act of removing the cover significantly disturbed the culture so that local testing of cells on a single to few habitat level was not possible. Such localized extraction was possible in our case due to the soft "resealable" nature of the Lumox membrane.

A

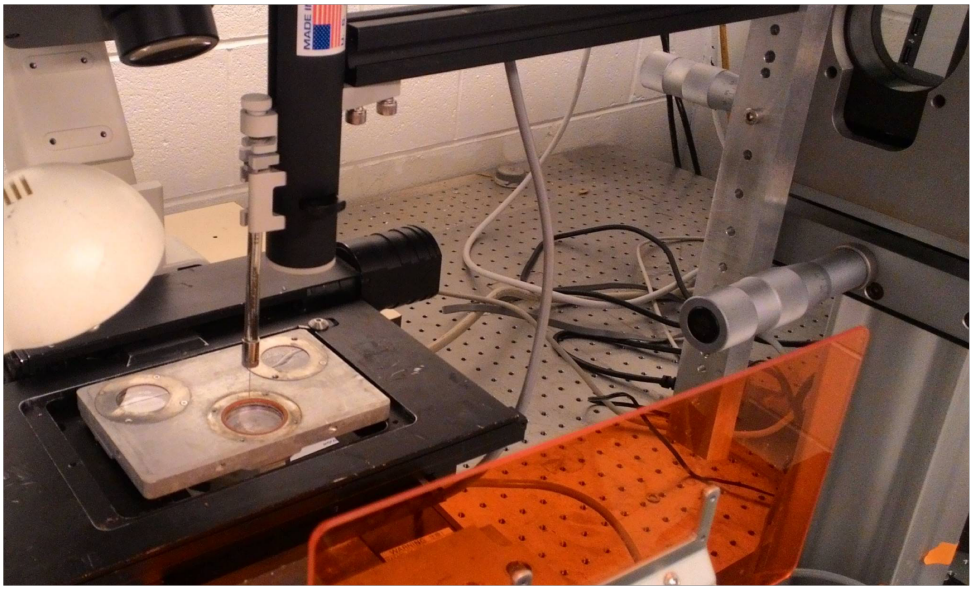

B

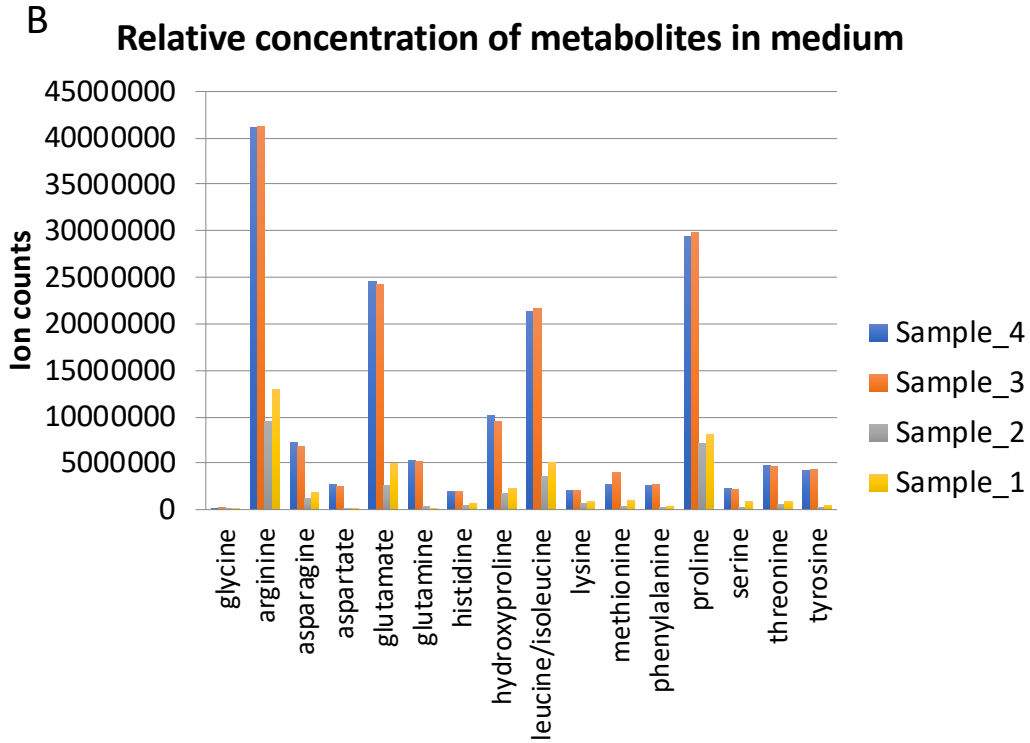

Figure 3.7: **Mass spectrometry of metabolic fluid.**(A) The experiment platform for downstream media extraction for mass spectrometry. (B) The abundance of metabolites at 4 randomly chosen positions in the EA, measured by mass spectrometry.

Chapter 4

The Application of Microfluidic Cell Culture Device: Investigating the Role of Emerging Polyploid Giant Cancer Cells as the Reservoir of Chemotherapeutic Stress from an Ecological Perspective

The ability of a population of PC3 prostate epithelial cancer cells to become resistant to docetaxel therapy and progress to a mesenchymal state remains a fundamental problem. The progression towards resistance is difficult to directly study in heterogeneous ecological environments such as tumors. In this chapter, we use our microfabricated "evolution accelerator" environment to create a complex heterogeneous yet

controllable *in vitro* environment with a spatially-varying drug concentration. With such a structure we observe the rapid emergence of a surprisingly large number of polyploid giant cancer cells (PGCCs) in regions of very high drug concentration, which does not occur in conventional cell culture of uniform concentration. This emergence of PGCCs in a high drug environment is due to migration of diploid epithelial cells from regions of low drug concentration, where they proliferate, to regions of high drug concentration, where they rapidly convert to PGCCs. Such a mechanism can only occur in spatially-varying rather than homogeneous environments.

Further, we also observe an epithelial to mesenchymal transition (EMT) of the polyploid giant cancer cells in the same high-drug regions where they are formed. This is consistent with prior work suggesting the PGCC cells are mediators of resistance in response to chemotherapeutic stress. Taken together, this work shows the key role of spatial heterogeneity and the migration of proliferative diploid cells to form PGCCs as a survival strategy for the cancer population, with implications for new therapies.

The results and figures presented in this chapter were published in Clinical and Experimental Metastasis [42]. Our collaborators at Johns Hopkins Medical Institute, Prof. Kenneth Pienta and Dr. Gonzalo Torga, provided much the cancer implications insight. Dr. Gonzalo Torga did much of the work in the downstream immunofluorescence and RT-qPCR assays. Prof. Robert Axelrod provided valuable mathematical insight. Yusha Sun at Princeton was involved in the discussion.

4.1 Review: polyploid giant cancer cells (PGCCs) and cancer stem cells

Polyploid giant cancer cells (PGCCs) are typically multi-nucleated or have an enlarged nucleus containing multiple sets of chromosomes in comparison to most of the cells comprising the bulk of the tumor. Clinical studies have shown that PGCCs,

morphologically-distinct cancer cells commonly observed in tumor biopsies [43], correlate with poor response to docetaxel chemotherapy in the context of castration-resistant prostate cancer [44].

There are multiple ways PGCCs can form: PGCCs can emerge from what would seem to be dead-end loss of function events such as abrogated mitotic checkpoint, cell fusion [45], failed cytokinesis [46], and DNA endoreduplication [47]. Particularly, fusion between cancer cells and normal cells, or among cancer cells themselves, has also been suspected to contribute to phenotypic evolution during different stages of cancer progression and metastasis [48].

It has been demonstrated that dual metastasis organotropisms can be achieved in the same cell through spontaneous fusion between bone- and lung-tropic sublines of the MDA-MB-231 breast cancer cell line. [49] However, PGCCs have also been observed to emerge from high-stress environments such as severe genotoxic stress (gamma irradiation [50, 45]), chemotherapy treatment (*e.g.* bleomycin [47], docetaxel [51, 52], cisplatin [53]), and hypoxia conditions [54, 55, 56], revealing a more important role for PGCCs. Furthermore, there is evidence that these PGCCs possess tumorigenic potential: both the mitotic-catastrophe-evaded PGCCs and the progeny derived from PGCCs may have an increased survival advantage [44].

4.2 Motivation: the emergence of polyploid giant cancer cells from an ecological perspective

Because of the evidence that PGCCs posses tumorigenic potential, it is important to understand the conditions that lead to the emergence of PGGCs with chemotherapy [57]. *In vivo* animal models have proved difficult to control systematically. However, most *in vitro* cancer cell studies are either done in a well-mixed conventional cell culture setting with uniform drug concentrations which do not replicate the true

complexity of *in vivo* tumors, or from spheroids which are difficult to image at the single cell level. For instance, PGCC PC3 cells have been previously described to emerge when cultured in the presence of docetaxel in conventional culture [44], But the true dynamics of PGCC emergence from an ecological perspective under stress remain unobserved in the context of the highly complex heterogeneity of the tumor ecosystem.

We chose a monomorphic sub-line epithelial phenotype of a widely established human prostate cancer cell to lower the intrinsic heterogeneity in the initial cancer population and highlight the emergence of the mesenchymal phenotype under chemotherapy stress. The sub-line we chose is the epithelial prostate cancer sub-line PC3-Epi, an E-cadherin/CDH1-positive-vimentin-negative PC3 derivative described by Roca *et al.* [35]. PC3-Epi cells were genetically engineered with nuclear fluorescence markers to visualize chromatin. The mCherry-expressing PC3-Epi cell line was transfected with a H2B-GFP plasmid delivered by transfection reagent lipofectamine 2000 and selected with neomycin (G418). The H2B-GFP plasmid (Addgene plasmid # 11680) allows high-resolution imaging of chromatin without affecting cell cycle progression or the chromosomal architecture [58] Utilizing this H2B-GFP system, we are able to quantify the number of nuclei and area at the single-cell level, allowing us to study the dynamics in the emergence of polyploidy as a function of time and variable stress level across the EA ecology.

4.3 Results

There are two important results: 1) A drug gradient vastly increases the emergence of PGCCs at higher levels of docetaxel concentration and improves overall survival of cancer population, a phenomenon that cannot be understood using fixed drug concentrations in conventional static culture. 2) By downstream immunofluorescent

analysis, the PGCCs emerging at the highest docetaxel concentrations in a gradient landscape show higher expression levels of ZEB1, a mesenchymal biomarker that is associated with cancer invasiveness and metastatic potential.

The PC3-EPI cells were seeded uniformly before the application of the drug in all the experiments. Cells were seeded and incubated 12 hours before the installation of the PDMS microfluidic device by placing the array over the cells on the Lumox surface and pressurizing at 0.2 psi pressure from below with 5% CO_2 conditioned gas under normoxia conditions. Media with no drug flow was injected through the left 3 sides of the hexagonal array of the EA while media with drug flow was injected through the right 3 sides of the hexagonal array of EA (Fig. 4.1). After the establishment of a docetaxel gradient over a 24-hour period (defined as $t = 0$), time lapse video-microscopy scanning was performed every 30 minutes throughout the experiment to capture the dynamics of each individual cell in the array of the EA. After 17 days of cell culture, the microfluidic array was detached from the Lumox film and and cells adhered to the Lumox were fixed and permeabilized for downstream immunofluorescent (IF) analysis as discussed below.

Two control experiments were performed to examine the relevance of gradients and sequestered microhabitats with weak communication (migration) of cells between them: 1) A series of fixed drug concentrations in a series of conventional cell culture. These control experiments were performed in triplicate with the same PC3-EPI subcell line but seeded into a multiple-well plate with fixed docetaxel concentrations from 0 to 10 nM. The media was replenished on a daily basis in each well to maintain constant nutrients level and docetaxel concentration. 2) The EA experiment was repeated, but with single uniform drug concentration across the EA landscape (not spatially-varying). This was to check if there were some unusual features of the EA experimental environment compared to conventional static cell cultures (besides the

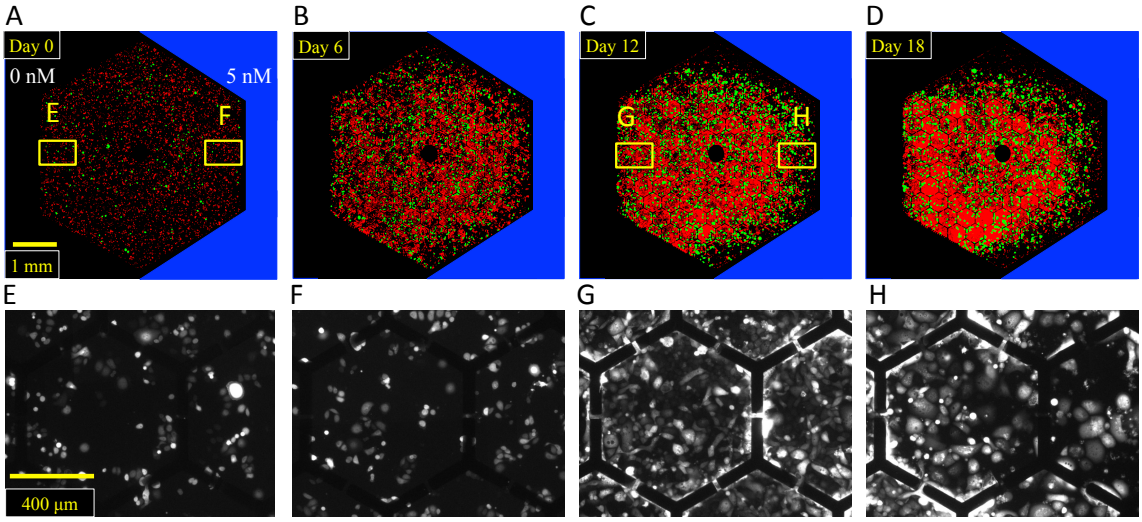

Figure 4.1: **PC3-EPI cultured in the EA in stress gradients (spatially-varying docetaxel concentration) (from 0 to 5 nM) for 18 days.**
Cells below 80 μm diameter are colored red and cells with diameter above 80 μm are colored green. Regions E and F at the 0 and 5 nM drug gradient at t=0 respectively are expanded, as are regions G and H at t=12 days. Note that at t=0, cells at low and high dosage region E and F had similar morphology and cell size, while at t=12, cells at high dosage region H had significantly larger size compared with cells at low dosage region G.

concentration gradient in the EA experiment described above). The results of the control experiment are discussion in Section 4.3.4 and shown in Fig 4.7 and Fig 4.8.

4.3.1 Emergence of PGCCs in complex docetaxel gradient

A docetaxel gradient ranging from 0 to 5 nM was established across the EA. Time-lapse video-microscopy using large-area image stitching was done throughout the span of the experiment. The concentration of docetaxel in each EA microhabitat was determined by a COMSOL Multiphysics® simulation. Fig. 4.1 presents the progression of the PC3-EPI cells in the EA versus time.

We developed a custom image processing macro on Fiji to track and pseudo-colorize the cells by mean diameter. Further details of the image processing method is described in Appendix B. The results of cell segmentation and categorization by size are shown in Fig. 4.1. Cells pseudo-colored green have diameters greater than

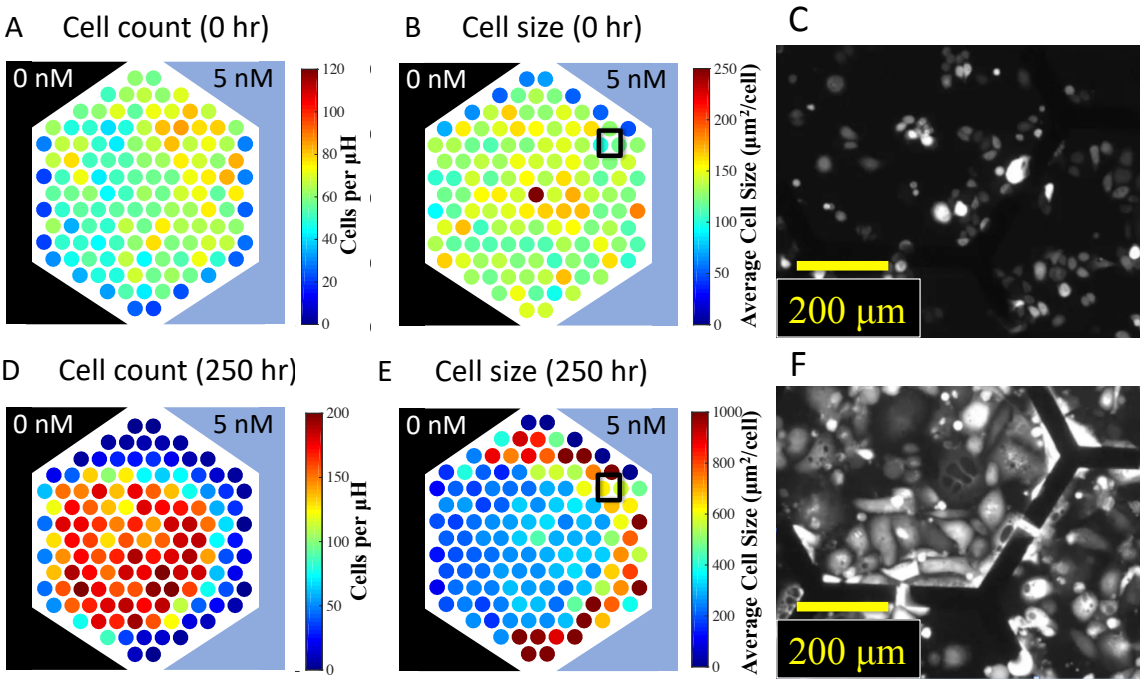

Figure 4.2: **The fluorescent (mCherry) images and the spatial distribution of cell number and average cell size in each microhabitat.** The experiment was done with PC3-EPI, with 0 drug boundary condition on the left 3 sides adn 5 nM docetaxel on the right 3 sides. In the beginning of the experiment, the cells were evenly distributed in terms of (A) cell number. The cell size (B) is rather uniform across the chip. After 250 hours, both (D) cell number dropped drastically around the edges with highest docetaxel concentration. (E) The average cell size is positively correlated with chemotherapy concentration. (C) The fluorescent images taken at 0 hour in high drug concentration region, as indicated in image B. (F) The fluorescent images taken at 250 hours in high drug concentration region, as indicated in image E.

80 μm; smaller cells are pseudo-colored red. The detection accuracy, defined as the ratio of number of detected large (green) cells to the number of "true" large cells counted manually, ranges from 75% to 90% depending on cell confluence. Fig. 4.2 shows the quantitative result of number of cells, average cell size of PC3-EPI in each microhabitats at t = 0 and t = 250 hours.

Before the application of chemotherapy, both the culture confluency and the number of cells in each microhabitats were relatively uniform. The average cell size was also identical across the device. After 250 hours of chemotherapy treatment, cells gradually died out around the edges with the highest dosage of docetaxel. However, there were still some extremely large cells that appeared and survived within the extreme environment at the high dosage areas. The distinct cell morphology and the increased number of GFP-labeled nuclei confirm the emerging large cells as PGCCs.

The large cells at the highest docetaxel concentrations had very distinct morphologies. The cell diameter had increased by an order of magnitude, from the ordinary 10 - 15 μm to 100 - 200 μm. Real-time single-cell characterization of nuclear dynamics was performed by simultaneous two-channel imaging of PC3-EPI cells co-expressing cytoplasmic mCherry protein and H2B-GFP labeled histones. Fig. 4.3 shows some examples of the heterogeneity of the mechanisms by which the original diploid PC3-EPI cells became PGCC cells. The mechanisms observed include failed cytokinesis, cell fusion, and cell engulfment. A near-continuous time-lapse scanning was done to ensure that the PGCCs did merge with the other cell during the cell fusion and cell engulfment process, instead of merely spatial overlap. These mechanisms have been previously observed among various type of cancers cells under high-stress environments such as severe genotoxic stress, chemotherapy treatments with different mechanism of actions, and hypoxia conditions. [45, 46, 47, 59, 60] The soft-condensed matter aspects of these dramatic cell fusion events is a subject that needs to be pursued [61].

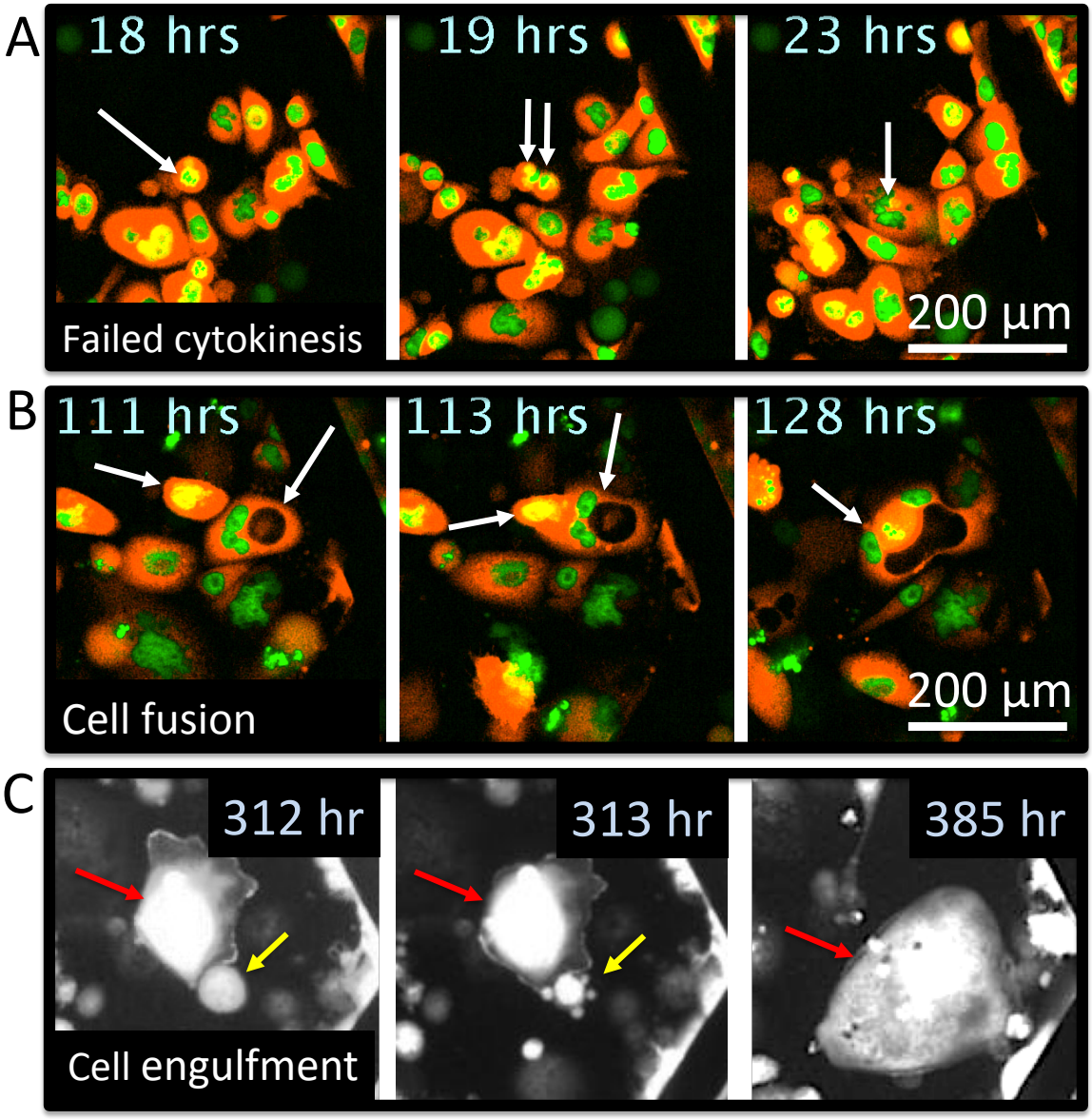

Figure 4.3: **Different mechanism of polyploidization process of cancer cells in docetaxel gradient.** The mCherry-expressing PC3-EPI cell line was transfected with H2B-GFP plasmid to visualize chro- matin. (A) Failed cytokinesis. A cancer cell at high dosage region attempted to divide but could not finish the mitosis process, ended up being polyploid. (B) Cell fusion. The two marked cells at high dosage region fused as one. (C) Cell engulfment. A PGCC (red arrow) approached and engulfed another cell (yellow arrow).

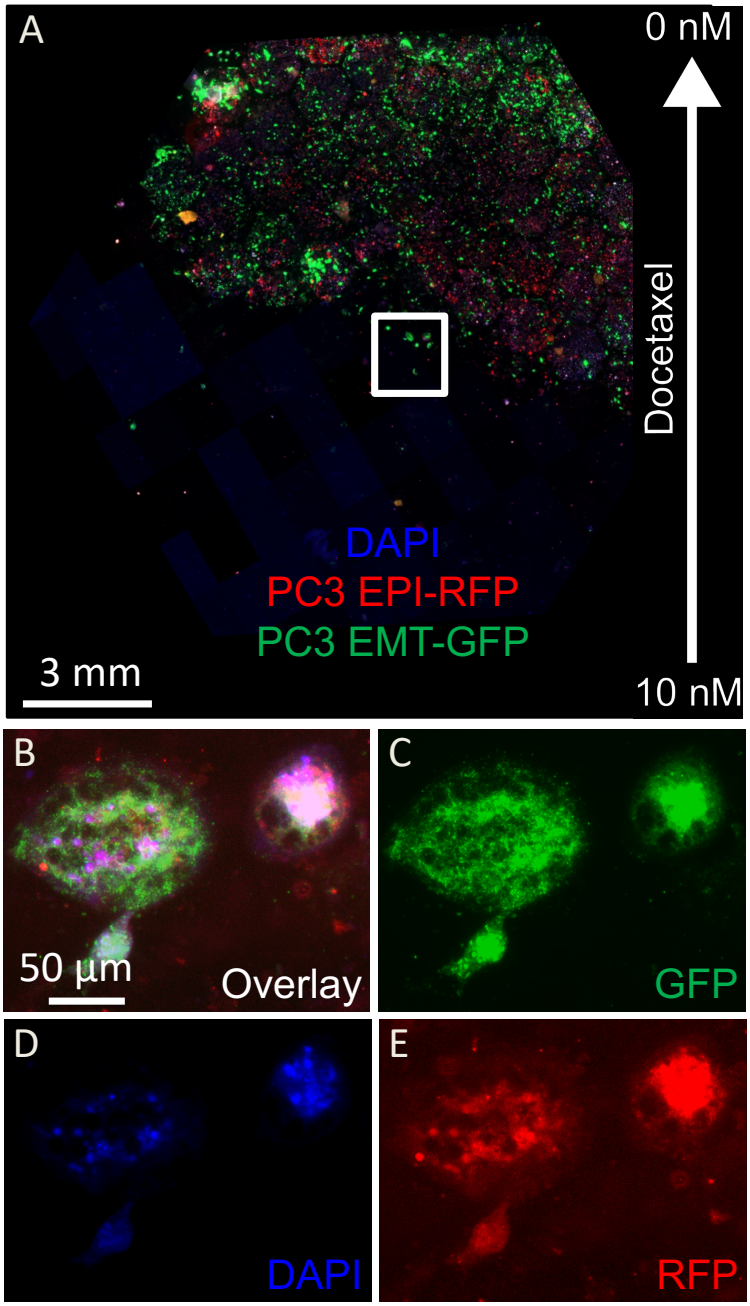

Figure 4.4: **Immunofluorescent (IF) staining of PC3-EPI(RFP) and PC3-EMT(GFP) co-cultured in docetaxel gradient for 20 days.** mCherry-expressing PC3-EPI cocultured with GFP-expressing PC3-EMT in docetaxel gradient. After 20 days, the microfluidic chip was removed and the cells were fixed and permeabilized for staining. A portion of PGCCs contained merged elements of PC3-EPI and PC3-EMT cells. (A) The overlay of GFP, RFP and DAPI channels of the entire chip. (B) The overlay of all three channels of the PGCCs as indicated in the square in A. (C) The GFP channel of B. (D) The DAPI channel of B. (E) The mCherry channel of B.

Cell fusion is not limited to individuals of the same phenotypes; fusion can occur amongst cells with different genetic or epigenetic content as well. We found the same heterokaryotic process in a co-culture experiment with the same docetaxel gradient of PC3-EPI and PC3-EMT. Some PGCCs contained merged elements of both epithelial and mesenchymal cells, as shown in Fig. 4.4, the downstream IF microscopy shows a portion of PGCCs contained merged elements of epithelial and mesenchymal cells and expressed green and red fluorescent protein simultaneously. This is a direct evidence indicating that cell fusion could occur among organisms with different genotypes or phenotypes, while preserving their original phenotypic behaviors as observed in other literature.[49, 62] These phenomenon suggests that the PGCCs have significant chromosomal instability and structural complexity that may increase their potential of phenotypic drifting in a fitness landscape, making them more adaptable and highly evolvable in response to stressful environments.[63, 64, 65]

4.3.2 Epithelial-mesenchymal transition (EMT) of PGCCs as a emergent cellular response

Most chemotherapeutic agents have been reported to induce EMT in the vast majority of solid cancers[66, 67, 68]. In order to probe the hypothesis that the emergence of PGCCs is a critical process in metastasis via the EMT process, we cultured PC3-EPI in the EA with a docetaxel gradient (from 0 to 5 nM) for 20 days and subsequently performed IF analysis to further characterize the expression level of ZEB1, a mesenchymal biomarker that is associated with cancer invasiveness and metastasis.

PC3-EPI is an established monomorphic cell sub-line without mesenchymal characteristics. After being exposed to docetaxel gradient for 20 days, there was a significant elevation of ZEB1 expression in the population, as shown in Fig. 4.5 (B). Each dot represents the average ZEB1 level of cells in the corresponding microhabitat. The

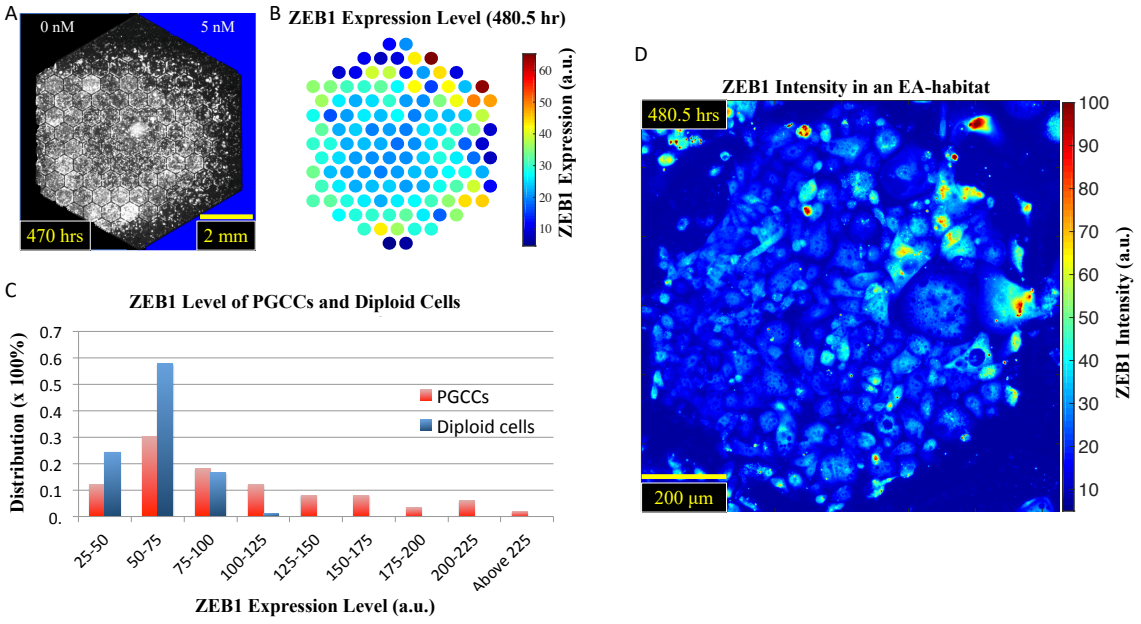

Figure 4.5: **ZEB1 expression level of PC3-EPI after being cultured in docetaxel gradient, from 0 to 5 nM, for 20 days.**
(A) The mCherry fluorescent image of the entire EA. (B) The heat-map of ZEB1 expression level across the device. Each dot represents the average ZEB1 level of cells in the corresponding EA. (C) The normalized histogram of ZEB1 level of PGCCs and diploid PC3-EPI cells showing the significant elevation of ZEB1 expression in PGCCs. (D) The color-mapped ZEB1 intensity in one EA element where PGCCs coexisted with diploid PC3-EPI cells. PGCCs stain more positively than diploid cells.

expression level increased significantly around and beyond the lethal high cytotoxicity boundary, similar to the PGCC distribution pattern demonstrated in Fig. 4.1.

Fig. 4.5 (C) shows that the ZEB1 level of PGCCs was increased compared with diploid cells. The fact that PGCCs have statistically significant mesenchymal biomarker expression compared with the diploid cells suggests that the PGCCs are equipped with greater phenotypic plasticity, conferring a superior adaptation potential in order to survive stressful environment. Our data show a great deal of heterogeneity within our EA, as would be expected in a tumor.

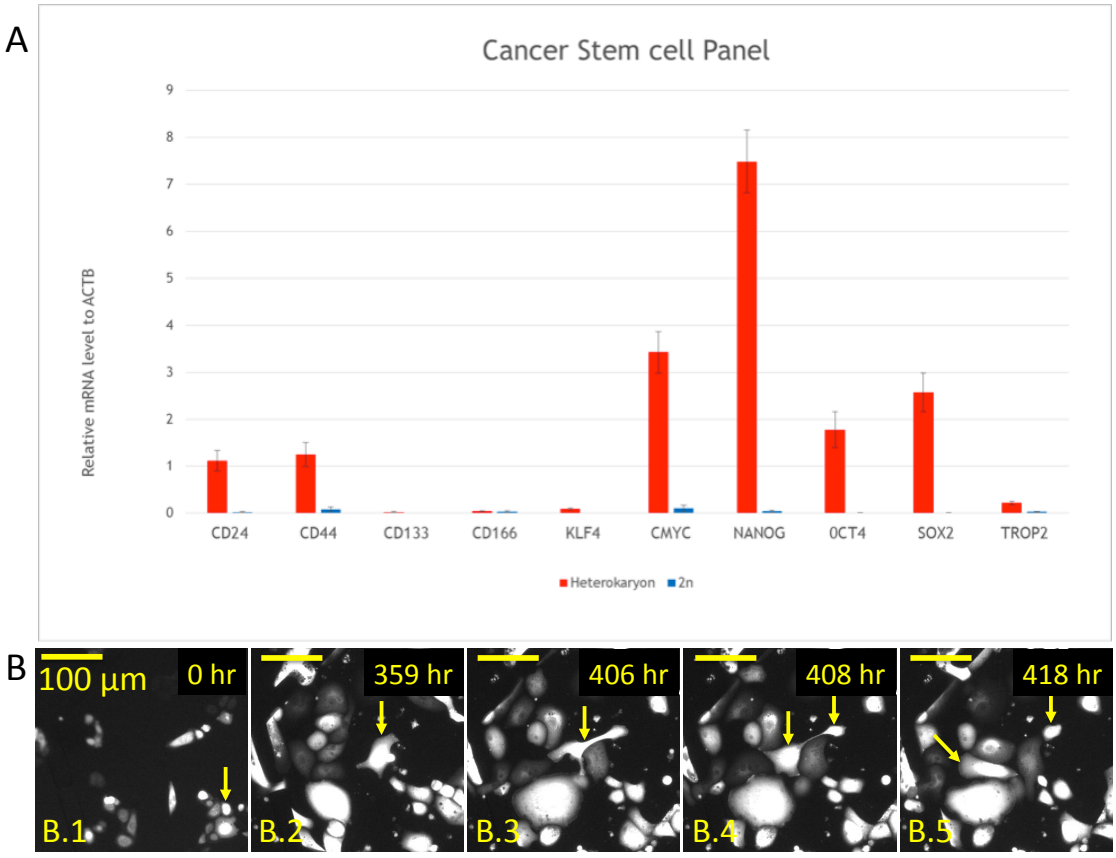

Figure 4.6: **The stem-like characteristics of PGCCs.** (A) A panel of relative mRNA level of stem cell biomarker in diploid cancer cells and in polyploid cells. (B) The neosis of PGCCs after the removal of docetaxel gradient. PC3-EPI cells were cultured under docetaxel gradient (0 to 10 nM) for 6 days, and then the docetaxel supply channel was switched to normal culture media so that the drug in the device was removed. The cell (marked by arrow in B.1) became polyploid (B.2) when exposed to docetaxel. After the removal of chemotherapeutic stress, the cell completed an asymmetric cell division (B.3 - B.5).

4.3.3 The stem-like characteristics of PGCCs

In addition to prolonged life time, better fitness advantage and higher phenotypic plasticity in chemotherapeutic stress, PGCCs are getting attention mostly due to their stem-like characteristics and tumorigenicity. [44, 69] To demonstrate the stem-like characteristics of PGCCs emerged in our microfluidic EA chips, two assays were performed: (1) the quantitative reverse transcription polymerase chain reaction (RT-qPCR) assay of a series of stem cell biomarkers including CD24, CD44, SOX2 and so on; (2) observing the tumorigenic potential of PGCCs treated by a time-dependent docetaxel therapy in the EA chip.

The result of RT-qPCR assays of diploid cells (the cancer population before docetaxel treatment) and PGCCs (after docetaxel treatment) is shown in Fig. 4.6 (A). A panel of cancer stem cell biomarkers has been made to compare the stemness of PGCCs with that of diploid cancer cells. The y-axis is the mRNA value of each stem cell biomarker over that of ACTB (actin beta) gene, which is commonly used to normalize RT-qPCR data.[70] The normalized stem cell biomarkers mRNA levels of PGCCs (red bars) are significantly higher than that of diploid cells (blue bars), suggesting that the PGCCs are metabolic active and share similar epigenetic characteristics with stem cells.

Secondly, the tumorigenic potential of PGCCs was also demonstrated *in vitro* in our experiments with the Evolution Accelerator chip. PC3-EPI cells were cultured under docetaxel gradient (0 to 10 nM) for 6 days, and subsequently the docetaxel supply channel was switched to normal culture media so that the drug in the habitats diffused back out to the outside channels and was then washed away. As shown in Fig. 4.6 (B), the diploid cell (B.1) indicated by yellow arrow became polyploid (B.2) after the docetaxel treatment. Around 406^{th} hour, the cell began the asymmetric cell division process (B.3, B.4) and successfully produced progeny.

Taken together, the two experimental results confirm that PGCCs indeed obtain stem-like properties and can undergo asymmetric cell division in regulating tumor heterogeneity. The functional behaviors of PGCCs observed in our EA chips are in accordance with that reported in other literature. [44]

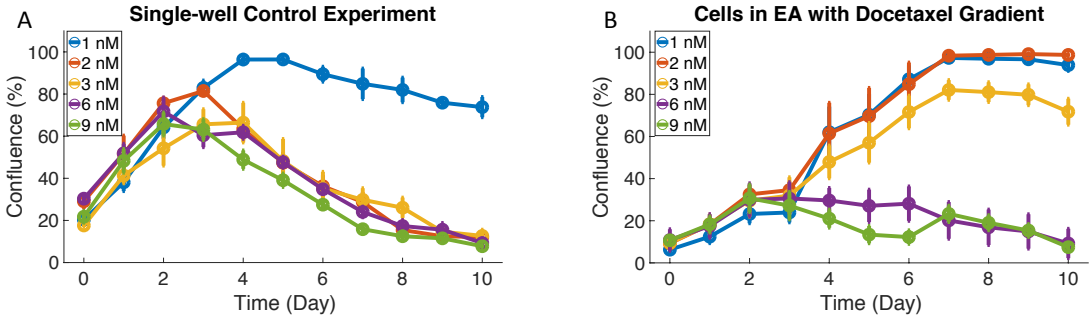

Figure 4.7: **The population dynamics of PC3 and PGCCs in the EA and isolated wells.**
(A) PC3-EPI cells were cultured in conventional single-well plates with different docetaxel concentrations. Growth media was replenished on a daily basis with assigned dosage of drug to maintain constant nutrients level and docetaxel concentration. The growth curves show the progression of PC3-EPI in terms of confluence in a well-mixed environment. (B) PC3-EPI were cultured in the presented microfluidic EA device with docetaxel gradient (0 to 10 nM). The progression of PC3-EPI was quantified by measuring the confluence of cells in each microhabitats as a function of time. Each microhabitat corresponds to a drug concentration determined by COMSOL Multiphysics® simulation. Note in single-well control, cell confluence dropped drastically at 2 nM docetaxel and higher dosage, while in EA experiment, cells remained highly confluent at 3 nM.

4.3.4 The transition in cell mortality in the docetaxel gradient

We now look inside the EA in detail and quantify cell populations as a function of the local drug concentration. Our results show that the number of PGCCs depends strongly on the existence of a gradient and not just the local value of the drug concentration. Three sets of experiments were performed and described as follows:

- An EA experiment was performed with 0-10 nM docetaxel to fully cover the cytotoxic response range of PC3-EPI cells. After seeding, the cells were incubated overnight (about 12 hrs) before the drug diffused in from one side of the array. In reporting of our data, "Day 0" is defined when the drug is first applied, not when the cells were seeded.

- Furthermore, a set of control experiments was performed with a series of fixed drug concentrations in a series of conventional cell culture. These control experiments were performed in triplicate with the same PC3-EPI sub-cell line but seeded into a multiple-well plate with fixed docetaxel concentrations from 0 to 10 nM. The media was replenished on a daily basis in each well to maintain constant nutrients level and docetaxel concentration.

- The EA experiment was repeated, but with single uniform drug concentration across the EA landscape. The purpose of this experiment was to check if there were some unusual feature of the EA experimental environment compared to conventional static cell cultures that could give rise to the phenomena we observed.

The growth of PC3-EPI cells in conventional single wells and in the EA is compared in Fig. 4.7 (A) (B). At the left edges of the EA where the drug concentration is 0 nM the cells reached and maintained 100% confluence. In regions of increasing docetaxel concentrations, the cell confluence was basically unchanged until a steep drop was observed in microhabitats with drug concentration from 3 to 6 nM. In the single-well control experiment by the 10^{th} day, the cell confluence decreased significantly at lower docetaxel concentrations of 2 nM.

To better visualize cell viability across docetaxel concentrations under both scenarios, the total cell confluence on the 10th day at different docetaxel concentrations is shown in Fig. 4.8 (A). Within each subpopulation, the density of PGCCs was

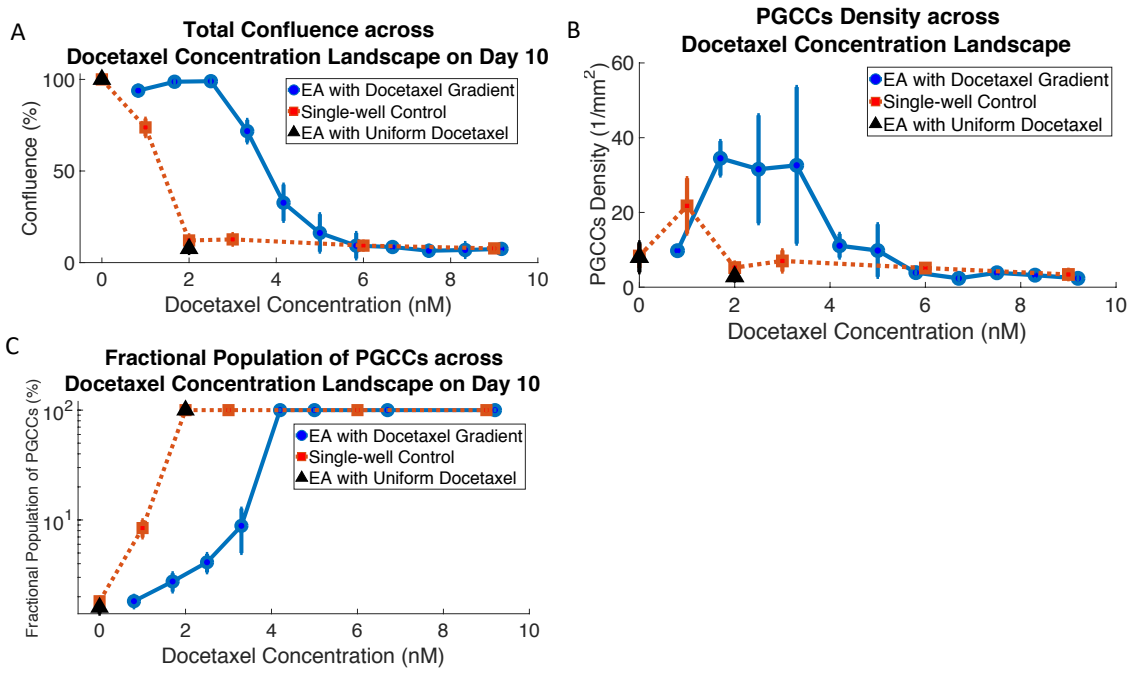

Figure 4.8: **Cell population versus docetaxel concentration on day 10.** (A) Total confluence. Compared with single-well control, in the EA with docetaxel gradient there were far more cells at higher docetaxel levels from 2 nM to 4 nM. (B) The density of PGCCs. Within the range of 2 nM to 4 nM docetaxel, the density of PGCCs increased by a large factor in the EA when with a drug gradient in comparison with the control conditions. (C) The fractional population of PGCCs. Within the region where PGCC density greatly increased, the fractional population of PGCCs was very low (10% or less), meaning there were an extremely large number of diploid cells. The coexistence of PGCCs and diploid cells could be correlated with elevated PGCC emergence. Under all scenarios, PGCCs were the only survivors at 4 nm and above.

quantified (Fig. 4.8 (B)), and the corresponding fractional population of PGCCs is shown in Fig. 4.8 (C).

As shown in Fig. 4.8 (A), the overall cell population boundary shifted positively by about 2 nM when the drug gradient was presented. The cell confluence profile of the EA gradient experiment shifted towards higher drug concentrations compared with control experiment - the population remained fully confluent until around 2 nM. This means that a large cell population was found with uniform drug concentration up to between 1 to 2 nM, with the EA a high population was observed at least to a habitat drug concentration of 3nM. Technically speaking, this doesn't necessarily

mean the cells were proliferating within this region, just that we observed living cells which may have migrated from elsewhere.

Compared with the control experiment, where the cells were cultured in conventional single-well with no docetaxel gradient, a striking result with respect to PGCCs was observed. The number of PGCCs per unit area was vastly enriched and more PGCCs resided in region with higher dosage of docetaxel (Fig. 4.8 (B)), revealing the importance of a gradient in PGCC emergence. Within the range of 2 nM to 4 nM docetaxel, the density of PGCCs increased by a remarkably large factor (from $\sim$4 $1/mm^2$ to $\sim$35 $1/mm^2$, nearly 10X) in the EA when with a drug gradient in comparison with both control conditions (the conventional single wells and the EA with uniform drug concentration).

For the control experiment, the fractional population of PGCCs without chemotherapeutic stress is 2%. At 1 nM, the fraction of PGCCs increased to 9%. Above 2 nM, the population was exclusively composed of PGCCs. In contrast, the fraction of PGCCs of the EA gradient experiment is significantly lower within the range of 1-3 nM docetaxel, which implies the coexistence of a large number of diploid cells (>300 $1/mm^2$) and PGCCs at 1-3 nM docetaxel. In contrast, in a conventional well plate, less than 1 $1/mm^2$ diploid cells survived after 10 days in 2 nM docetaxel.

In order to verify that the difference in population dynamics between the EA gradient experiment and the single-well control experiment was not due to technical artifacts associated with our cell culture platform, we performed a set of control experiments in the EA with uniform docetaxel dosage, 0 nM and 2 nM. As shown in Fig. 4.8, the result was in accordance with the single-well controls.

Therefore, two conclusions can be made: (1) The phenomena of increased survival of PC3-EPI population under high dosage are indeed the result of the heterogeneous environment (the stress gradient). (2) The surviving population exists mainly as polyploid cells.

4.3.5 Physical mechanism of polyploid cell generation: quantification of cancer population dynamics and cell migration

To identify the underlying mechanism of the increased polyploidization events in docetaxel gradient, it is necessary to quantify key parameters which regulate population dynamics. Here we modified the well-known logistic growth equation applied to both diploid and polyploidy cells by introducing the polyploid transformation term. We can fit the equation to data from single-well control experiments to determine the parameters. We also tracked cell motion and quantified the migration events that occurred in the EA with docetaxel gradient. The acquired parameters would then be used to described cancer population dynamics with and without cell migration factors as discussed in the Discussion section, revealing the fundamental role of cells migration over a stress gradient in tumor development.

First, we assume that the cancer population is composed of 2 interchangeable phenotypes, the diploid cancer cells (u) and the PGCCs (v). The cancer population is broken up into 11 subpopulations in a linear microhabitat array. Each subpopulation i is locally homogeneous and connected to the adjacent subpopulations $i-1$ and $i+1$. A docetaxel gradient (0 to 10 nM) is stably established across the microhabitat array so that the local docetaxel concentration within each subpopulation is $C_i = i - 1$ (nM). The local population dynamics of diploid cells (u_i) and PGCCs (v_i) in the subpopulation i can be described using a set of non-linear differential equations based on the logistic growth equation,

$$\begin{aligned} \frac{du_i}{dt} &= u_i(G_i - k_u(u_i + v_i) - T_i - D_{ui}) + M_{im,i} - M_{em,i}, \\ \frac{dv_i}{dt} &= u_i T_i + v_i(-k_v(u_i + v_i) - D_{vi}), \end{aligned} \tag{4.1}$$

The form of the equations are modified from a well-known model of population growth first published by Pierre Verhulst in 1845 and 1847, decribing the growth dynamics of a population with limited carrying capacity. Relevant mechanisms that we included in the model are:

(i) G_i is the proliferation rate of diploid cells as a function of drug concentration C_i.

(ii) T_i is the transformation rate from diploid to PGCCs as a function of drug concentration C_i. The transformation from PGCCs to diploid progeny was not observed within the time frame of the experiment and is therefore absent in the equation.

(iii) D_{ui} and D_{vi} are death rate of diploid cells and PGCCs, respectively, as a function of drug concentration C_i;

(vi) k_u and k_v are the cell capacity limiting constants of diploid cells and PGCCs, which are independent of the dosage of docetaxel.

(v) $M_{im,i}$ and $M_{em,i}$ are the amount of cell migration into / out of the subpopulation i. The mathematical form of $M_{im,i}$ and $M_{em,i}$ can be determined by experiment data.

Although PGCCs have been observed to be extremely deformable and can migrate through the slits, the migration probability is very low compared with diploid cells. Therefore we assume the migration of PGCCs to be zero. In addition, $u_i(G_i - k_u(u_i + v_i))$ is considered the density-dependent effective proliferation rate of diploid cells, while $u_i T_i - k_v v_i(u_i + v_i)$ is considered the effective PGCC emergence rate.

The aforementioned parameters G_i, T_i, D_{ui}, D_{vi}, k_u and k_v can be obtained by fitting the equations to single-well control data of diploid and PGCCs as a function of time in different docetaxel concentration. The migration terms were ignored in the single-well control experiment where no migration occurred. The number of diploid cells and PGCCs as a function of time measured in single-well control experiments were fitted using the minimum chi-square fitting method. As shown in Fig. 4.9,

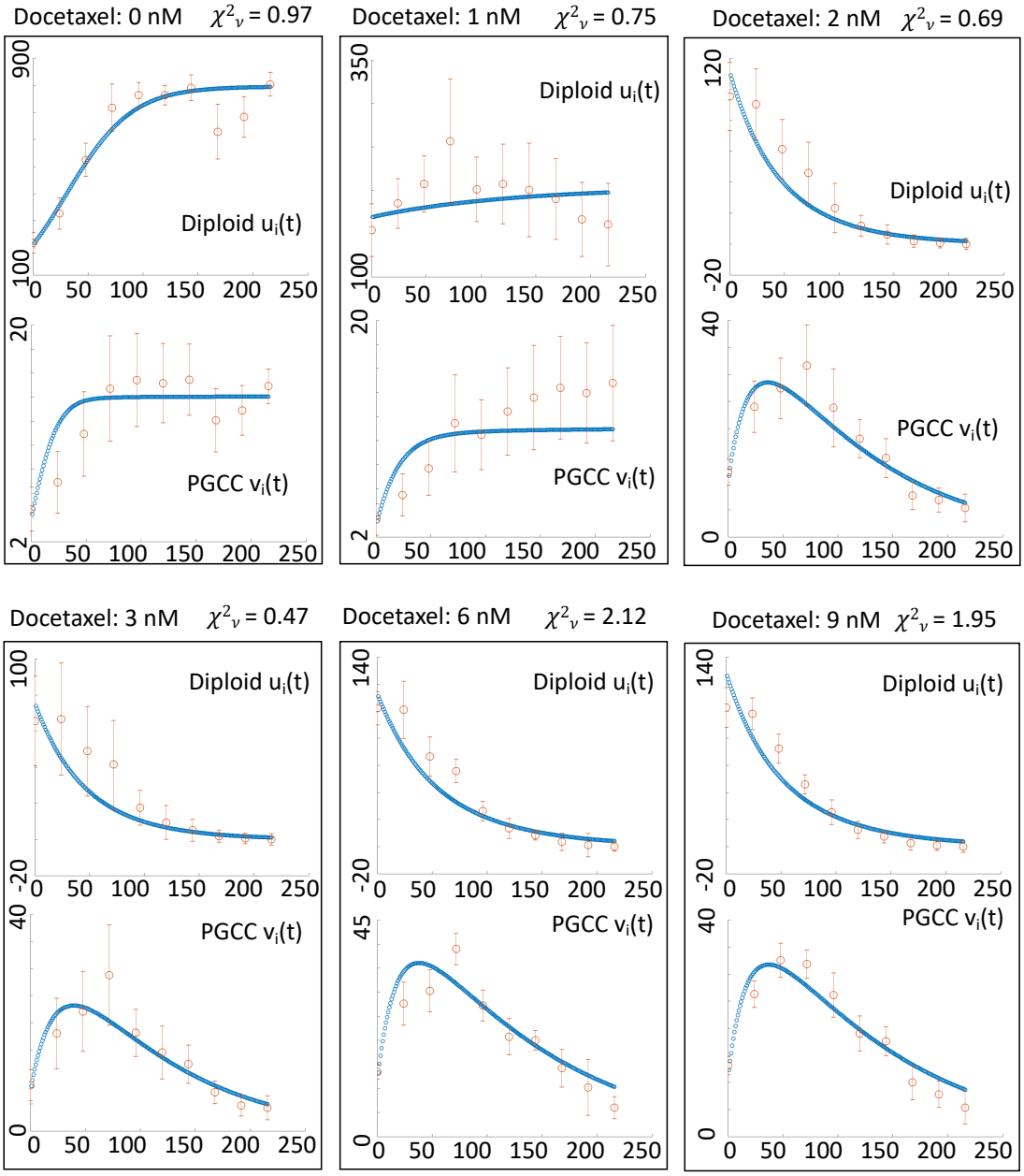

Figure 4.9: **Curve fitting of the single-well control experiments using Eq. 4.1.** The population of PGCCs and diploid cells treated at each dosage of docetaxel in the single-well control, $u_i(t)$ and $v_i(t)$, are fitted using the minimum chi-square fitting method to obtain the parameters described in equation 4.1. The parameters which were fitted are: G_i, T_i, D_{ui}, D_{vi}, k_u and k_v, u_0 and v_0 (the initial cell count of diploid cells and PGCCs).

C (nM)	G (1/d)	T (1/d)	D_u (1/d)	D_v (1/d)	k_u (1/d)	k_v (1/d)	μ (1/d)
0	0.89	0.072	0	0			
1	0.79	0.072	0.50	0.25			
2	0.48	0.41	0.48	0.34	0.0010	0.0050	0.02
3	0.55	0.43	0.55	0.34			
6	0.70	0.50	0.50	0.34			
9	0.60	0.41	0.53	0.34			

Table 4.1: **The value of parameters used in the cancer population model as a function of drug concentration C.**

the equation describes the population progression reasonably well. The parameters are listed in Table 4.1. The parameters G_i, T_i, D_{ui}, and D_{vi} are functions of drug concentration, as visualized in Fig. 4.10.

The migration factor is determined by cell tracking measurement of the EA experiment with docetaxel gradient (0 - 10 nM). As shown in Fig. 4.11, the cell emigration events in each microhabitat is roughly linearly correlated to the cell number within the microhabitat in a period of 45 hours. This was quite surprising as one might assume that the drug would affect a cell's metabolism and thus slow down its migration. In addition, there is no dependency between drug concentration and emigration/cell count ratio. If they are alive, they migrate independent of drug concentration. Finally, an important point is that there is no observable tendency for diploid cells to migrate toward higher or lower drug concentration. Their migration is random in direction, as would be expected with no chemotaxis response. Later, this was assumed in our model when there was a drug gradient. Therefore, the emigration and immigration terms M_{em} and M_{im} can be described as

$$\begin{aligned} M_{em,i} &= \mu u_i, \\ M_{im,i} &= \frac{1}{2}(M_{em,i-1} + M_{em,i+1}) = \frac{\mu}{2}(u_{i-1} + u_{i+1}), \end{aligned} \tag{4.2}$$

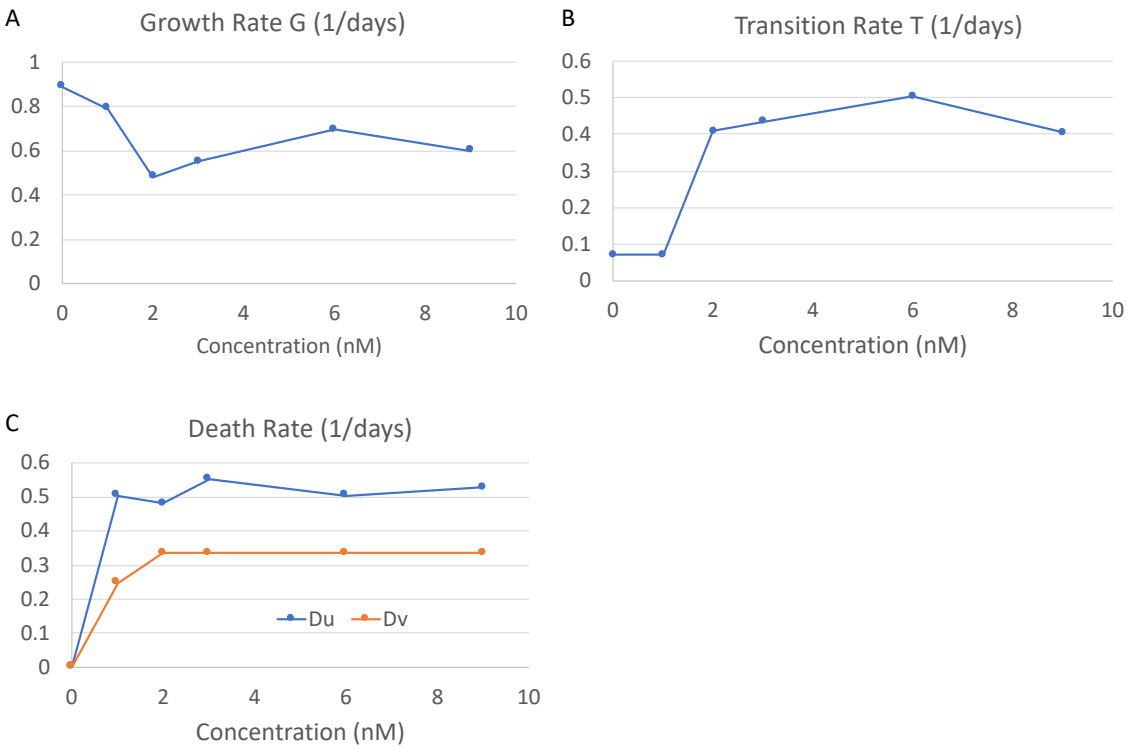

Figure 4.10: **The parameters of the cancer population model based on the fitting result of single-well control experiments.** (A) The growth rate of diploid cells at different docetaxel concentrations. The growth rate G_i tends to decrease at higher drug concentrations. (B) The transformation rate from diploid to PGCCs T_i increased up to 5-fold above 2 nM of docetaxel. (C) The death rate of diploid cells D_u and PGCCs D_v shoot up as the dosage of drug increases. PGCCs have comparably lower death rate.

The slope of the regression line in Fig. 4.11 is about 0.9, which means the migration probability μ for each cell is $\approx 0.9/45 = 0.02$ (1/hr).

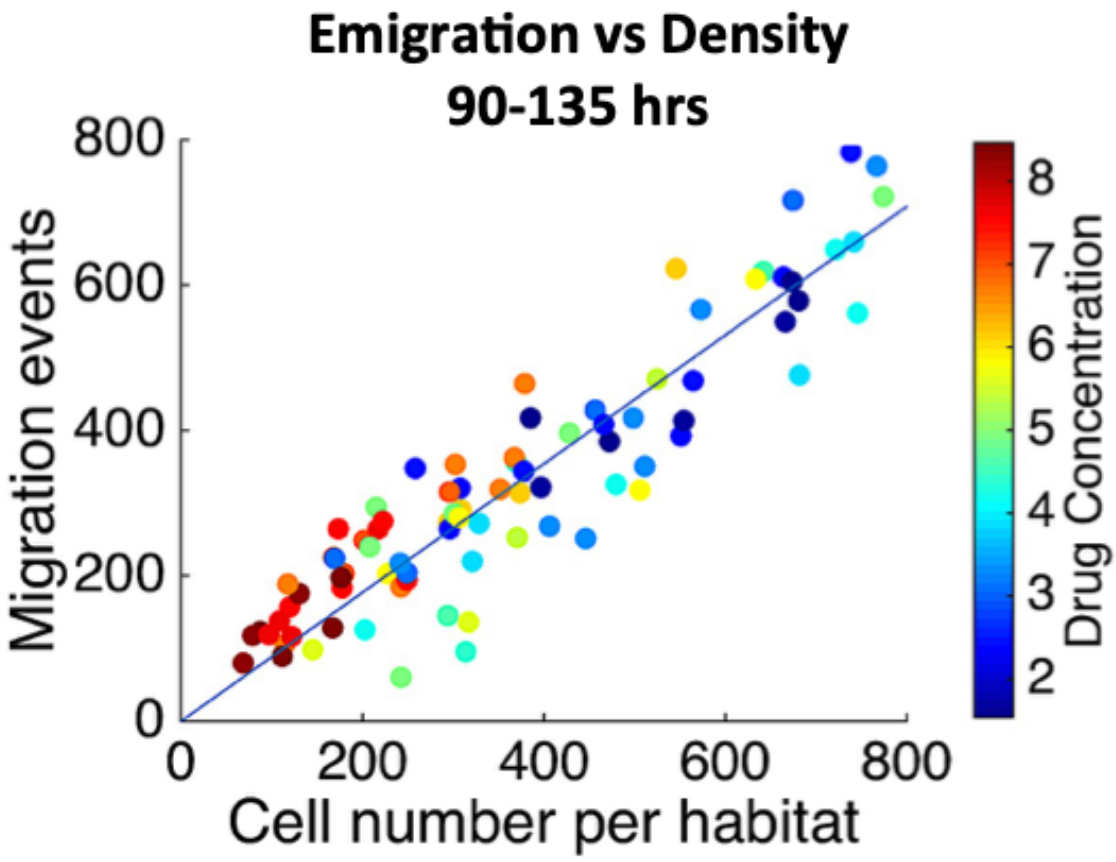

Figure 4.11: **The number of emigration events occurred within 45 hours versus the number of cells in each corresponding microhabitat.** Cell tracking analysis of EA experiments with docetaxel gradient (0 - 10 nM) is performed using TrackMate[37]. The scatter plot shows the number of emigration events occurred within 45 hours versus the number of cells in each corresponding microhabitat. The data points are color-coded to present local docetaxel concentration. The slope of the linear regression line determines the probability of a cell leaving current habitat within 45 hours, which leads to the value of μ, the migration probability as described in equation 4.2.

4.4 Physical mechanism leading to high PGCC formation: Migration

4.4.1 Modelling PGCC formation in the EA with drug gradients by adding migration

The population study of Fig. 4.8 demonstrated that the gradient stress environment generated a population that could survive at stress levels that could not be achieved when the environment had no gradient. When a stable docetaxel gradient was applied in the EA for 10 days, we observed a cytotoxic transition between fully confluent zone and the PGCC-dominant zone. Compared with the control experiment, the lethal high cytotoxicity boundary shifted from 2 nM to 6 nM for the overall population, and the density of PGCCs was enriched in region with higher dosage of docetaxel by upto 10X.

The underlying mechanism of the aforementioned observation is studied using mathematical model described in equation (4.1). The model demonstrated that the coexistence of proliferative and resistant phenotypes with the ability to migrate across a spatially-varying stress landscape could lead to significant improvement of survival of cancer cells. With the parameters in equation (4.1) quantified based on single-well experimental data, the population dynamics of the both single-well control and EA experiment with docetaxel gradient can be reconstructed without introducing any other free parameters, as demonstrated in Fig. 4.12 (A) (B).

The only difference between the modeled single-well control and modeled EA experiment, and the key physical result, is the migration factor. Compared with experimental result presented in Fig. 4.8 (A) (C), the modeling results share similar features. The total cell confluence shifted about 2 nM, and the density of PGCCs increased dramatically within the similar range of docetaxel concentration. To be clear,

equation (4.1) does not include other potential mechanisms such as niche construction in densely populated domain or the diffusion of cell signaling molecules which may confer an advantage to cells in adjacent regions. These were not necessary to successfully model the data.

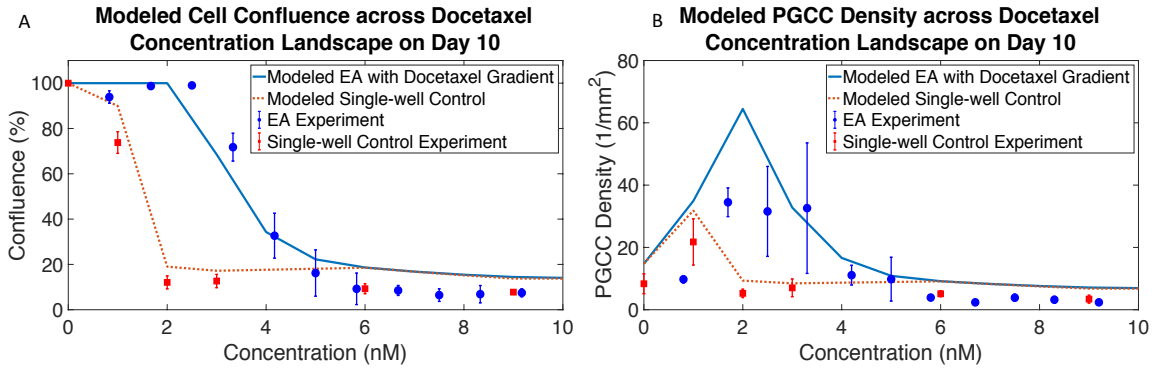

Figure 4.12: **The modeling of cancer population as a function of docetaxel concentration on day 10.** (A) Total cell confluence versus docetaxel concentration. (B) Density of PGCCs versus docetaxel concentration. The modeling of both cell confluence shifting and PGCC abundance are in accordance with the features of experimental results.

The basic reasoning for the observed population dynamics can be grasped from a game theory analogy [71], as shown in Fig. 4.13 (A). In a conventional cell culture plate, when the cells are exposed to chemotherapy above a certain dosage, the cells will either become polyploid or more likely apoptotic. The maximum number of PGCCs would be pre-determined by the initial diploid density, since diploid proliferation would be limited.

Now consider the case when the cancer cells are exposed to a stress gradient. In the high drug concentration region the cells die but a portion of the population become polyploid in response to the chemotherapy, but with low numbers and slow to zero growth rates. In the meantime, the population in the low drug concentration region is dominated by the highly-proliferative diploid phenotype that continues to proliferate. Most significantly, this large number of diploids can now migrate into higher drug regions, where they can then serve as the generators of PGCCs. Therefore, unlike the

conventional cell culture plate, the population in the high stress zone is replenished by cell migration and thus the number of PGCCs is not limited by the initial size of the population in the high drug region. This qualitative explanation is supported by our quantitative model as demonstrated in Fig. 4.13 (B) (C). The diffusive migration of diploid cells creates a positive cell influx from low to high drug concentration (Fig. 4.13 (B)). The accumulated cell influx, which consists of proliferative diploid cells, leads to higher diploid population in region with higher docetaxel concentration. The migrated diploid cells then rapidly transform to PGCCs, because the transformation rate is increased by the stress from the drug. As a result, many more PGCCs are formed in a gradient environment than in uniform drug environments.

To emphasize how and where PGCCs are produced in the EA, the effective PGCC emergence rate can be calculated by multiplying local diploid population u_i and transformation rate T_i and subsequently subtracting the population capacity limiting term $v_i k_v(u_i + v_i)$, as shown in Fig. 4.13 (C). The modeling result shows that the random migration of diploid cells is sufficient to give rise to an elevated PGCC emergence observed in experiment.

4.4.2 Discussion of PGCC formation in drug gradient environments and imlications for new therapies

We have demonstrated that the observed increased survival of the cancer population and the enrichment of PGCCs in the chemotherapeutic stress environment is facilitated by a gradient in stress levels. We have also demonstrated with our microfluidic EA that the the emergent PGCCs have significant up-regulation of mesenchymal biomarker ZEB1 compared with the diploid cells, implying that PGCCs were more capable of exploring the phenotypic landscape and finding better survival and metastatic strategies. The mechanism of how PGCCs become resistant is beyond the scope of this paper. Instead, the highlight of this work is that what appears to be

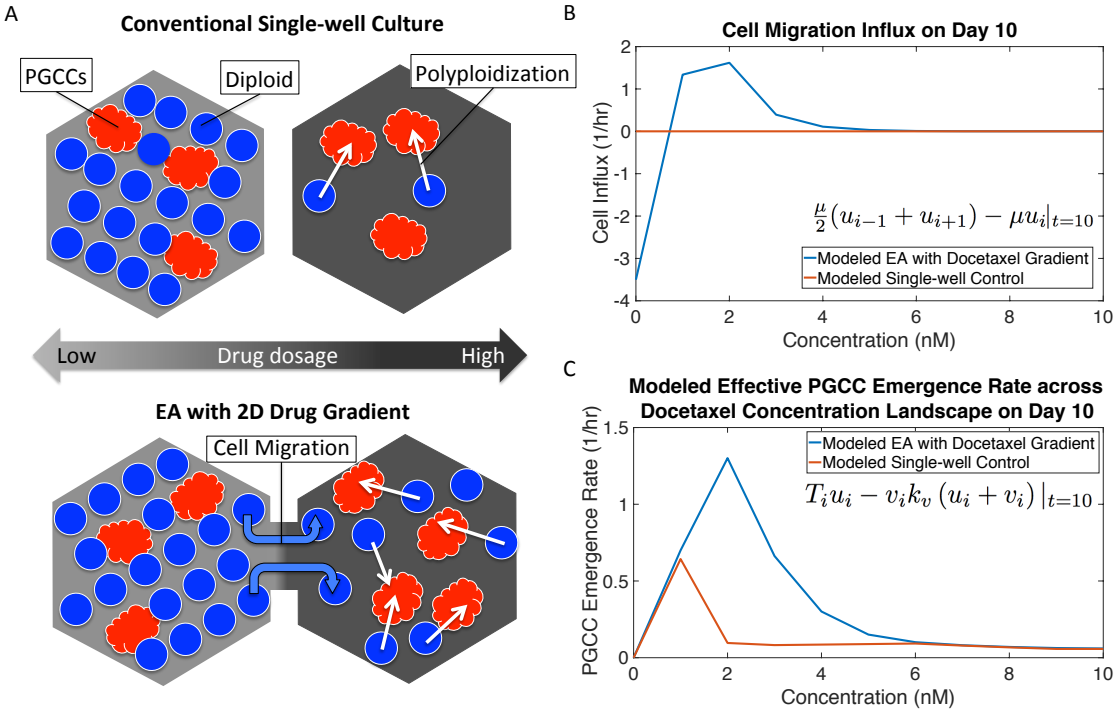

Figure 4.13: **Explanation of elevated PGCC emergence in chemotherapy gradient as opposed to a well-mixed environment.** (A) Schematic figure of the game theory analogy. In conventional culture, cells with drug dosage reach high confluence and the fraction of PGCCs remains low. The cells in high dosage well either undergo apoptosis or polyploidization, leaving only the PGCCs in the culture. In the EA gradient experiment, on the other hand, the populations under different level of stress are interconnected. The diploid cells continue to proliferate in EA areas with low drug, and can migrate to high drug EA areas, providing new source of PGCCs but at a high risk of death. (B) Diploid cell migration influx as a function of docetaxel concentration on day 10. Diploid cells are constantly supplied into higher docetaxel concentration region. (C) The effective PGCC emergence rate defined as $T_i u_i$ subtracted by population capacity limiting term $v_i k_v (u_i + v_i)$. By simply allowing cell migration, the effective PGCC emergence rate can be greatly affected.

a rare event in homogeneous environments can be amplified in a stress gradient. Our observation provides an insight into the development of drug resistance in a tumor tissue: when more tumorigenic and highly-evolvable polyploid cell subpopulations are generated during the treatment due to the environmental heterogeneity, it is more likely that the tumor becomes resistant.

It has been reported that the technology based on semi-isolated populations in a gradient environment accelerates the evolutionary dynamics to take place over weeks in the lab rather than months in conventional static culture *in vitro* assays[33, 39, 40]. For instance, Wu *et al.* demonstrated that the degree of doxorubicin resistance of multiple myeloma increased 16-fold after 48 hrs of doxorubicin gradient exposure [39], and Lin *et al.* presented the microfluidic system which allows the observation of on-chip docetaxel resistance development and relapse of prostate cancer PC3 in 2 weeks[33]. However, there has been no satisfactory explanation for how the rapid evolution is achieved. Our results and the game theory analogy could also provide microscopic evidence for the underlying mechanism: the continuous production of PGCCs which possess high phenotypic plasticity and chromosomal instability.

There is in addition a strong resemblance between the polyploidization response of cancer cells to chemotherapy resulting in increased fitness and the emergence of multi-nucleated bacterial [72] when *E. coli* are treated with the genotoxic antibiotic ciprofloxacin. Multi-chromosome-containing bacteria are able to divide asymmetrically at sub-lethal concentrations of ciprofloxacin and produce progeny with increased resistance. The mechanism of bacterial filament formation is analogous to the generation of PGCCs, which suggests a unified fundamental role of polyploidy emergence in conferring resistance.

We note that it has been extensively demonstrated that cell dynamics within tumor microenvironment can be a crucial factor in tumor progression, drug resistance development, and cancer metastasis. [73, 74] For instance, stromal cells have been

demonstrated to suppress the apoptosis signal of cancer cells, mediate *de novo* drug resistance,[75] and contribute to CCR5-dependent promotion of metastatic tumor growth. [76] Immune cells are also known to promote epithelial-mesenchymal transition (EMT) and generate cancer stem cells within the cancer ecosystem. [77, 78] These intercellular dynamics are typically difficult to study *in vitro* in the context of environmental heterogeneity. Although not presented in this paper, our current work includes co-cultures of cancer and stromal cells in an effort to address these issues.

Using a heterogeneous environment typical of a real biological system has allowed us to see how the mixture of normal diploid cells and the PGCCs can result in better fitness to high levels of a therapy such as docetaxel. This suggests the clinical value of identifying vulnerabilities of PGCCs might be targeted as critical targets [79]. Ideally, we should be able to identify some vulnerabilities of PGCCs that even diploid cancer cells generically do not have, in a way that would not trigger a stress response in the diploid cancer cell tumor population, which unfortunately usually leads to increased resistance. An important therapeutic implication of our findings is that inhibiting centrosome clustering might well retard the development of drug resistance in tumors. Inhibiting centrosome clustering would be a promising therapeutic target because it would be likely prevent an effective response to a stressful drug.

4.4.3 Future perspectives

Our model relies entirely on cell migration, not on other mechanism such as signalling , for example. This could be experimentally tested by making the slits between habitats smaller to reduce or eliminate cell migration. Reducing the width to 4 μm should be sufficient. Signalling molecules or proteins could still pass through, and multiple slits could be made in parallel so the total ability of signalling molecules could be made the same as of one wide slit.

Although the data support the association of polyploidization with drug resistance, the asymmetric division process of PGCCs remain poorly characterized in the context of heterogeneous microenvironment where polyploid cells evade mitotic catastrophe and produce viable progeny of chemotherapy resistant clones.[80] Using our EA chips, we can monitor and quantify the asymmetric cell division dynamics of PGCCs in a spatially-varying and time-varying stress landscape. We may further test the hypothesis that targeting KIFC1, a mediator of centrosome clustering necessary for the multipolar cell division process, would prevent PGCCs from producing viable resistant progeny.[81]

Chapter 5

Cellular Dynamics between Cancer Cells and the Host Stromal Cells with the Static Diffuser

In the previous chapters, we focused on the emergence of phenotypic variations and interaction among cancer population given a spatially varying chemotherapy concentration as the source of environmental heterogeneity. In this chapter, we proceed to incorporate different cell types into the artificial microenvironment on chip. Further, we use this experiment as demonstration of the "static diffuser" approach towards maintaining a long-term drug gradient without external pumps or pressure sources.

The complex intercellular interactions between cancer cells and host stromal cells have been increasingly recognized as fundamental for drug resistance development and tumor progression.[82] We report in this chapter the co-culture of human bone marrow stromal cell line (HS-5) and bone-metastatic prostate cancer cell line (PC3) across a gradient of chemotherapy using the microfluidic static diffuser described in Chapter 2. The microfluidic static diffuser allows quantitative study of cell dynamics

by monitoring in real time the interactions of multiple cell types over time with considerable experiment throughput.

Although the experimental data was noisy due to the bright-field quantification method, we may still observe qualitatively that (1) in the no-drug scenario, the system tends toward a cancer wins state; (2) in the low-drug region within the static diffuser, the system tends either toward stromal cells wins or coexistence; (3) in the high-drug region within the drug gradient, the system moves toward either coexistence or mutual death.

Although the quantification method leaves much room for improvement, this preliminary work demonstrates that the complex nonlinear interactions between cancer and host stromal cells, including the cooperative and competitive dynamics within a heterogeneous fitness landscape, can be observed and measured using the static diffuser technology.

The results and figures presented in this chapter are still in progress for a journal publication. Our collaborators at Johns Hopkins Medical Institute, Prof. Kenneth Pienta and Dr. Gonzalo Torga, provided much the cancer implications insight. Dr. Gonzalo Torga at Johns Hopkins and Yusha Sun at Princeton contributed to the development of the static diffuser technology. Yusha Sun did a considerable amount of work in the HS5-PC3 co-culture experiment.

5.1 Intercellular interactions between cancer cells and host stromal cells as a contributor to microenvironment-mediated drug resistance

One of the mainstream cancer research topics in the past 30 years has been unraveling the correlation between various permanent genetic mutations and the corresponding

behavioral consequences. These studies provide us with fundamental understanding of cell biology and functional networks of cancer. However, it has also been increasingly recognized that the cellular dynamics and stress response of cancer can not be fully described without considering the local tumor microenvironment constructed by a mixture of cancer and host cells including the vasculature, reactive stromal fibroblasts, immune cells and the extracellular matrix (ECM).[83, 75] Furthermore, the cooperative interaction between tumor cells and the surrounding environment has been characterized as survival strategies against drugs. [84, 82]

Specifically, prostate cancer is well-known for predominantly metastasizing into bone marrow, which leads to almost inevitable failure of treatments. The bone marrow provides an inclusive environment for metastasized prostate cancer, allowing the cancer cells to stay dormant for a period of time before transitioning into the proliferating phase. [85, 86] The process of how and why prostate cancer can be triggered to exit dormancy state and proceed to subsequent secondary tumor growth remains poorly understood.

Therefore, in this work we recreated the microenvironment in bone marrow using the microfluidic static diffuser described in Chapter 2. By generating static chemotherapy gradients across the metapopulation of bone marrow stromal cell line (HS-5) co-cultured with bone-metastatic prostate cancer cell line (PC3), we seek to demonstrate the potential of using static diffuser as a experiment platform to predict deterministically the population dynamics of the cancer-stroma system.

5.2 Experimental Design

As shown in Fig.5.1 (A), the static diffusers are installed into a specially-designed 6-well plate to ensure mechanical stability of the chip on the Lumox dishes, which had a mixture of PC3-EPI and HS-5 seeded a day before the initiation of the exper-

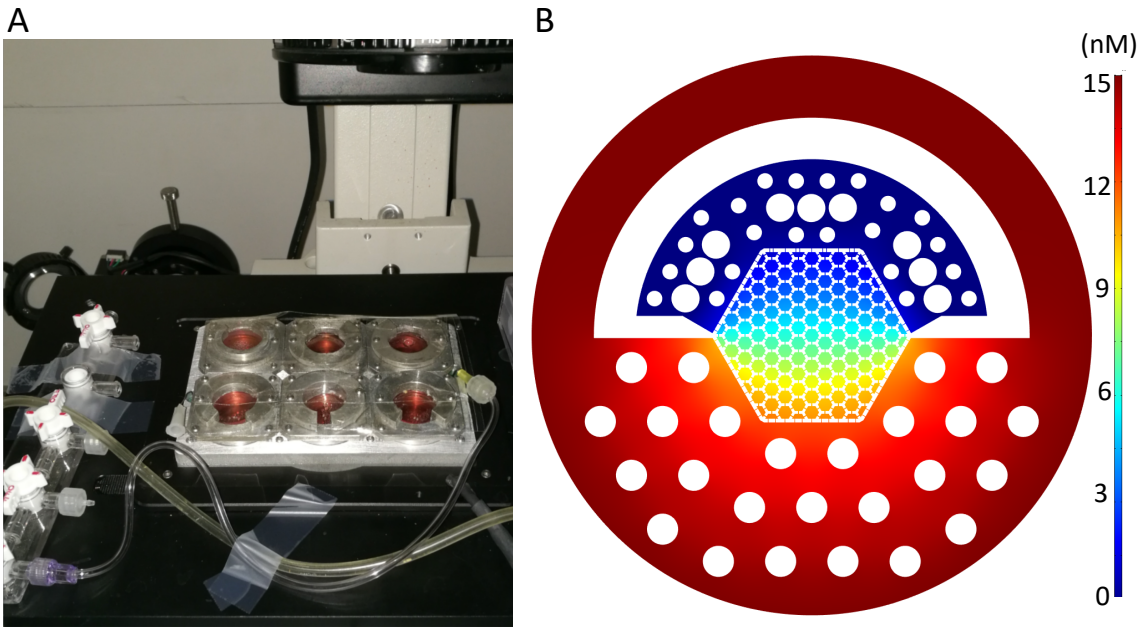

Figure 5.1: **The experimental setup of the static diffuser.** (A) Six devices are installed into the customized 6-well plate to secure the mechanical steadiness of the chip on cell culture membranes. The plate sits in the ibidi^{TM} incubator for continuous on-stage imaging over several weeks. (B) The spatial distribution of docetaxel in the static diffuser.

iment. The customized 6-well plate allows the user to run six experiments on-stage simultaneously. The ibidi^{TM} on-stage thermal control enclosure, a brand of products for microbiological experiments, is used to keep the cells at 37 °C. A custom gas supply system mixes ambient air with the desired 5% CO_2 before getting humidified in the bubbler. The humid mixed gas connects to the customized 6-well plate and pressurizes the Lumox membrane against the chip, ensuring sealing of the chip and providing efficient gas exchange. The plate sits in the ibidi^{TM} incubator on a microscope platform for continuous bright-field and fluorescent imaging over the course of weeks.

The generation of drug gradient is achieved by adding 15 nM of docetaxel in the outer (red) region as shown in Fig.5.1 (B). The blue region is connected to a large reservoir of media without drugs, located above the chip, as described in Chapter 2. Due to the large volume of the reservoir, we have presented in Chapter 2 that such a

gradient can be maintained stably over several weeks. The media on the outer region is replenished with fresh media with 15 nM docetaxel every other day.

5.3 Results

5.3.1 The generation of quantifiable image of unlabeled cells using bright-field microscopy

In this experiment, unlabeled bone marrow stromal cells (HS-5) are mixed with PC3-EPI cells co-expressing cytoplasmic mCherry protein and H2B-GFP labeled histones. Having cytoplasmic and histone fluorescent labels in cancer cells allows us to keep track of the polyploidization process as presented in the previous chapter. That being said, the use of two fluorescent labels in one cell type limits the emission bandwidth for the rest of the cell types. Therefore, as a preliminary test, we use unlabeled HS-5 and seek to establish a image processing protocol for bright-field image analysis and cell quantification.

A stitched mosaic composed of unprocessed 10X bright-field images is shown in Fig. 5.2 (A). It is apparent that the background intensity differs dramatically across the field of view due to the flat field effect, the optical configuration, and most importantly the unexpected objects that scatter the transmission light source. In the case shown in Fig. 5.2 (A), a small air bubble in the top reservoir casts a shadow, both literally and figuratively, at the bottom left corner of the image and hinders the visibility.

To obtain a quantifiable bright-field image, the nonuniformity of background signal intensity needs to be ironed out. Moreover, the signal intensity of the cells across the field of view should be normalized properly for a satisfying cell segmentation performance. We therefore created a custom image processing macro based on existing algorithm on Fiji.

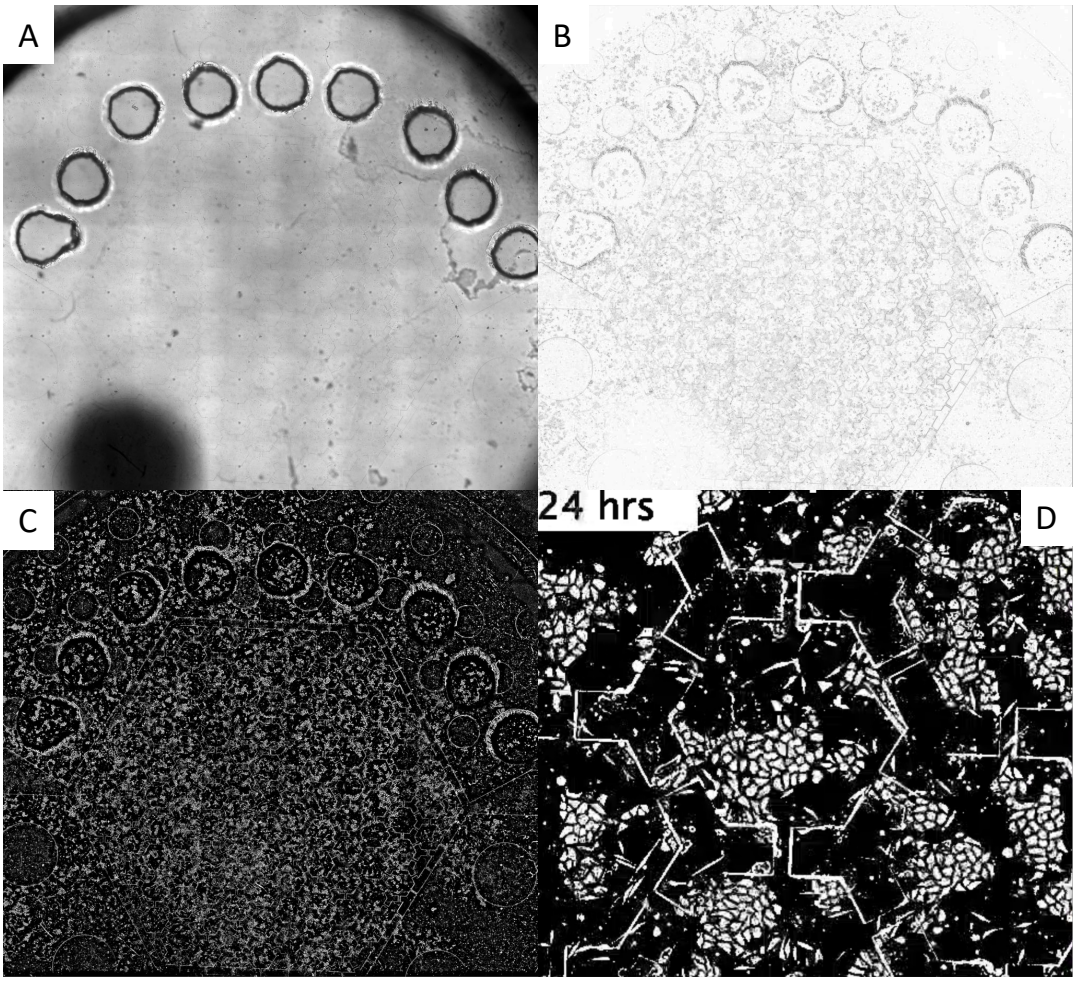

Figure 5.2: **The result of bright-field image processing protocol.** (A) The mosaic of original bright-field images. (B) Background-subtracted image. Uneven illuminated background has been corrected. (C) Processed image after Phansalkar local thresholding algorithm. (D) A close-up image of C.

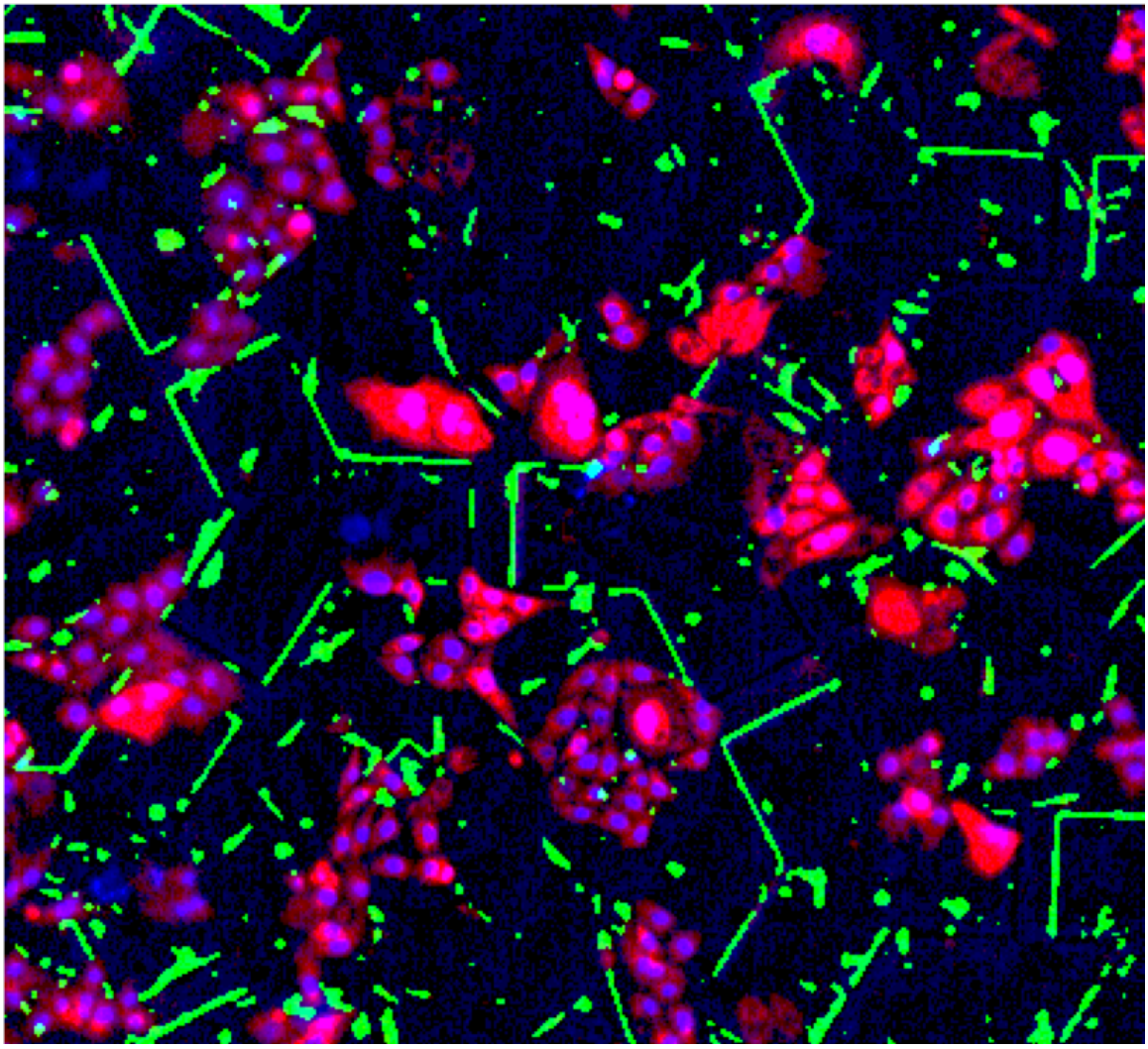

Figure 5.3: **The overlay of cytoplasmic- and histone-labeled PC3-EPI and the processed bright-field channel.** The green fluorescent protein histone label is pseudo-colored as blue. The mCherry cytoplasmic label is pseudo-colored as red. The mCherry image is subtracted from the processed bright-field image to generate a HS5-only image, pseudo-colored as green.

(1) The first step is to correct for uneven illuminated background by using a "rolling ball" algorithm (`https://imagej.net/Rolling_Ball_Background_Subtraction`). A local background signal is calculated by averaging over a large circle with assigned radius around the pixel. Sequentially, the calculated local background value is subtracted from the original image in order to remove coarse background variations. The result after background subtraction is shown in Fig. 5.2 (B). However, the signal intensity of cells still differs between the shading region and the surroundings.

(2) The second step is to determine local threshold value at each pixel to transform the background-subtracted 8-bit image into a binary mask with cells illuminated. The adaptive local thresholding algorithm, Phansalkar[87], is implemented via the Auto Local Threshold plugs-in in Fiji (`https://imagej.net/Auto_Local_Threshold`). This local thresholding scheme is developed to solve the problem of nonuniform staining, or nonuniform bright-field intensity in our case. The result is shown in Fig. 5.2 (C). The cells within the shading region are now clearly visible.

A close-up image of Fig. 5.2 (C) is presented in (D) where cells are properly segmented. Typical image quantification methods can now be applied, including confluence, morphology (e.g. circularity, diameter, etc.), velocity, and so on.

5.3.2 Running 6 experiments simultaneously with the static diffuser EA chips

As discussed previously in Section 2.4.2, the static diffuser EA chips simplify the experiment setup by getting rid of the active growth media source. Without the bulky peripheral equipment for the generation of media flow, the system allows high-throughput experimentation.

As shown in Fig. 5.4, in this work we demonstrated that with the customized 6-well plate and the static diffuser EA chips, up to 6 experiments can be performed

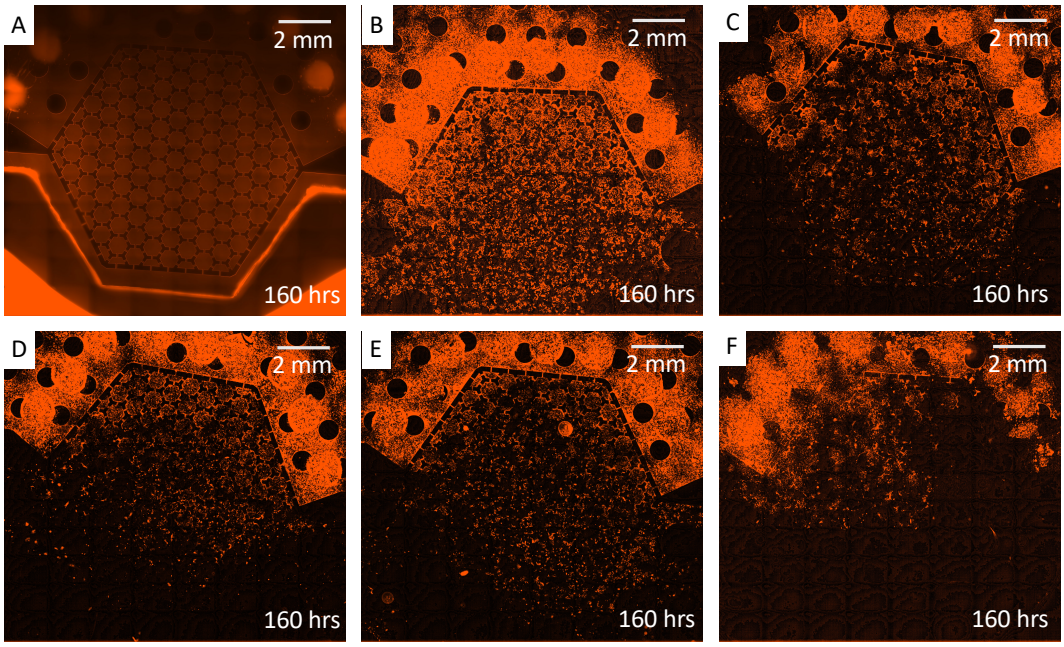

Figure 5.4: **6 experiments running simultaneously on the customized 6-well plate with static diffuser EA chips.** The cells used in this set of experiments are PC3-EPI (Red cells) and HS-5 (unlabeled). (A) The Rhodamine 6G (fluorescent dye) gradient test. (B) The control experiment, without any drug. (C)(D) PC3-EPI treated by docetaxel gradient from 0 - 15 nM for 160 hours. (E)(F) PC3-EPI treated by docetaxel gradient from 0 - 25 nM for 160 hours.

simultaneously for continuous high-resolution image acquisition. Fig. 5.4 (A) is a gradient generation test using a fluorescent dye, Rhodamine 6G. Fig. 5.4 (B) is a control experiment done with mCherry-labeled PC3-EPI and unlabeled HS-5 cells. Cells reached high confluence after a week of culture. (C) and (D) are the PC3-EPI (Red cells) and HS-5 (unlabeled) coculture experiments treated by docetaxel gradient ranging from 0 nM (the top three sides of the chips) to 15 nM (the bottom sides of the chips). (E) and (F) are similar to (C) and (D), only changing the maximum dosage from 15 nM to 25 nM. As a result, the amount of experiment throughput is 2X to 3X higher than that of previous syringe-pump-driven EA, allowing us to explore wider parameter space and to perform more experiment replicates in a short period of time. We note that the number of experiments can be easily scaled up for parallel

experimentation by keeping the experiments running on multiple customized 6-well plates inside a normal cell culture incubator.

5.3.3 Quantification of PC3-EPI and HS-5 population

The number of PC3-EPI cells can be easily determined on GFP channel by either particle analysis or local maximum counting feature in Fiji. However, it is more challenging for the processed bright-field image. The reason is that unlike the GFP-histone label, processed bright-field image of cells can capture the inner structure of cells which lead to overestimation of cell population if we apply particle-based methods. Therefore, instead of the direct counting of cells on the bright-field channel, we measure the confluence of cells as a indication of cell population.

mCherry image, the cytoplasmic-label of PC3-EPI, is subtracted from the processed binary bright-field image to generate a HS5-only binary mask. The fluorescent channels (GFP and mCherry) and the HS5-only binary mask is combined and pseudo-colored as demonstrated in Fig.5.3. The confluence of cells in each microhabitat is in turn measured to yield the total HS-5 coverage in each microhabitat. The number of HS-5 can then be estimated by dividing the HS-5 coverage area by the average cell size of HS-5.

5.3.4 The population dynamics across docetaxel gradient

A docetaxel gradient ranging from 0 to 15 nM was established across the static diffuser. Time-lapse video-microscopy using large-area image stitching was done throughout the course of the experiment. The concentration of docetaxel in each microhabitat can be determined by COMSOL Multiphysics simulation. Fig.5.5 presents the progression of the PC3-EPI and HS-5 in the static diffuser versus time.

Under the scenario when no chemotherapy was applied, as shown in Fig.5.5 (A) (B), PC3-EPI (red) and HS-5 (green) grew homogeneously across the microhabitat

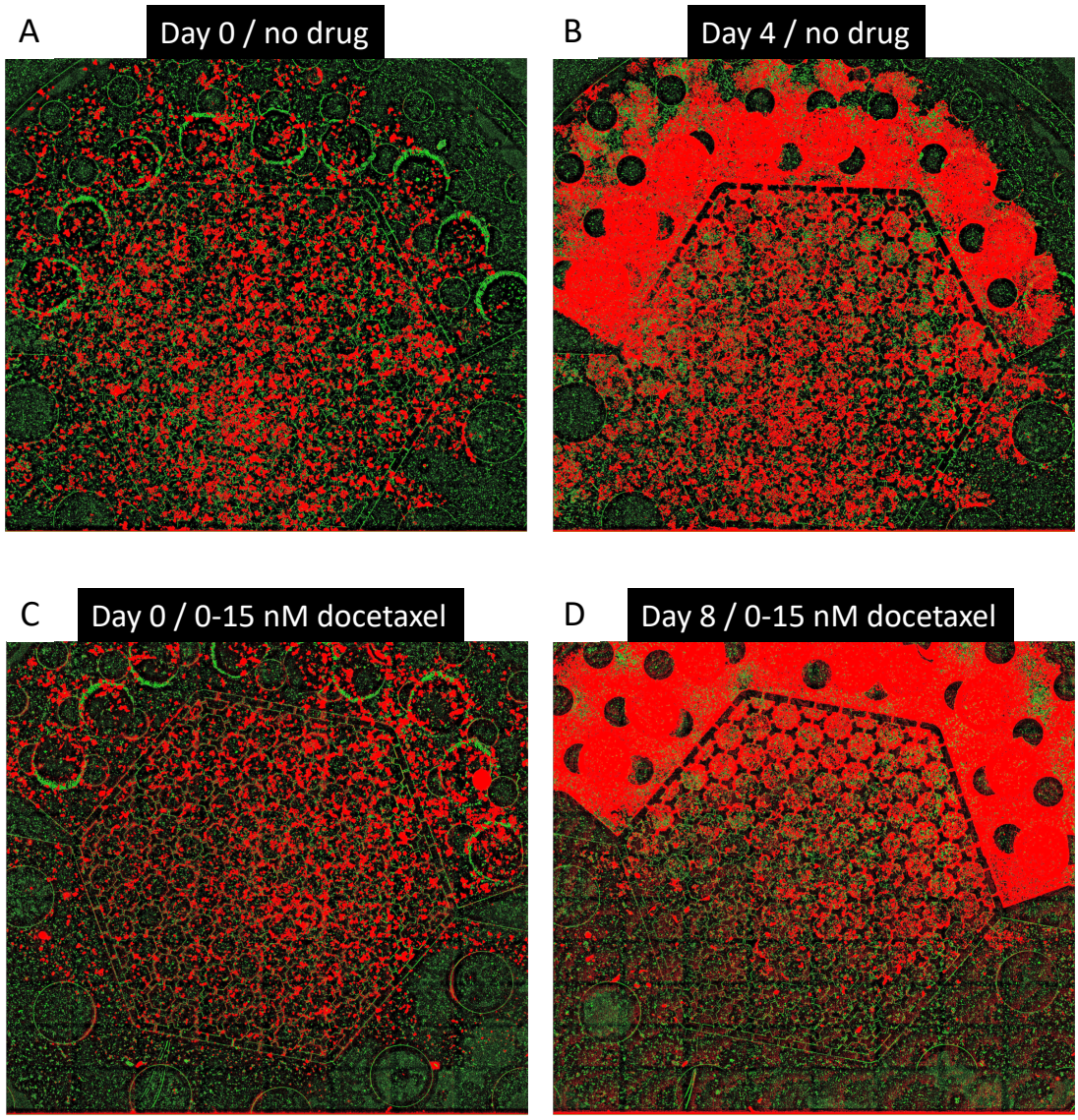

Figure 5.5: **The coculture of PC3-EPI (mCherry, colored as red) and HS-5 (processed bright field, colored as green) without drug and with docetaxel gradient (0 to 15 nM).** (A)(B) The coculture of PC3-EPI and HS-5 without drug, observed on day 0 and day 4. (C)(D) The coculture of PC3-EPI and HS-5 with docetaxel gradient ranging from 15 nM (the outer region) to 0 nM (the top reservoir).

array and reached high confluence in 4 days. The time scale and growth rate are comparable to the previous experiments done with the syringe-pump driven devices. When a docetaxel gradient (0 to 15 nM) was applied, the cancer cells gradually died out around the edges with the highest dosage of docetaxel as shown in Fig.5.5 (C) (D).

Using the method articulated in the previous section, both the number of PC3-EPI and HS-5 can be quantified as a function of time in each microhabitat. The fractional population of cancer is then calculated: $p_\gamma = p_\gamma/(p_\gamma + p_s)$ where p_γ and p are the number of PC3-EPI and HS-5, respectively. Cancer fractional populations on day 1 and day 7 for control experiment and the gradient experiment are presented in the form of heatmaps in Fig. 5.6. For the control experiment, we observe a general tendency from lower cancer fractional population to a relatively higher fractional populations (Fig. 5.6 (A) to (B)), which is expected due to the fact that cancer cells generally have a faster proliferation rate compared with stromal cells. In the case with drug gradient from 0 to 15 nM, as shown in Fig. 5.6 (C) day 1 to (D) day 7, a clear transition in terms of population dominance is evident.

5.4 Discussion

The aforementioned results are qualitatively consistent with the direct observations on the original images. However, there have been significant errors in the estimated HS-5 population for both low drug and high drug scenarios. In the low drug region, both cancer and stromal cells proliferate and reach high confluence. When cancer and stromal cells are tightly packed, subtracting cytoplasmic-labeled cancer from the processed bright-field image often causes underestimation of HS-5, because the HS-5 cells are overlooked whenever there is an overlap between cancer and HS-5. On the other hand, in the high dosage region, the cells die and leave behind cellular debris.

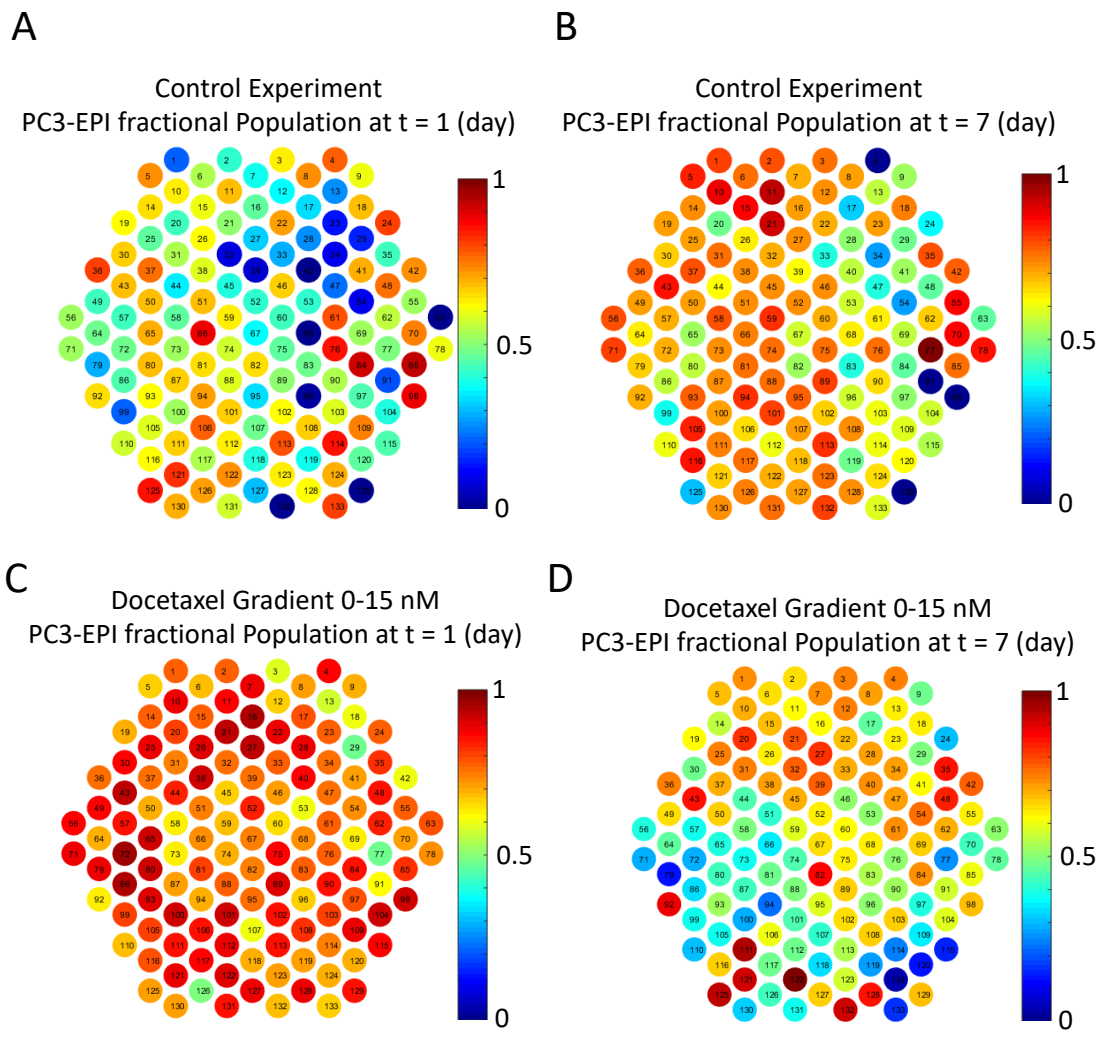

Figure 5.6: **The spatial distribution of fractional PC3-EPI population for the control and gradient experiment on day 1 and day 7.** The fractional population of PC3-EPI cancer cells at each microhabitat without drug on (A) day 1 and (B) day 7. (C) and (D) show the fractional population of PC3-EPI with the presence of docetaxel gradient (0-15 nM) on day 1 and day 7.

The cellular debris is included in the processed bright-field image, mistakenly counted as a part of HS-5 confluence, which then leads to significant overestimation of HS-5.

These factors fundamentally restrict the feasibility of using bright-field imaging to quantify population dynamics. This preliminary result suggests that in order to acquire quantitative experimental data, it is necessary to have each cell type labeled prior to image acquisition. Although the quantification method leaves much room for improvement, this work demonstrates that the complex interactions between cancer and stromal cells within a heterogeneous stress landscape can surely be monitored and measured using the static diffuser technology.

Finally yet importantly, we successfully demonstrated the ability to run 6 static diffuser EA experiments simultaneously on an inverted microscope. The amount of experiment throughput is 2X to 3X higher than that of previous syringe-pump-driven EA, and the experiment setup for the static diffuser EA can be done 5X faster without complicated media flow generation.

Chapter 6

Conclusion

6.1 Summary

Throughout the history of mankind, the advance in science and technology has always been made through the iteration of two necessary processes: (i) the better understanding of fundamental science which brings about revolution in technology, and (ii) the improvement of technology that in turn catalyzes the progress of research and discovery. As scientists and engineers, we play a significant role as the driver in these processes and are responsible for the advance in civilization and expanding the boundaries of human knowledge. The materials presented in this dissertation, to a certain degree, demonstrates how the improvement of technology could lead to scientific discovery that might be overlooked in conventional research paradigm.

In this dissertation, we introduce the microfluidic cancer-on-chip devices we have developed and how we implemented the technology to explore cancer population dynamics and how cancer acquire drug resistance. Two experimental configurations are presented in Chapter 2, the syringe-pump-driven microfluidic evolution accelerator (EA), and the static diffuser. The syringe-pump-driven EA provides superior control over boundary biochemical conditions. The concentrations of chemicals are

strictly fixed as given. The syringe-pump-driven EA is also capable of generating precise time-dependent stress gradients, which can be utilized as an experimental platform for studying maximum tolerated dose (MTD) strategy, metronomic therapy, and adaptive therapy. That being said, the bulky peripheral equipment and the complicated experiment setup would limit the throughput of experiment.

In comparison, the static diffuser is not only way less labor-intensive in the setup process, the number of experiment replicates can also be scaled up easily due to the lack of active media source. The media in the outer region does need to be replenished every other day, but it can be incorporated into the work flow in a automated molecular biology lab or pharmaceutical lab. Their superiority in respect of high-throughput experimentation makes them stand out from the crowd.

For both the syringe-pump-driven EA and the static diffuser EA, the setup of the portable on-stage platform allows for long-term coculture of multiple cell types in a heterogeneous microenvironment under stable physical and biochemical conditions with high-resolution real-time imaging. The significant improvement in the spatial and temporal resolution is a complete game changer. Without the high-magnification real-time scanning, it would not be possible to observe the cellular dynamics reported in Chapter 3, 4 and 5, including the cell migration events, emerging phenotypic transformation, endoreduplication, cell fusion, cell engulfment, etc. These observations directly attract our attention on the correlation between the emergence of polyploid giant cancer cells (PGCCs) and drug resistance.

It has been shown in the literature that PGCCs correlate with poor response to docetaxel chemotherapy in the context of castration-resistant prostate cancer[44] and are suspected to contribute to phenotypic evolution during different stages of cancer progression and metastasis[48]. However, the cell dynamics of PGCC emergence from an heterogeneous tumor micro-ecology under stress remain unobserved. As reported in Chapter 4, with our improved technology, we can quantitatively measure

population progression and relevant physical quantities, reaching a conclusion that environmental heterogeneity combined with cell migration within tumor population would cause amplification on the emergence of PGCCs.

In Chapter 5, we further incorporate different cell types into the artificial tumor microenvironment on chip. The goal is to quantitatively study cell dynamics between bone marrow stroma and cancer cells by monitoring in real-time with considerable experiment throughput. Although the quantification method leaves much room for improvement and the quantitative analysis on bright-field images is error-prone, this preliminary work shows that the static diffuser can indeed be used as an *in vitro* tumor microenvironment model.

Last but not least, the same experimental setup and back-pressure sealing method is not only implemented in this dissertation, but also utilized to study the collective dynamic of bacteria within mazes and complicated physical barriers. [88]

In summary, the devices and experiment platform presented in this dissertation have been shown to support valuable scientific studies with different research topics in biology. The system is compatible to a wide variety of materials and organisms of interests. This dissertation is an example of how the improvement of technology may highlight some pieces of information which has been overlooked in conventional methodology. We hope this work can one day serve as a foundation of further cancer research and eventually create positive impact on human society.

Appendix A

Protocols

A.1 Device fabrication

A.1.1 Fabrication of photomask

Heidelberg DWL66 laser writer (Heidelberg Instruments Mikrotechnik, Heidelberg, Germany) is used to write pattern on a soda-lime glass plate coated with 100 nm Cr and 500 nm photoresist AZ1518. After laser writing, the photoresist is development with developer AZ300MIF for 60 seconds. Chromium without the protection from photoresist is then etched away with Cr-7 Chromium Etchant. Finally, the residual photoresist is stripped off using Microposit Remover 1165 at 70 °C for 45 minutes.

A.1.2 Photoresist patterning

HMDS and photoresist AZ4330 are in turn spin coated on Si wafer with 4000 rpm 40 sec and 4000 rpm 40 sec respectively, followed by softbake at 95 °C for 60 seconds. KarlSuss MA6 mask aligner (SUSS MicroTec, Garching near Munich, Germany) was employed for UV exposure on Si wafer. Photoresist is developed with developer AZ300MIF for 4 minutes.

A.1.3 DRIE etching

The wafer patterned with photoresist is then dry-etched by Samco RIE800iPB (Samco, Kyoto, Japan) for 100 microns in depth. Photoresist is stripped off with acetone and plasma etching with TePla M4L plasma etcher (PVA TePla America, California, US).

A.1.4 Wafer oxidation and silanization

Thermal oxidation in performed on etched Si wafer in a furnace at 1100 °C for one hour. After cooling down, the Si wafer is then placed into a desiccator with a few droplets of trichloro (1H, 1H, 2H, 2H-perfluorooctyl) silane (PFOTS) dripped in a small container near the wafer. The pressure is pumped down to 0.5 atm at room temperature for 60 minutes. The Si mold become hydrophobic after proper silanization.

A.1.5 Soft lithography

The pre-polymer and cross-linker in PDMS Sylgard 184 package are mixed at a 10:1 weight ratio. Mixed PDMS is poured up to create a 10 mm film in height onto a previously silanized Si wafer mold, and is then degased in a desiccator for 30 minutes. Sequentially, the Si mold covered with mixed PDMS is incubated at 70 °C overnight. Once the PDMS is cured, the PDMS film can be carefully peeled off from the Si mold, followed by punching through-holes at the inlet ports with biopsy needles and cut to 27 mm in diameter using a circular punch.

A.1.6 PDMS layer bonding

Heat cure two other stacks of 27 mm-PDMS cylinders as the reservoir layer and the capping layer. Cut out two 7 mm circles around the inlets on the reservoir layer,

and punch the through-holes at the inlet ports on the capping layer. Bond the three stacks of PDMS with oxygen plasma treatment, and then punch the through-holes at the outlets and the center port.

A.2 Cell culture and cellular assay

A.2.1 Cell culture and subculture (trypsinization)

The human prostate cancer lines used in this dissertation, including PC3-EPI, PC3-EMT parental PC3, are routinely maintained in RPMI 1640 (Gibco, Grand Island, NY) supplemented with 10% fetal bovine serum (Sigma-Aldrich, St. Louise, MI) and 1X Anti-anti (Gibco, Grand Island, NY) at 37 °C in a humidified atmosphere containing 5% CO_2 in commercial incubator. Growth media needs to be replenished before the media turns yellow, usually 2 or 3 times a week. Once the cells reached 100% confluence, cells need to be trypsinized and subcultured into lower density into new culturewares.

To do so, remove culture medium from cultureware and rinse the cells gently with a 1X PBS free of Ca2+ and Mg2+ as serum, Ca2+ and Mg2+ inhibit the function of trypsin. Remove PBS and then dispense trypsin/EDTA solution into the cultureware and incubate at 37 °C for 2 to 5 minutes, depending on the cell lines. After cell detachment, add fresh media with serum into the cultureware and centrifuge the mixture of cells, media and trypsin/EDTA solution. Afterwards, aspirate the excessive fluid and resuspend the cells. The cells can then be subcultured or frozen.

A.2.2 Cell freezing and thawing

A rule of thumb is to freeze cells slow and thaw cells fast. After trypsinization, mix the concentrated cells with 900 ml of media and 100 ml of dimethyl sulfoxide (DMSO) into a cryotube vial. The cryotube vials are placed in a cell freezing container filled with

isopropyl alcohol. The container is then transferred into a -80 °C fridge to achieve a cooling rate of roughly -1 °C/min. The vials can be left in the fridge overnight, and then transferred to a liquid nitrogen tank for long-term storage.

Cell thawing is recommended to be done fast (within 1 min). Warm up the frozen vial in a 37 °C hot bath until it's fully thawed, and then immediately dilute the thawed cells gently using pre-warmed growth medium. Centrifuge the cell suspension and then transfer the cells into the appropriate cultureware.

A.2.3 Lipotransfection

Lipotransfection is a technique used to introduce external materials into the cells by means of liposomes. In our experiment, we use lipotransfection to trasfect a plasmid into the cells so that the cells would produce histone labeled with fluorescent protein. The trasfected cells will also gain resistance to a specific reagent, in this case Gentamicin (G418), so we can use G418 later as selection agent.

In order to determine the concentration of G418 used on each cell line, before transfection, we culture cells of each cell line in one 6 well plate and then add increasing concentration from 0, 1:100, 1:75 and 1:50 of antibiotic G418. Examine cell death after 5 days, if not all cells are dead in any of the wells, do the experiment and increase the concentration until we find out a minimal dosage that kills all the cells. This dosage would be the concentration of G418 later used in the selection process.

After deciding the dosage of G418, mix 600 µL of serum free RPMI-1640 with 6 µg of the plasmid, vortex 10 seconds, and then incubate 10 min at room temperature. Sequentially, add 18 µL of lipofectamine into the solution, vortex 10 seconds, and then incubate 20 min at room temperature. Afterwards, add the solution into the cultureware. Change media after 4 to 12 hours. Cells should start to be fluorescence the next day. After 72 hours from transfection, selection agent G418 is added to

the culture. Fluorescence-activated cell sorter (FACS) can also be used to select a subpopulation of cells with desired fluorescent protein expression level.

A.2.4 Fixation and permeabilization

Before conducting downstream immunofluorescence (IF) assay, the cells need to be fixed and permeabilized so that intracellular staining can be performed. The protocol is enumerated as follows.

Prior to start: a. Put a 15 mL tube full of Methanol in ice. b. Make 4% paraformaldehyde (PFA) from the 16% stock. Mix 1 part PFA stock with 3 parts PBS. For instance, 2 mL PFA (16%) should be mixed with 6 mL PBS to make 4 mL of 4% PFA.

1. Add 2x1 mL of PBS slowly, pointing the tip of the pipette towards the wall of the Lumox dish.

2. Retrieve 2x1 mL of PBS from the Lumox pointing the tip of the pipette towards the wall of the Lumox.

3. Repeat (1) followed by (2) 2 more times (total of 3 washes).

4. Add 2x1mL of PFA slowly, pointing the tip of the pipette towards the wall of the Lumox 300 µL per rectangle of 4% PFA and incubate for 30 min at room temperature.

5. Repeat (1) followed by (2) 3 times (total of 3 washes).

6. Add 2x1 mL of iced methanol slowly, pointing the tip of the pipette towards the wall of the Lumox and incubate for 10 min at room temperature.

7. Repeat (1) followed by (2) 3 times (total of 3 washes).

8. Add PBS and fill up the Lumox and keep the cells at 2 - 8 °C before immunostaining.

Appendix B

Image Processing

B.1 Cell Segmentation and Categorization by Size

To properly categorize cells by size, we created a custom image processing macro on Fiji based on the rolling ball algorithm (`https://imagej.net/Rolling_Ball_Background_Subtraction`) to enhance cell segmentation and improve the performance of Particle Analysis feature in Fiji (`https://imagej.net/Particle_Analysis`). To begin with, we performed rolling ball algorithm on the original image with the rolling ball diameter set to be larger than that of the largest cell in the region of interest in order to remove coarse background variations. Sequentially, we performed rolling ball algorithm on the background-subtracted image with the rolling ball diameter lower than that of the smallest cell. This process is sensitive to intensity variations and therefore highlights the cell boundaries. Finally, we subtracted the boundary-highlighted image from the background-subtracted image to create a better-segmented image, which was then analyzed using Particle Analysis feature in Fiji for cell categorization by given diameter threshold.

Appendix C

Publications and Conference Presentations

A significant portion of the materials in Chapter 2 and Chapter 3 is based on our paper published in Convergent Science Physical Oncology[33]. Chapter 4 is based on our paper published in Clinical & Experimental Metastasis[42]. A portion of the materials presented in Chapter 2 and Chapter 5 will be covered in our next paper, which is still in progress.

The publications and presentations arising from my Ph.D. studies are listed as follows.

C.1 Journal articles

1. Ke-Chih Lin, Gonzalo Torga, Yusha Sun, Robert Axelrod, Kenneth J. Pienta,James C. Sturm, and Robert H. Austin. The role of heterogeneous environment and docetaxel gradient in the emergence of polyploid, mesenchymal and resistantprostate cancer cells. *Clinical Experimental Metastasis*, 36(2): 97-108, Apr 2019.

2. Amy Wu, David Liao, Vlamimir Kirilin, Ke-ChihLin, Gonzalo Torga, Junle Qu, Liyu Liu,James C. Sturm, Kenneth Pienta and Robert Austin, Cancer dormancy and criticality from a game theory perspective, *Cancer Convergence*, 2:1 (2018)

3. Ke-chih Lin, Gonzalo Torga, Amy Wu, Joshua D Rabinowitz, Wesley J Murray,James C Sturm, Kenneth J Pienta, and Robert Austin. Epithelial and mes-enchymal prostate cancer cell population dynamics on a complex drug landscape. *Convergent Science Physical Oncology*, 3(4):045001, 2017.

4. Ryan J Morris, Trung V Phan, Matthew Black, Ke-Chih Lin, Ioannis G Kevrekidis, Julia A Bos and Robert H Austin, Bacterial population solitary waves can defeat rings of funnels, *New Journal of Physics*, 19: 035002 (2017)

C.2 Conference Presentations

1. Gonzalo Torga, Ke-Chih Lin, Bernat Navarro Serer, Cathleen Nguyen, Robert H. Austin and Kenneth J. Pienta, Multinucleation precedes the emergence of drug resistance in prostate cancer, *Cancer Research* 78 (16 Supplement), B039-B039 (2018)

2. Gonzalo Torga, Ke-Chih Lin, Bernat Navarro Serer, Cathleen Nguyen, Robert H. Austin and Kenneth J. Pienta, KIFC1 is a potential target to prevent treatment resistance in prostate cancer, *Cancer Research* 78 (13 Supplement), 1977-1977 (2018)

3. Ke-Chih Lin, Gonzalo Torga, James C Sturm, Kenneth J Pienta, Robert Austin, The Emergence of Polyploid Giant Cancer Cells as the Reservoir of Therapeutic Resistance, *APS Meeting Abstracts*: V46.003 (2018)

4. Ke-Chih Lin, Robert Austin, Greg Ducker, James Sturm, James Sturm, Serine, Glycine and One-carbon Metabolism in Colorectal Cancer Cell in Heterogeneous Microenvironment, *APS Meeting Abstracts*: Y6.011 (2017)

5. Ke-Chih Lin, Gonzalo Torga, Amy Wu, Joshua D Rabinowitz, Kenneth J Pienta, James C Sturm, Robert Austin, Cancer cell populations in a complex ecology at the timberline of existence, *European biophysics journal* 46, S114 (2017)

6. Ke-Chih Lin, Gonzalo Torga, Kenneth J Pienta, James C Sturm, Robert Austin, Multiple Cancer Cell Population Dynamics in a Complex Ecology, *APS Meeting Abstracts*: E35.003 (2016)

7. Gonzalo Torga, Ke-Chih Lin, Robert H. Austin and Kenneth J. Pienta, Microenvironment-on-chip: Development of a microfluidics-based tumor ecosystem, *Cancer Research* 76 (14 Supplement): 2418-2418 (2016)

Bibliography

[1] Denis Wirtz, Konstantinos Konstantopoulos, and Peter C. Searson. The physics of cancer: the role of physical interactions and mechanical forces in metastasis. *Nature Reviews Cancer*, 11:512 EP –, 06 2011.

[2] Jun Yokota. Tumor progression and metastasis . *Carcinogenesis*, 21(3):497–503, 03 2000.

[3] Paolo Vineis, Arthur Schatzkin, and John D. Potter. Models of carcinogenesis: an overview. *Carcinogenesis*, 31(10):1703–1709, 04 2010.

[4] Miguel López-Lázaro. A new view of carcinogenesis and an alternative approach to cancer therapy. *Molecular Medicine*, 16(3):144–153, Mar 2010.

[5] Lauren M. F. Merlo, John W. Pepper, Brian J. Reid, and Carlo C. Maley. Cancer as an evolutionary and ecological process. *Nature Reviews Cancer*, 6:924 EP –, 11 2006.

[6] David Basanta and Alexander R. A. Anderson. Exploiting ecological principles to better understand cancer progression and treatment. *Interface Focus*, 3(4):20130020, 2013.

[7] David Caballero, Sophie M. Blackburn, Mar de Pablo, Josep Samitier, and Lorenzo Albertazzi. Tumour-vessel-on-a-chip models for drug delivery. *Lab Chip*, 17:3760–3771, 2017.

[8] D. Caballero, S. Kaushik, V.M. Correlo, J.M. Oliveira, R.L. Reis, and S.C. Kundu. Organ-on-chip models of cancer metastasis for future personalized medicine: From chip to the patient. *Biomaterials*, 149:98 – 115, 2017.

[9] Tao Xu, Peter Molnar, Cassie Gregory, Mainak Das, Thomas Boland, and James J. Hickman. Electrophysiological characterization of embryonic hippocampal neurons cultured in a 3d collagen hydrogel. *Biomaterials*, 30(26):4377 – 4383, 2009.

[10] Virginia Brancato, Valentina Comunanza, Giorgia Imparato, Davide Cor, Francesco Urciuolo, Alessio Noghero, Federico Bussolino, and Paolo A. Netti. Bioengineered tumoral microtissues recapitulate desmoplastic reaction of pancreatic cancer. *Acta Biomaterialia*, 49:152 – 166, 2017.

[11] Pu Chen, Zhengyuan Luo, Sinan Gven, Savas Tasoglu, Adarsh Venkataraman Ganesan, Andrew Weng, and Utkan Demirci. Microscale assembly directed by liquid-based template. *Advanced Materials*, 26(34):5936–5941.

[12] Eelco Fennema, Nicolas Rivron, Jeroen Rouwkema, Clemens van Blitterswijk, and Jan de Boer. Spheroid culture as a tool for creating 3d complex tissues. *Trends in Biotechnology*, 31(2):108 – 115, 2013.

[13] Yi Jiang, Jelena Pjesivac-Grbovic, Charles Cantrell, and James P. Freyer. A multiscale model for avascular tumor growth. *Biophysical Journal*, 89(6):3884 – 3894, 2005.

[14] I. K. Guttilla, K. N. Phoenix, X. Hong, J. S. Tirnauer, K. P. Claffey, and B. A. White. Prolonged mammosphere culture of mcf-7 cells induces an emt and repression of the estrogen receptor by micrornas. *Breast Cancer Research and Treatment*, 132(1):75–85, Feb 2012.

[15] Leoni A. Kunz-Schughart, Paula Heyder, Josef Schroeder, and Ruth Knuechel. A heterologous 3-d coculture model of breast tumor cells and fibroblasts to study tumor-associated fibroblast differentiation. *Experimental Cell Research*, 266(1):74 – 86, 2001.

[16] AYSHA AKHTAR. The flaws and human harms of animal experimentation. *Cambridge Quarterly of Healthcare Ethics*, 24(4):407419, 2015.

[17] Max I. Bogorad, Jackson DeStefano, Johan Karlsson, Andrew D. Wong, Sharon Gerecht, and Peter C. Searson. Review: in vitro microvessel models. *Lab Chip*, 15:4242–4255, 2015.

[18] Boyang Zhang, Anastasia Korolj, Benjamin Fook Lun Lai, and Milica Radisic. Advances in organ-on-a-chip engineering. *Nature Reviews Materials*, 3(8):257–278, 2018.

[19] Mariana R. Carvalho, Daniela Lima, Rui L. Reis, Vitor M. Correlo, and Joaquim M. Oliveira. Evaluating biomaterial- and microfluidic-based 3d tumor models. *Trends in Biotechnology*, 33(11):667 – 678, 2015.

[20] Esak Lee, H-H Greco Song, and Christopher S Chen. Biomimetic on-a-chip platforms for studying cancer metastasis. *Current Opinion in Chemical Engineering*, 11:20 – 27, 2016. Biological Engineering / Material Engineering.

[21] Kyung Eun Sung, Patricia J. Keely, Carolyn Pehlke, David J. Beebe, Kevin W. Eliceiri, Ning Yang, and Andreas Friedl. Transition to invasion in breast cancer: a microfluidic in vitro model enables examination of spatial and temporal effects. *Integrative Biology*, 3(4):439–450, 12 2010.

[22] Qian Zhang, Tingjiao Liu, and Jianhua Qin. A microfluidic-based device for study of transendothelial invasion of tumor aggregates in realtime. *Lab Chip*, 12:2837–2842, 2012.

[23] Tingjiao Liu, Bingcheng Lin, and Jianhua Qin. Carcinoma-associated fibroblasts promoted tumor spheroid invasion on a microfluidic 3d co-culture device. *Lab Chip*, 10:1671–1677, 2010.

[24] Duc-Huy T. Nguyen, Sarah C. Stapleton, Michael T. Yang, Susie S. Cha, Colin K. Choi, Peter A. Galie, and Christopher S. Chen. Biomimetic model to reconstitute angiogenic sprouting morphogenesis in vitro. *Proceedings of the National Academy of Sciences*, 110(17):6712–6717, 2013.

[25] Sudong Kim, Hyunjae Lee, Minhwan Chung, and Noo Li Jeon. Engineering of functional, perfusable 3d microvascular networks on a chip. *Lab Chip*, 13:1489–1500, 2013.

[26] Lauren L. Bischel, Edmond W.K. Young, Brianah R. Mader, and David J. Beebe. Tubeless microfluidic angiogenesis assay with three-dimensional endothelial-lined microvessels. *Biomaterials*, 34(5):1471 – 1477, 2013.

[27] Jonathan W. Song, Stephen P. Cavnar, Ann C. Walker, Kathryn E. Luker, Mudit Gupta, Yi-Chung Tung, Gary D. Luker, and Shuichi Takayama. Microfluidic endothelium for studying the intravascular adhesion of metastatic breast cancer cells. *PLOS ONE*, 4(6):1–10, 06 2009.

[28] Ioannis K. Zervantonakis, Shannon K. Hughes-Alford, Joseph L. Charest, John S. Condeelis, Frank B. Gertler, and Roger D. Kamm. Three-dimensional microfluidic model for tumor cell intravasation and endothelial barrier function. *Proceedings of the National Academy of Sciences*, 109(34):13515–13520, 2012.

[29] Hyunjae Lee, Woohyun Park, Hyunryul Ryu, and Noo Li Jeon. A microfluidic platform for quantitative analysis of cancer angiogenesis and intravasation. *Biomicrofluidics*, 8(5):054102, 2014.

[30] Jessie S. Jeon, Simone Bersini, Mara Gilardi, Gabriele Dubini, Joseph L. Charest, Matteo Moretti, and Roger D. Kamm. Human 3d vascularized organotypic microfluidic assays to study breast cancer cell extravasation. *Proceedings of the National Academy of Sciences*, 112(1):214–219, 2015.

[31] Michelle B Chen, Jordan A Whisler, Julia Fröse, Cathy Yu, Yoojin Shin, and Roger D Kamm. On-chip human microvasculature assay for visualization and quantification of tumor cell extravasation dynamics. *Nature Protocols*, 12:865 EP –, 03 2017.

[32] Michelle B. Chen, John M. Lamar, Ran Li, Richard O. Hynes, and Roger D. Kamm. Elucidation of the roles of tumor integrin 1 in the extravasation stage of the metastasis cascade. *Cancer Research*, 76(9):2513–2524, 2016.

[33] Ke-chih Lin, Gonzalo Torga, Amy Wu, Joshua D Rabinowitz, Wesley J Murray, James C Sturm, Kenneth J Pienta, and Robert Austin. Epithelial and mesenchymal prostate cancer cell population dynamics on a complex drug landscape. *Convergent Science Physical Oncology*, 3(4):045001, 2017.

[34] Xiaofeng Zheng, Julienne L. Carstens, Jiha Kim, Matthew Scheible, Judith Kaye, Hikaru Sugimoto, Chia-Chin Wu, Valerie S. LeBleu, and Raghu Kalluri. Epithelial-to-mesenchymal transition is dispensable for metastasis but induces chemoresistance in pancreatic cancer. *Nature*, 527(7579):525–530, 2015.

[35] Hernan Roca, James Hernandez, Savannah Weidner, Richard C. McEachin, David Fuller, Sudha Sud, Taibriana Schumann, John E. Wilkinson, Alexander Zaslavsky, Hangwen Li, Christopher A. Maher, Stephanie Daignault-Newton, Patrick N. Healy, and Kenneth J. Pienta. Transcription Factors OVOL1 and OVOL2 Induce the Mesenchymal to Epithelial Transition in Human Cancer. *PLoS ONE*, 8(10), 2013.

[36] Johannes Schindelin, Ignacio Arganda-Carreras, Erwin Frise, Verena Kaynig, Mark Longair, Tobias Pietzsch, Stephan Preibisch, Curtis Rueden, Stephan Saalfeld, Benjamin Schmid, Jean-Yves Tinevez, Daniel James White, Volker Hartenstein, Kevin Eliceiri, Pavel Tomancak, and Albert Cardona. Fiji: an open-source platform for biological-image analysis. *Nature Methods*, 9:676 EP –, 06 2012.

[37] Jean-Yves Tinevez, Nick Perry, Johannes Schindelin, Genevieve M. Hoopes, Gregory D. Reynolds, Emmanuel Laplantine, Sebastian Y. Bednarek, Spencer L. Shorte, and Kevin W. Eliceiri. Trackmate: An open and extensible platform for single-particle tracking. *Methods*, 115:80 – 90, 2017. Image Processing for Biologists.

[38] Eleftheria Tsakalozou, Allison M. Eckman, and Younsoo Bae. Combination effects of docetaxel and doxorubicin in hormone-refractory prostate cancer cells. *Biochemistry Research International*, 2012, 2012.

[39] Amy Wu, Qiucen Zhang, Guillaume Lambert, Zayar Khin, Robert a. Gatenby, Hyunsung John Kim, Nader Pourmand, Kimberly Bussey, Paul C. W. Davies, James C. Sturm, and Robert H. Austin. Ancient hot and cold genes and chemotherapy resistance emergence. *Proceedings of the National Academy of Sciences*, 112(33):10467–10472, 2015.

[40] Jeonghun Han, Yukyung Jun, So Hyun Kim, Hong-Hoa Hoang, Yeonjoo Jung, Suyeon Kim, Jaesang Kim, Robert H. Austin, Sanghyuk Lee, and Sungsu Park. Rapid emergence and mechanisms of resistance by U87 glioblastoma cells to doxorubicin in an in vitro tumor microfluidic ecology. *Proceedings of the National Academy of Sciences*, 113(50):14283–14288, 2016.

[41] Jessie Huang Ulf D. Kahlert James R. Hernandez Gonzalo Torga Jelani C. Zarif Tamir Epstein Robert Gatenby Annemarie McCartney Jennifer H. Elisseeff Steven M. Mooney Steven S. An Takumi Shiraishi, James E. Verdone and Kenneth J. Pienta. *Oncotarget*, 6:130–143, 2015.

[42] Ke-Chih Lin, Gonzalo Torga, Yusha Sun, Robert Axelrod, Kenneth J. Pienta, James C. Sturm, and Robert H. Austin. The role of heterogeneous environment

and docetaxel gradient in the emergence of polyploid, mesenchymal and resistant prostate cancer cells. *Clinical & Experimental Metastasis*, 36(2):97–108, Apr 2019.

[43] William H. Wolberg, W. Nick Street, and Olvi L. Mangasarian. Importance of nuclear morphology in breast cancer prognosis. *Clinical Cancer Research*, 5(11):3542–3548, 1999.

[44] Karuna Mittal, Shashi Donthamsetty, Ramneet Kaur, Chunhua Yang, Meenakshi V Gupta, Michelle D Reid, Da Hoon Choi, Padmashree C G Rida, and Ritu Aneja. Multinucleated polyploidy drives resistance to Docetaxel chemotherapy in prostate cancer. *British Journal of Cancer*, 116(9):1186–1194, 2017.

[45] Jekaterina Erenpreisa, Andrei Ivanov, Sally P Wheatley, Elizabeth A Kosmacek, Fiorenza Ianzini, Alim P. Anisimov, Michael Mackey, Paul J. Davis, Grigorijs Plakhins, and Timothy M. Illidge. Endopolyploidy in irradiated p53-deficient tumour cell lines: Persistence of cell division activity in giant cells expressing Aurora-B kinase. *Cell Biology International*, 32(9):1044–1056, 2008.

[46] Antonia P Sagona and Harald Stenmark. Cytokinesis and cancer. *FEBS Letters*, 584(12):2652–2661, 2010.

[47] Yuji Nakayama, Asae Igarashi, Ikue Kikuchi, Yuuki Obata, Yasunori Fukumoto, and Naoto Yamaguchi. Bleomycin-induced over-replication involves sustained inhibition of mitotic entry through the ATM/ATR pathway. *Experimental Cell Research*, 315(15):2515–2528, 2009.

[48] Xin Lu and Yibin Kang. Cell fusion as a hidden force in tumor progression. *Cancer Research*, 69(22):8536–8539, 2009.

[49] Xin Lu and Yibin Kang. Efficient acquisition of dual metastasis organotropism to bone and lung through stable spontaneous fusion between mda-mb-231 variants. *Proceedings of the National Academy of Sciences*, 106(23):9385–9390, 2009.

[50] Timothy M Illidge, Mark S Cragg, Birgitta Fringes, Peggy Olive, and J a Erenpreisa. Polyploid giant cells provide a survival mechanism for p53 mutant cells after DNA damage. *Cell biology international*, 24(9):621–33, 2000.

[51] A N Makarovskiy, E Siryaporn, D C Hixson, and W Akerley. Survival of docetaxel-resistant prostate cancer cells in vitro depends on phenotype alterations and continuity of drug exposure. *Cellular and Molecular Life Sciences*, 59(7):1198–1211, 2002.

[52] Angela Ogden, Padmashree C G Rida, Beatrice S. Knudsen, Omer Kucuk, and Ritu Aneja. Docetaxel-induced polyploidization may underlie chemoresistance and disease relapse. *Cancer Letters*, 367(2):89–92, 2015.

[53] Pierre Emmanuel Puig, Marie Noëlle Guilly, André Bouchot, Nathalie Droin, Dominique Cathelin, Florence Bouyer, Laure Favier, François Ghiringhelli, Guido Kroemer, Eric Solary, François Martin, and Bruno Chauffert. Tumor cells can escape DNA-damaging cisplatin through DNA endoreduplication and reversible polyploidy. *Cell Biology International*, 32(9):1031–1043, 2008.

[54] Shiwu Zhang, Imelda Mercado-Uribe, Samir Hanash, and Jinsong Liu. ITRAQ-based proteomic analysis of polyploid giant cancer cells and budding progeny cells reveals several distinct pathways for ovarian cancer development. *PLoS ONE*, 8(11):1–16, 2013.

[55] S Zhang, I Mercado-Uribe, Z Xing, B Sun, J Kuang, and J Liu. Generation of cancer stem-like cells through the formation of polyploid giant cancer cells. *Oncogene*, 33(1):116–28, 2014.

[56] Laura M. Lopez-Sánchez, Carla Jimenez, Araceli Valverde, Vanessa Hernandez, Jon Peñarando, Antonio Martinez, Chary Lopez-Pedrera, Juan R. Muñoz-Castañeda, Juan R. De La Haba-Rodríguez, Enrique Aranda, and Antonio Rodriguez-Ariza. CoCl2, a mimic of hypoxia, induces formation of polyploid giant cells with stem characteristics in colon cancer. *PLoS ONE*, 9(6), 2014.

[57] Z. Storchova and D. Pellman. From polyploidy to aneuploidy, genome instability and cancer. *Nat Rev Mol Cell Biol*, 5(1):45–54, 2004.

[58] Teru Kanda, Kevin F. Sullivan, and Geoffrey M. Wahl. Histone-GFP fusion protein enables sensitive analysis of chromosome dynamics in living mammalian cells. *Current Biology*, 8(7):377–385, 1998.

[59] Jekaterina Erenpreisa and Mark S. Cragg. Three steps to the immortality of cancer cells: senescence, polyploidy and self-renewal. *Cancer Cell International*, 13(1):92, Sep 2013.

[60] Andrei Ivanov, Mark S. Cragg, Jekaterina Erenpreisa, Dzintars Emzinsh, Henny Lukman, and Timothy M. Illidge. Endopolyploid cells produced after severe genotoxic damage have the potential to repair dna double strand breaks. *Journal of Cell Science*, 116(20):4095–4106, 2003.

[61] F. Wottawah, S. Schinkinger, B. Lincoln, R. Ananthakrishnan, M. Romeyke, J. Guck, and J. Kas. Optical rheology of biological cells. *Phys Rev Lett*, 94(9):098103, 2005.

[62] Ruoxiang Wang, Xiaojuan Sun, Christopher Y. Wang, Peizhen Hu, Chia-Yi Chu, Shurong Liu, Haiyen E. Zhau, and Leland W. K. Chung. Spontaneous cancer-stromal cell fusion as a mechanism of prostate cancer androgen-independent progression. *PLOS ONE*, 7(8):1–11, 08 2012.

[63] Jeffrey L. Platt, Xiaofeng Zhou, Adam R. Lefferts, and Marilia Cascalho. Cell fusion in the war on cancer: A perspective on the inception of malignancy. *International Journal of Molecular Sciences*, 17(7), 2016.

[64] Jochen B. Geigl, Anna C. Obenauf, Thomas Schwarzbraun, and Michael R. Speicher. Defining chromosomal instability. *Trends in Genetics*, 24(2):64 – 69, 2008.

[65] Andrew J. Holland and Don W. Cleveland. Boveri revisited: chromosomal instability, aneuploidy and tumorigenesis. *Nature Reviews Molecular Cell Biology*, 10:478 EP –, 07 2009.

[66] Haixia Long, Tong Xiang, Wei Qi, Jiani Huang, Junying Chen, and Luhang He. cancer cell metastasis via CCL5 induced epithelial-mesenchymal transition. *Oncotarget*, 6(8):13–14, 2015.

[67] Michele Cioffi, Crescenzo Dalterio, Rosalba Camerlingo, Virginia Tirino, Claudia Consales, Anna Riccio, Caterina Ieranò, Sabrina Chiara Cecere, Nunzia Simona Losito, Stefano Greggi, Sandro Pignata, Giuseppe Pirozzi, and Stefania Scala. Identification of a distinct population of CD133 + CXCR4 + cancer stem cells in ovarian cancer. *Scientific Reports*, 5:1–11, 2015.

[68] Hyun Hee Lee, Vanessa Bellat, and Benedict Law. Chemotherapy induces adaptive drug resistance and metastatic potentials via phenotypic CXCR4-expressing cell state transition in ovarian cancer. *PLoS ONE*, 12(2):1–17, 2017.

[69] Fei Fei, Dan Zhang, Zhengduo Yang, Shujing Wang, Xian Wang, Zhengsheng Wu, and Qiang Wu. The number of polyploid giant cancer cells related proteins are associated with invasion and metastasis in human breast cancer. *Journal of Experimental & Clinical Cancer Research*, pages 1–13, 2015.

[70] Raquel Weber, Ana Paula Santin Bertoni, Laura Walter Bessestil, Beatriz Maria de Azevedo Assis Brasil, llma Simoni Brum, and Tania Weber Furlanetto. Validation of Reference Genes for Normalization Gene Expression in Reverse Transcription Quantitative PCR in Human Normal Thyroid and Goiter Tissue. *BioMed Research International*, 2014:1–5, 2014.

[71] R Axelrod and WD Hamilton. The evolution of cooperation. *Science*, 211(4489):1390–1396, 1981.

[72] Julia Bos, Qiucen Zhang, Saurabh Vyawahare, Elizabeth Rogers, Susan M. Rosenberg, and Robert H. Austin. Emergence of antibiotic resistance from multinucleated bacterial filaments. *Proceedings of the National Academy of Sciences*, 112(1):178–183, 2015.

[73] Mark B. Meads, Lori A. Hazlehurst, and William S. Dalton. The bone marrow microenvironment as a tumor sanctuary and contributor to drug resistance. *Clinical Cancer Research*, 14(9):2519–2526, 2008.

[74] Kenneth H Shain and William S Dalton. Environmental-mediated drug resistance: a target for multiple myeloma therapy. *Expert Review of Hematology*, 2(6):649–662, 2009.

[75] Yulia Nefedova, Pingyan Cheng, Melissa Alsina, William S. Dalton, and Dmitry I. Gabrilovich. Involvement of notch-1 signaling in bone marrow stroma-mediated de novo drug resistance of myeloma and other malignant lymphoid cell lines. *Blood*, 103(9):3503–3510, 2004.

[76] Robert L Mango, Hendrik W van Deventer, Qing Ping Wu, and Jonathan S Serody. Pulmonary stromal cells expressing cc-chemokine receptor 5 promote metastasis via erythroid differentiation regulator 1. *Blood*, 114(22):3601–3601, 2009.

[77] Jelani C Zarif, Russell S Taichman, and Kenneth J Pienta. Tam macrophages promote growth and metastasis within the cancer ecosystem. *OncoImmunology*, 3(7):e941734, 2014. PMID: 25954596.

[78] Jennifer M. Reiman, Keith L. Knutson, and Derek C. Radisky. Immune promotion of epithelial-mesenchymal transition and generation of breast cancer stem cells. *Cancer Research*, 70(8):3005–3008, 2010.

[79] Jermaine Coward and Angus Harding. Size Does Matter: Why Polyploid Tumor Cells are Critical Drug Targets in the War on Cancer. *Frontiers in oncology*, 4(May):123, 2014.

[80] Gonzalo Torga, Ke-Chih Lin, Robert H. Austin, and Kenneth J. Pienta. Abstract b039: Multinucleation precedes the emergence of drug resistance in prostate cancer. *Cancer Research*, 78(16 Supplement):B039–B039, 2018.

[81] Gonzalo Torga, Ke-Chih Lin, Bernat Navarro Serer, Cathleen Nguyen, Robert H. Austin, and Kenneth J. Pienta. Abstract 1977: Kifc1 is a potential target to prevent treatment resistance in prostate cancer. *Cancer Research*, 78(13 Supplement):1977–1977, 2018.

[82] Kenneth C. Valkenburg, Amber E. de Groot, and Kenneth J. Pienta. Targeting the tumour stroma to improve cancer therapy. *Nature Reviews Clinical Oncology*, 15(6):366–381, 2018.

[83] Thea D. Tlsty and Lisa M. Coussens. Tumor stroma and regulation of cancer development. *Annual Review of Pathology: Mechanisms of Disease*, 1(1):119–150, 2006. PMID: 18039110.

[84] Mark B. Meads, Robert A. Gatenby, and William S. Dalton. Environment-mediated drug resistance: a major contributor to minimal residual disease. *Nature Reviews Cancer*, 9:665 EP –, 08 2009.

[85] Sun H Park, Evan T Keller, and Yusuke Shiozawa. Bone marrow microenvironment as a regulator and therapeutic target for prostate cancer bone metastasis. *Calcified tissue international*, 102(2):152–162, 02 2018.

[86] Colm Morrissey and Robert L. Vessella. The role of tumor microenvironment in prostate cancer bone metastasis. *Journal of Cellular Biochemistry*, 101(4):873–886.

[87] Ashish Sabale Neerad Phansalkar, Sumit More and Madhuri Joshi. Adaptive local thresholding for detection of nuclei in diversity stained cytology images. In *2011 International Conference on Communications and Signal Processing*, pages 218–220, Feb 2011.

[88] Ryan J Morris, Trung V Phan, Matthew Black, Ke-Chih Lin, Ioannis G Kevrekidis, Julia A Bos, and Robert H Austin. Bacterial population solitary waves can defeat rings of funnels. *New Journal of Physics*, 19(3):035002, mar 2017.